

# Inverse design of a pyrochlore lattice of DNA origami through model-driven experiments

Hao Liu,<sup>1</sup> Michael Matthies,<sup>1</sup> John Russo,<sup>2</sup> Lorenzo Rovigatti,<sup>2</sup> Raghu Pradeep Narayanan,<sup>1</sup> Thong Diep,<sup>1</sup> Daniel McKeen,<sup>3</sup> Oleg Gang,<sup>3,4,5</sup> Nicholas Stephanopoulos,<sup>1</sup> Francesco Sciortino,<sup>2</sup> Hao Yan,<sup>1</sup> Flavio Romano,<sup>6,7</sup> and Petr Šulc<sup>1,8</sup>

<sup>1</sup>*School of Molecular Sciences and Center for Molecular Design and Biomimetics, The Biodesign Institute, Arizona State University, 1001 South McAllister Avenue, Tempe, Arizona 85281, USA*

<sup>2</sup>*Dipartimento di Fisica, Sapienza Università di Roma, P.le Aldo Moro 5, 00185 Rome, Italy*

<sup>3</sup>*Department of Chemical Engineering, Columbia University, 817 SW Mudd, New York, NY 10027, USA*

<sup>4</sup>*Department of Applied Physics and Applied Mathematics, Columbia University, New York, NY 10027, USA*

<sup>5</sup>*Center for Functional Nanomaterials, Brookhaven National Laboratory, Upton, NY, 11973, USA*

<sup>6</sup>*Department of Molecular Sciences and Nanosystems, Ca' Foscari University of Venice, Via Torino 155, 30171 Venezia-Mestre, Italy*

<sup>7</sup>*European Centre for Living Technology (ECLT), Ca' Bottacin, 3911 Dorsoduro Calle Crosera, 30123 Venice, Italy*

<sup>8</sup>*School of Natural Sciences, Department of Bioscience, Technical University Munich, 85748 Garching, Germany*

Sophisticated statistical mechanics approaches and human intuition have demonstrated the possibility to self-assemble complex lattices or finite size constructs, but have mostly only been successful *in silico*. The proposed strategies quite often fail in experiment due to unpredicted traps associated to kinetic slowing down (gelation, glass transition), as well as to competing ordered structures. An additional challenge that theoretical predictions face is the difficulty to encode the desired inter-particle interaction potential with the currently available library of nano- and micron-sized particles. To overcome these issues, we conjugate here SAT-assembly — a patchy-particle interaction design algorithm based on constrained optimization solvers — with coarse-grained simulations of DNA nanotechnology to experimentally realize trap-free self-assembly pathways. As a proof of concept we investigate the assembly of the pyrochlore (also known as tetrastack) lattice, a highly coveted 3D crystal lattice due to its promise in construction of optical metamaterials. We confirm the successful assembly with two different patchy DNA origami designs via SAXS as well as SEM visualization of the silica-coated lattice. Our approach offers a versatile modeling pipeline that starts from patchy particles designed *in silico* and ends with wireframe DNA origami that self-assemble into the desired structure.

## I. INTRODUCTION

The experimental realization of nano- and mesoscopic structures with precise geometry is one of the central goals of nanotechnology. To this end, one of the most promising bottom-up approaches is self-assembly, where the building blocks are specifically designed to spontaneously aggregate into the target structure. Despite its potential impact, progress in this direction is hindered by the lack of a general framework that can discover designs that can self-assemble with high yield without encountering kinetic traps or unwanted byproducts. Some of the proposed solutions to this problem include statistical mechanical approaches [1–11], machine learning-inspired protocols [12], and optimization methods [13]. So far, these approaches have been mostly *in-silico*, with experiments relying more heavily on ingenious intuition [14–18], or painstakingly difficult trial-and-error attempts.

Several potential pitfalls typically encountered in self-assembly can considerably lower the yield of the desired structure: i) metastable states that can compete with the final product; ii) dynamically arrested states (kinetic traps); iii) low aggregation rates; iv) lack of knowledge of

the underlying phase behavior of the building-blocks, especially for mixtures with many components. Additionally, from an experimental point-of-view, one has to consider the difficulty of realizing the building blocks, their size and interaction polydispersity, as well as their mechanical and molecular properties, such as softness and flexibility, that are difficult to take into account in theoretical modeling.

Here we use the synergy between theory, simulations, and experiments to address the aforementioned problems. We introduce a new modeling-driven design pipeline based on patchy particles as building blocks. Patchy particles are a model for units that interact with addressable directional bonds [19], which have recently been experimentally realised at the colloidal scale [16, 20–23]. In particular, we select as patchy particles DNA origami [24] where the scaffold is complemented by single-stranded overhangs (sticky sequences) located in controllable positions. The possibility of controlling the interaction between different patches in a unique way (by designing their DNA sequence) serves as a key strength of DNA nanotechnology as a nanofabrication technique. We show that our approach that couples optimization

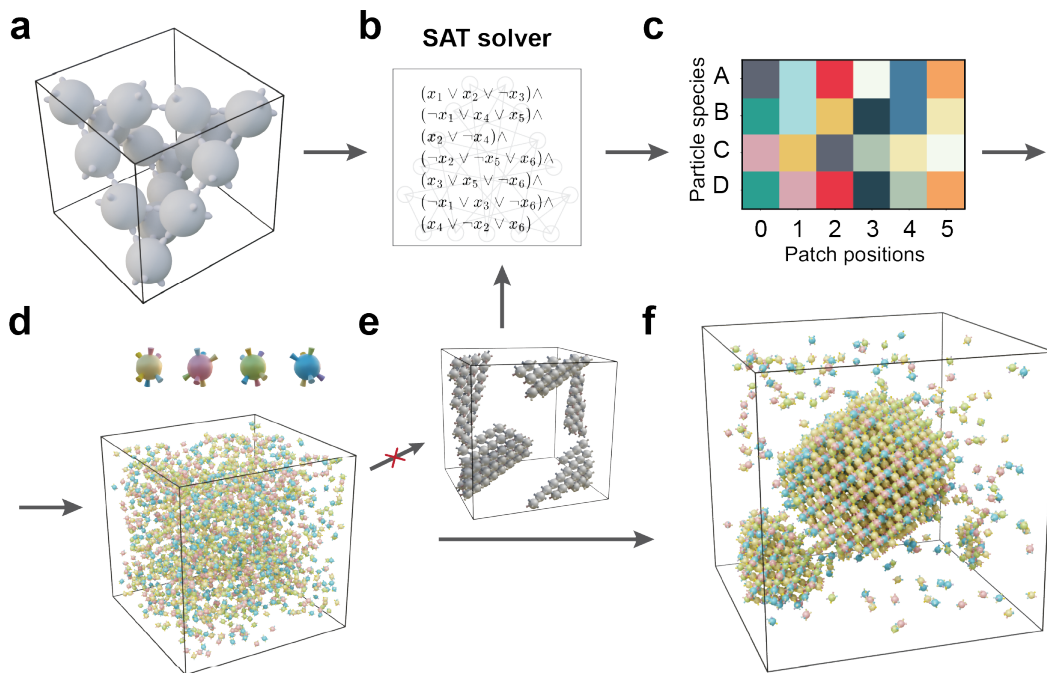


FIG. 1. Workflow of the computational design with SAT-assembly: **a**) The topology of the unit cell of a pyrochlore lattice, where each particle has six neighbors. **b**) The design problem to find a fixed number of species of patchy particles that satisfy the unit cell lattice is translated into a set of Boolean clauses (shown schematically here and listed in Supp. Mat. Sec. S1 ). **c**) From the defined clauses the SAT solver generates an interaction matrix corresponding to the assignment of colors to patches on respective species of patchy particles that can be arranged to satisfy the unit lattice interactions. **d**) We simulate the bulk assembly of patchy particles in a range of temperatures and screen for undesired assemblies that prevent the formation of the desired lattice. **e**) The identified undesired states are included as negative design in the SAT solver pipeline, explicitly banning solutions that can form these competing states. **f**) The process is iterated until we find a patchy assignment that only results in successful nucleation and assembly of the desired lattice.

methods, multiscale simulations, and DNA-origami experiments, can actively guide the assembly into the target structure.

As a test case, we focus on the pyrochlore (tetrastack) lattice, which so far has not been successfully experimentally realized by self-assembly. The pyrochlore lattice is of particular interest since it has been identified as having an omnidirectional photonic band gap, which is both wide and robust with respect to defects in the lattice [25, 26]. The self-assembly of this lattice is particularly challenging due to the presence of several competing structures with similar bonding topologies but different stacking orders which have so far prevented experimental realization [27]. To further demonstrate the versatility of our method we employ two different DNA origami wireframe nanostructure designs (icosahedral and octahedral shapes respectively) and show that they both robustly self-assemble into the pyrochlore superlattice, as confirmed by SAXS and SEM experiments of the silica-coated lattice.

## II. INVERSE DESIGN IN SILICO

We developed a multiscale approach to design DNA nanoparticles and test *in silico* their assembly into the pyrochlore lattice (Fig. 1). First we use the SAT-assembly method for positive (to target the desired lattice) and negative (excluding competing structures) designs. The second step is to numerically investigate the assembly process based on a coarse-grained patchy particle model, where each nanoparticle is represented as a sphere with colored interaction sites, where only compatible colors can form a bond. The colors represent single-stranded DNA sequences, where compatible colors correspond to complementary sequences. If the simulations reveal the presence of unwanted competing structures, these are translated into additional SAT clauses that are fed back to the optimization solver to look for solutions that exclude them. This feedback loop can be iterated until we obtain a solution for which the simulations produce the target structure with a high yield. The last step uses nucleotide-level modeling that translates the patchy particle design into a DNA origami amenable to experimental realization.

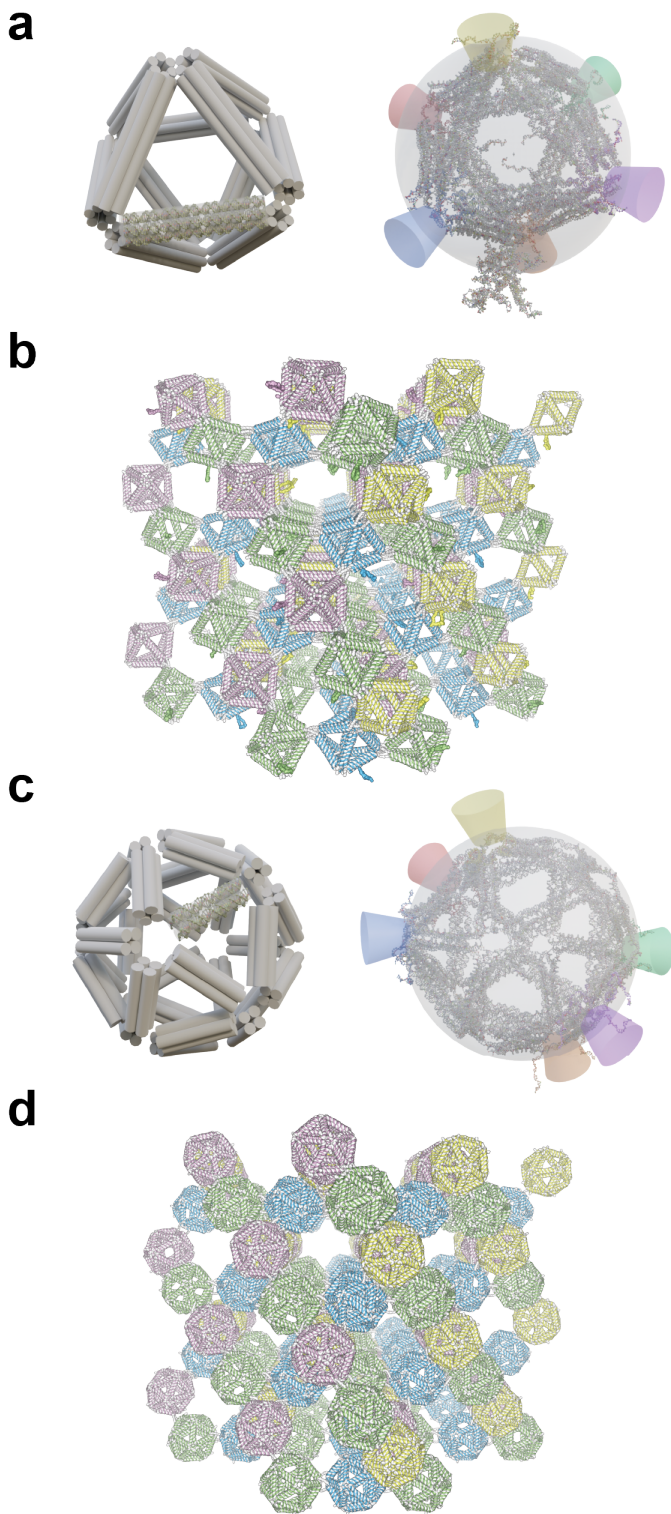


FIG. 2. Transferring the patchy particle design to the sequence design of DNA nanostructures with oxDNA simulations of the assembled lattice. **a** Octahedral and **c** icosahedral DNA origamis are selected for the experimental implementation of patchy particles, with patches realized as single-stranded overhangs. Both structures have multi-helical bundle edges to ensure their structural rigidity. We ran large-scale oxDNA simulations of large clusters (consisting of 128 DNA origami) with pyrochlore lattice geometry to ensure that the lattices are mechanically stable for chosen single-stranded overhang placements and lengths. The mean structures produced from the oxDNA simulations are shown in **b** and **d** respectively.

## A. SAT-assembly

The goal of the SAT-assembly procedure is to assign an interaction matrix that sets whether there is an attraction between any pair of building blocks so that the target lattice assembles without any kinetic traps or alternative free-energy minima that would lead to misassembled structures or defects in the lattice. The number of possible ways to design interaction matrices between patchy particles explodes combinatorially with an increasing number of possible colors and particle species, which in turn makes the search of the design space very challenging. To find an interaction matrix that can avoid these trapped states, we employed the SAT-assembly framework [13, 28] that maps the inverse design problem into a Boolean Satisfiability problem (SAT). SAT is a well studied NP-complete problem for which highly efficient solvers are available [29], allowing us to efficiently find solutions to the design problem; these solutions are represented as a set of binary variables that specify which color is assigned to which particle and which colors can interact. It further specifies restrictions that the interactions need to satisfy in terms of binary logic clauses composed of AND and OR and negation operations on the binary variables. These restrictions include that each color can only have one complementary color, each patch can only be assigned one color, and that the patchy particles can be arranged into the unit lattice so that all the patches on each particle are bound to a patch of complementary color (see Supp. Mat. Sec. S1 for details). Thus, as a positive design task, we can specify in terms of binary variables and logic clauses that the target lattice is an energy minimum of the patchy particle system, and let the SAT solver find color interactions and a patch color assignment that satisfy this condition. The first step of the SAT-assembly method is to specify the target unit cell of the lattice (Fig. 1). In the case of the pyrochlore lattice, the unit cell is composed of 16 individual particles, where each particle has six neighbors.

## B. Patchy particle simulations

We next verify that the solutions found by SAT solver can homogeneously nucleate a pyrochlore crystal via molecular dynamics simulations (Fig. 1). The goal of our pipeline is to realize the building blocks with DNA origami nanostructures. For simulations of DNA nanotechnology, we typically use a nucleotide-level coarse-grained model, oxDNA [30–33], which has been shown to reproduce the structural, mechanical and thermodynamic properties of single- and double-stranded DNA. However, the oxDNA model is still too slow to simulate the kinetics of assembly of individual origami into the lattice. Hence, to study assembly kinetics, we used a coarser model where the individual DNA nanostructures are represented as patchy spheres (Fig. 1d). Each patch is assigned a color, as given by the solution from

SAT solver. If two colors are compatible, they are considered to correspond to complementary single-stranded DNA overhangs and, in the patchy representation, to a short-range attractive potential. The spheres interact with excluded volume interactions to prevent two particles from overlapping with each other. We have used the oxDNA model to parameterize the patchy particle model (see Supp. Mat. Sec. S1).

We run multiple patchy particle simulations in a range of temperatures to probe the assembly kinetics for each possible solution (see Supp. Mat. Sec. S1 for details). We first try a solution that uses only one species of particles, but our simulations show that it always leads to misassembled states. At high temperatures, the assembly will remain in the gas phase, whereas at low temperature the system will form a quenched glassy state; at intermediate temperatures, where one would hope to observe nucleation and assembly of the lattice, the system forms misassembled states (shown in Fig. 1e and Supp. Fig. S2), which are stabilized by two bonds formed between two complementary pairs of patches on two patchy particles.

As a first iteration of the feedback loop, we introduce a new negative design requirement: no pair of particles can bind to each other by more than one bond, so that we explicitly prevent the system from forming the misassembled state that we previously identified in the molecular dynamics simulations. For our pyrochlore lattice design, the SAT solver proved that no solution exists that satisfies the conditions above if we allow only one patchy particle species, forcing us to go to multicomponent systems.

In multicomponent systems it is possible to add an additional requirement that a particle cannot form any bond with a particle of the same species. In the context of DNA origami interacting via single-stranded overhangs, as we will discuss later, this will be important in order to prevent possible aggregations or blocking by unpaired staple strands when each DNA nanostructure is prepared individually. SAT shows that this requirement suppresses all solutions with only two particle species. In fact, the SAT solver identifies that the smallest number of distinct particle species required is four (Supp. Mat. Sec. S1).

Our simulations show that kinetic traps are formed when a low number of colors is used. To decrease the chance of kinetic traps we then set the solver to find solutions with the maximum number of colors, 24 (that is 12 pairs of complementary colors). The resulting interaction matrix between patches is shown in Fig. 1c. As shown in Fig. 1f, simulations confirm the successful assembly of the 24 color solution into the desired pyrochlore lattice.

### C. Realization of patchy particles with DNA nanotechnology

We next design nucleic acid nanostructures that realize the patchy particles and their interactions found by

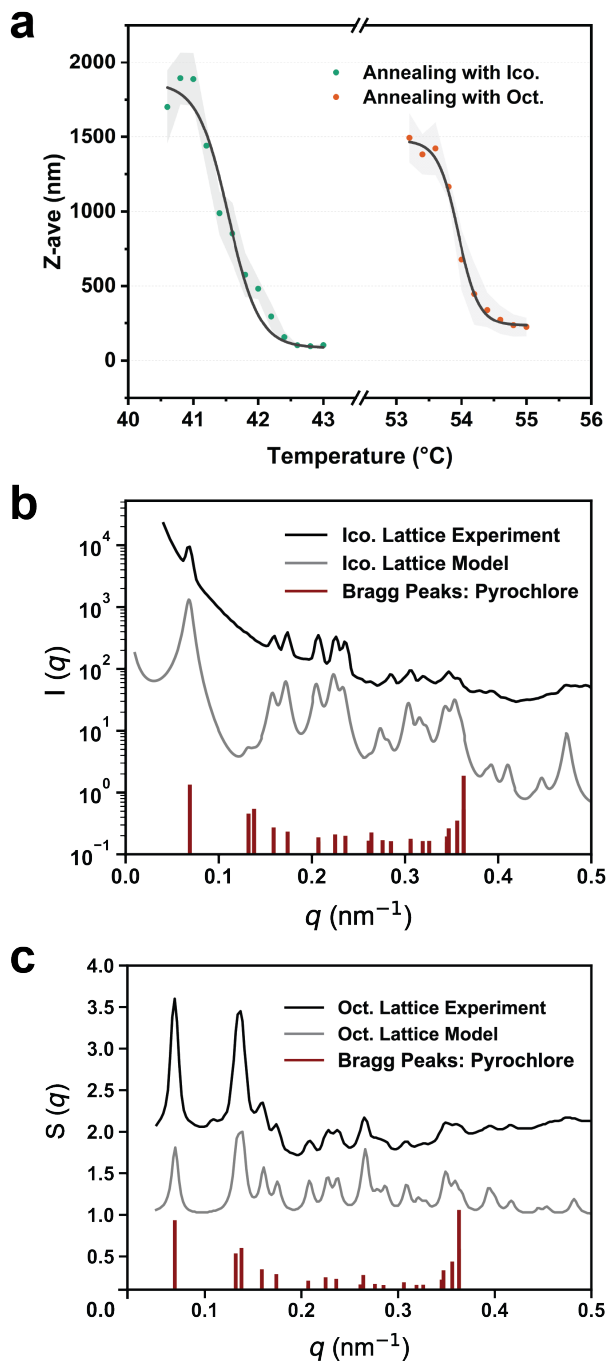


FIG. 3. **a**) Dynamic light scattering as a function of temperature during the lattice assemblies (from icosahedral and octahedral DNA origami respectively), used to identify the approximate assembly temperature. Experimental characterizations of the pyrochlore lattices with SAXS with **b**) icosahedral and **c**) octahedral building blocks. In black lines, we show the scattered intensity for lattice of icosahedral DNA origami in **b**) and structural factors are shown in **c**) for lattice of octahedral origami with encaged gold nanoparticles. The SAXS measurements are compared to the predicted scattering model for DNA origami arranged in the pyrochlore lattice (grey lines) and the Bragg peak positions (red lines).

the SAT assembly and verified in patchy particle simulation (Fig. 2). We use the oxDNA model and interactive modeling tool oxView [34] to design DNA nanostructures to represent the patchy particles with wireframe DNA origami, where patches correspond to single-stranded overhangs with spacers (Fig. 2 and Supp. Fig. S3). We considered two DNA wireframe origami designs: an icosahedral shape based on origami used in Ref. [35], and a second one based on an octahedral origami from Ref. [36] (Fig. 2a,c). In the icosahedral origami, each “patch” corresponds to three single-stranded overhangs (“handles”) placed in the vertex of the DNA origami, making the overall geometry fully compatible with the corresponding patchy particle model. Each overhang has a 15-nucleotide poly-T spacer followed by the 8-nucleotide binding region at the 3’ flanking end. The binding region sequences are the same on each of the three sequences in the patch, so that there is no imposed orientational control over binding of the two patches. We have optimized the assigned binding regions so that for each complementary pair, the binding free energy of complementary sequences is as close as possible for all twelve binding pairs, while making the binding between overhangs that are not supposed to interact as unfavorable as possible (see Supp. Mat. Sec. S4).

In order to demonstrate the robustness of the overhang-driven assembly and inverse-design strategy, we also employ a octahedral origami design where the vertex positions do not perfectly correspond to the patch positions. This in turn requires that each handle is sufficiently long to adapt to the imposed geometry, which is not compatible with octahedra touching their vertices. We hence design the handles with longer poly-T spacers (22 nucleotides) at each vertex to ensure that the DNA origami can arrange into the pyrochlore lattice, and use a 9-nucleotide long binding region. We verified in patchy particle simulations with patches placed in the octahedron vertex positions that the design with four particles species and 24 colors is still capable of assembling into a pyrochlore lattice (see Supp. Sec. S1).

Both icosahedral and octahedral designs were tested in a large scale simulation with the oxDNA model to investigate the mechanical stability and design the position and lengths of handle sequences accordingly. We therefore assembled a pyrochlore lattice cluster measuring  $2 \times 2 \times 2$  unit cells in each dimension (total: 128 DNA origami, corresponding to over two million nucleotides in the simulation). Molecular dynamics simulations were conducted for both designs (icosahedron and octahedron units) at 293 K, and used to calculate the mean structure as shown in Fig.2b,d. We assessed the movement trajectory of the center of mass (COM) for each DNA origami incorporated into the lattice and superimposed it onto the mean structure. A qualitative comparison of the relative positions of the COM trajectory and the mean structure indicates that the lattice assembled using the proposed origami design satisfies the pyrochlore geometry and is mechanically stable. We also verified that

the extra single-stranded scaffold loop in the octahedral origami design (Fig. 2a,b and Supp. Fig. S4) does not interfere with the desired pyrochlore geometry.

### III. EXPERIMENTAL LATTICE ASSEMBLY AND CHARACTERIZATIONS

For each DNA origami design, we prepared each species in a separate PCR tube by thermal annealing, after which, depending on the folding result of the origami, we use individually determined purification method for the lattice assembly. For icosahedral DNA origami, well-folded monomeric structures, isolated using rate-zonal purification [37], are preferentially utilized to ensure optimal lattice assembly, minimizing interference from multimeric side products. While for the octahedral DNA origami, despite further purification to exclude the influence of undesirably folded structures might produce better superlattices, we determined that removing the excess free staple strands with ultrafiltration is sufficient for the lattice to emerge, given the superior yield of the target monomeric structure. The four different origami species were then mixed together and annealed over a temperature ramp (Supp. Mat. Sec. S2).

We monitored the size change of the system with a fast annealing protocol using Dynamic Light Scattering (DLS) (Fig. 3a). The measured spectrum allows us to approximately identify the temperature range at which the monomers start associating ( $T_1$ ) and the temperature where the size of the assemblies reaches a stable size ( $T_2$ ). In particular, for the octahedral origami system  $T_1$  is 54 °C and  $T_2$  is 51 °C, while for the lattice assembled from icosahedral origami, it is 43 and 40 °C respectively. We then use an annealing protocol with a slow ramping rate from  $T_1$  to  $T_2$ , after incubation of the system at a slightly higher temperature to dissociate any bonds between monomers. The annealing process, during which the mixed origami nanoparticles nucleate and further crystallize, requires at least one week for the superlattice to emerge, and both elongating and fine-tuning the annealing protocol should give rise to superlattices with enlarged sizes and improved qualities.

The assembly of octahedral and icosahedral origami systems happens at different temperature ranges, as a result of the different particle geometry, patch distribution, and binding strength (Fig. 3a). We observe in the experiments that a higher binding strength is required for the octahedral system to assemble into the designed lattice, presumably because the icosahedron has more optimal patch positions, as supported by coarse-grained models (Supp. Mat. Sec. S1).

For characterization, we coat the annealed sample with a thin layer of silica to preserve the structural details for scanning electron microscopy (SEM) characterization [38]. We used SEM to visualize the deposited silica-DNA hybrid structure and the representative results are shown in Fig. 4 and Supp. Mat. Sec. S3. We optimized the

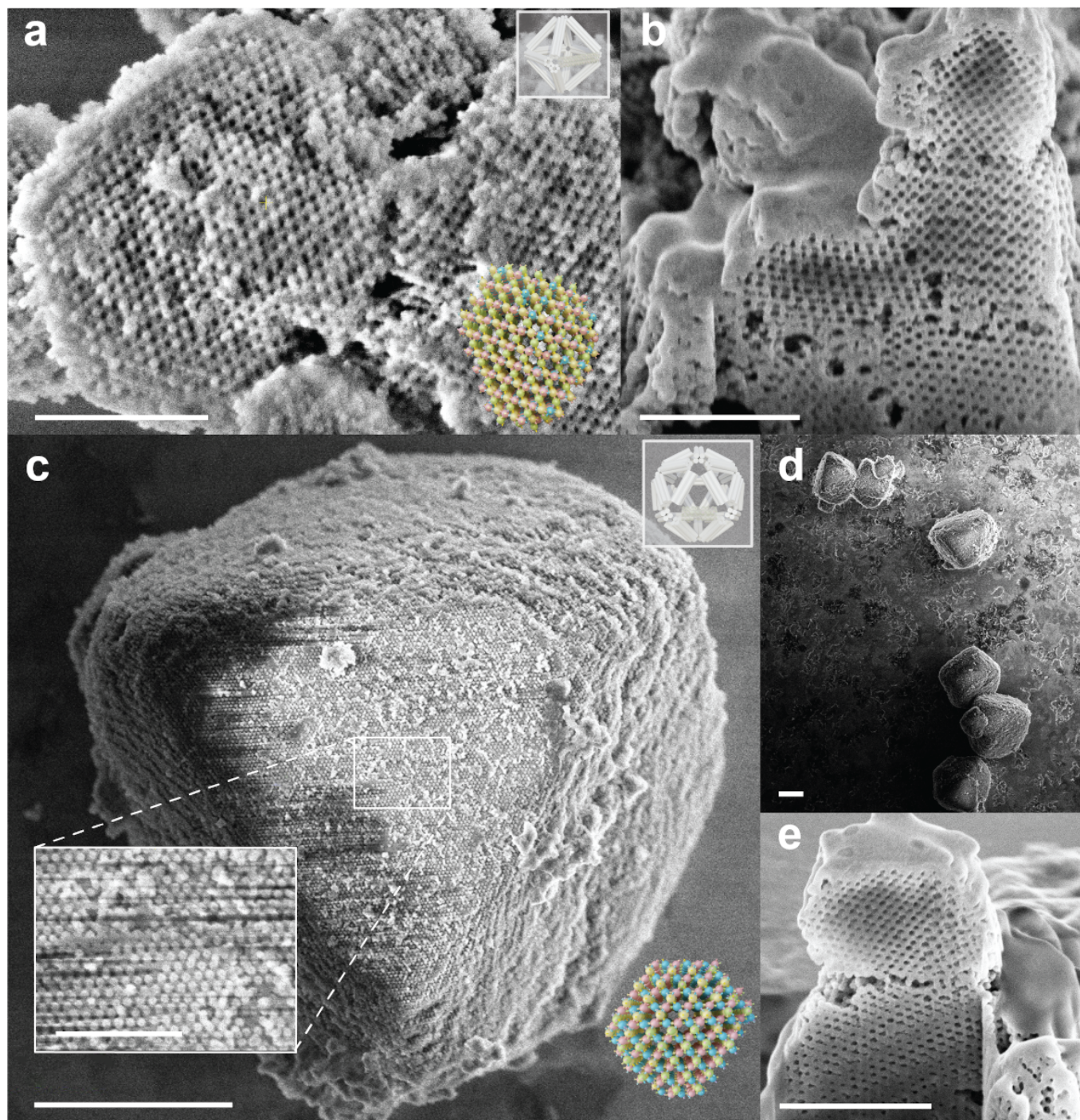


FIG. 4. Experimental characterization of the fabricated pyrochlore lattice embedded with silica. Representative SEM image of the assembled pyrochlore lattice with **a** octahedral and **c** icosahedral DNA origami building blocks and **b,d** the associated cross-section of the lattice created by focused ion beam from picked smaller lattice grains. In **d**, a typical zoomed-out view of the lattice assembled from icosahedral origami is shown. Insets for **a**, **c** are model for monomer and assembled lattice fitted to the projected view. In **a**, **b**, **e**, scale bars are 1  $\mu\text{m}$  and for **c**, **d**, scale bars are 5  $\mu\text{m}$ .

assembly conditions that affect the lattice formation, besides the annealing time, including origami concentration and ionic strength (in this case, magnesium ion concentration), based on the feedback of SEM characterization. Limited by the high binding strength, the octahedral system annealed best with the concentration of origami and magnesium being 10 nM and 12.5 mM respectively, to ensure the structural integrity of the nanostructure itself during lattice assembly. While with the icosahedral origami we determined (using a slow temperature ramp around the melting point) that concentrations of 10 nM origami and 25 mM magnesium produced the best superlattice, with increased ionic strength allowing larger lattices to emerge. For both systems, clear periodicity corresponding to the pyrochlore lattices is observed. The octahedral DNA origami produces on average smaller lattice grains and more poly-crystalline assemblies, with size on average 1  $\mu\text{m}$ . With icosahedral building blocks we are able to achieve larger and faceted lattices over 5  $\mu\text{m}$ . For the icosahedral system, we additionally also tried a mix-and-anneal strategy, where we provide mechanical agitation to the solutions while annealing. Through facilitating the diffusion of DNA origami particles and rocking the sedimented lattice in the bottom of the tube, we partially overcome the limitation of precipitation during thermal annealing. We find that this approach produced even larger lattices, with the largest dimension exceeding 20  $\mu\text{m}$  (Fig. 4c,d).

We next investigated the internal structures of the selected lattice grains with focused ion beam (FIB) cross-sectional analysis. It appears that internally associated long-range order persists without obvious assembly defects, confirming the successful experimental realization of the pyrochlore lattice (Fig. 4). To confirm the lattice structure, we have further performed SAXS measurements (see Supp. Mat. Sec. S2.8) of the assembled lattices: for the octahedral design, we have additionally attached a DNA-coated gold nanoparticle inside the origami to help the SAXS characterization. By fitting the SAXS measurements with a model of diffraction pattern for pyrochlore lattice (Supp. Mat. Sec. S2.8), we obtained lattice parameters of 156.4 nm for the octahedron origami lattice, and 159.1 nm for the lattice made out of icosahedral origami. The comparison of measured structure factor shows agreement with the one expected for the pyrochlore lattice (Fig. 3).

#### IV. CONCLUSION

We have developed a pipeline that uses multiscale modeling and optimization algorithms to design DNA nanostructures that self-assemble into the pyrochlore lattice. Our computational tools can be generalized to also design and guide the experimental realization of other types of lattices or finite-size multicomponent assemblies [34]. The method could also be used to design initial seeding substructures for improving the yields and resulting

sizes of the seeded nucleation and growth of the lattice, as well as design other sought-after lattice geometries such as clathrates [39]. This first successful realization of the pyrochlore lattice geometry opens a pathway towards optical metamaterials.

The reason for the generality of the procedure is that the design pipeline does not rely on the specific shape of the building blocks: the geometrical information of the local environment is only taken into account via a matrix of contacts. The nucleotide-level coarse-grained model is then used to verify that a particular DNA nanostructure realization is compatible with the designed patchy particle self-assembled system. One therefore has significant freedom in choosing the internal features, as well as the size, of the building blocks. Our approach allowed us to build upon the vast literature of successful DNA nanostructure designs, while being able to choose the size provides a handle on the lattice parameters which in turn controls the bandgap and other properties of the final lattice. The complexity of the unit cell is also not a limiting factor for the design process, since our approach is able to deal with many different building block species. Finally, the pipeline presented is not limited to long-range structures, but can be just as easily exploited to realise finite-size assemblies. The design and simulation tools are provided as free open-source software.

#### ACKNOWLEDGMENTS

We acknowledge support from the ONR Grant N000142012094 and ONR DURIP Grant N000142112876. We acknowledge the use of the Extreme Science and Engineering Discovery Environment (XSEDE), which is supported by National Science Foundation grant number TG-BIO210009. We acknowledge the use of facilities within the Eyring Materials Center at Arizona State University supported in part by NNCI-ECCS-1542160. This material is based upon work supported by the National Science Foundation under Grant No. 2227650. Research reported in this publication was supported by The National Institute of General Medical Sciences of the National Institutes of Health under grant number DP2GM132931 to N.S. The content is solely the responsibility of the authors and does not necessarily represent the official views of the National Institutes of Health. J.R. and P.Š. further acknowledge support from the Universit' a Ca' Foscari for a Visiting Scholarship. J.R. acknowledges support from the European Research Council Grant DLV-759187. J.R., L.R., and F.S. acknowledge support from ICSC — Centro Nazionale di Ricerca in High Performance Computing, Big Data and Quantum Computing, funded by the European Union—NextGenerationEU. This research used the CMS beamline at the National Synchrotron Light Source II, which is a US DOE Office of Science Facilities at Brookhaven National Laboratory under contract no. DE-SC0012704. D.M and O.G were sup-

ported by the US Department of Energy, Office of Basic Energy Sciences, Grant DE-SC0008772. This research used resources of the Advanced Light Source, which is a DOE Office of Science User Facility under contract no.

DE-AC02-05CH11231. We thank Ye Tian, Yang Yang, Andreas Neophytou, Eileen Seo, Chad Simmons, Youli Li, Di Liu, Tim Liedl, and Gregor Posnjak for helpful discussions.

- 
- [1] J. D. Halverson and A. V. Tkachenko. DNA-programmed mesoscopic architecture. *Physical Review E*, 87(6):062310, 2013.
- [2] M. Z. Miskin, G. Khaira, J. J. de Pablo, and H. M. Jaeger. Turning statistical physics models into materials design engines. *Proceedings of the National Academy of Sciences*, 113(1):34–39, 2016.
- [3] R. Kumar, G. M. Coli, M. Dijkstra, and S. Sastry. Inverse design of charged colloidal particle interactions for self assembly into specified crystal structures. *The Journal of chemical physics*, 151(8):084109, 2019.
- [4] M. Dijkstra and E. Luijten. From predictive modelling to machine learning and reverse engineering of colloidal self-assembly. *Nature Materials*, 20(6):762–773, 2021.
- [5] M. C. Rechtsman, F. H. Stillinger, and S. Torquato. Optimized interactions for targeted self-assembly: application to a honeycomb lattice. *Physical review letters*, 95(22):228301, 2005.
- [6] E. Marcotte, F. H. Stillinger, and S. Torquato. Optimized monotonic convex pair potentials stabilize low-coordinated crystals. *Soft Matter*, 7(6):2332–2335, 2011.
- [7] A. Jain, J. R. Errington, and T. M. Truskett. Dimensionality and design of isotropic interactions that stabilize honeycomb, square, simple cubic, and diamond lattices. *Physical Review X*, 4(3):031049, 2014.
- [8] W. M. Jacobs and D. Frenkel. Self-assembly of structures with addressable complexity. *Journal of the American Chemical Society*, 138(8):2457–2467, 2016.
- [9] A. Bupathy, D. Frenkel, and S. Sastry. Temperature protocols to guide selective self-assembly of competing structures. *Proceedings of the National Academy of Sciences*, 119(8):e2119315119, 2022.
- [10] N. Patra and A. V. Tkachenko. Layer-by-layer assembly of patchy particles as a route to nontrivial structures. *Physical Review E*, 96(2):022601, 2017.
- [11] S. Mushnoori, J. A. Logan, A. V. Tkachenko, and M. Dutt. Controlling morphology in hybrid isotropic/patchy particle assemblies. *The Journal of Chemical Physics*, 156(2):024501, 2022.
- [12] S. Whitelam and I. Tambllyn. Learning to grow: Control of material self-assembly using evolutionary reinforcement learning. *Physical Review E*, 101(5):052604, 2020.
- [13] F. Romano, J. Russo, L. Kroc, and P. Šulc. Designing patchy interactions to self-assemble arbitrary structures. *Physical Review Letters*, 125(11):118003, 2020.
- [14] Y. Tian, J. R. Lhermitte, L. Bai, T. Vo, H. L. Xin, H. Li, R. Li, M. Fukuto, K. G. Yager, J. S. Kahn, et al. Ordered three-dimensional nanomaterials using DNA-prescribed and valence-controlled material voxels. *Nature materials*, 19(7):789–796, 2020.
- [15] T. Zhang, C. Hartl, K. Frank, A. Heuer-Jungemann, S. Fischer, P. C. Nickels, B. Nickel, and T. Liedl. 3D DNA origami crystals. *Advanced Materials*, 30(28):1800273, 2018.
- [16] M. He, J. P. Gales, É. Ducrot, Z. Gong, G.-R. Yi, S. Sacanna, and D. J. Pine. Colloidal diamond. *Nature*, 585(7826):524–529, 2020.
- [17] A. Michelson, B. Minevich, H. Emamy, X. Huang, Y. S. Chu, H. Yan, and O. Gang. Three-dimensional visualization of nanoparticle lattices and multimaterial frameworks. *Science*, 376(6589):203–207, 2022.
- [18] R. J. Macfarlane, B. Lee, M. R. Jones, N. Harris, G. C. Schatz, and C. A. Mirkin. Nanoparticle superlattice engineering with DNA. *science*, 334(6053):204–208, 2011.
- [19] J. Russo, F. Leoni, F. Martelli, and F. Sciortino. The physics of Empty Liquids: from Patchy particles to Water. *Reports on Progress in Physics*, 2021.
- [20] E. Duguet, A. Désert, A. Perro, and S. Ravaine. Design and elaboration of colloidal molecules: an overview. *Chemical Society Reviews*, 40(2):941–960, 2011.
- [21] P. Swinkels, S. Stuij, Z. Gong, H. Jonas, N. Ruffino, B. v. d. Linden, P. Bolhuis, S. Sacanna, S. Woutersen, and P. Schall. Revealing pseudorotation and ring-opening reactions in colloidal organic molecules. *Nature communications*, 12(1):2810, 2021.
- [22] I. Chakraborty, D. J. Pearce, R. W. Verweij, S. C. Matysik, L. Giomi, and D. J. Kraft. Self-assembly dynamics of reconfigurable colloidal molecules. *ACS nano*, 16(2):2471–2480, 2022.
- [23] R. Khalaf, A. Viamonte, E. Ducrot, R. Méridol, and S. Ravaine. Transfer of multi-DNA patches by colloidal stamping. *Nanoscale*, 2023.
- [24] P. W. K. Rothmund. Folding DNA to create nanoscale shapes and patterns. *Nature*, 440(7082):297–302, 2006.
- [25] T. Ngo, C. Liddell, M. Ghebrebrhan, and J. Joannopoulos. Tetrastack: Colloidal diamond-inspired structure with omnidirectional photonic band gap for low refractive index contrast. *Applied physics letters*, 88(24):241920, 2006.
- [26] É. Ducrot, J. Gales, G.-R. Yi, and D. J. Pine. Pyrochlore lattice, self-assembly and photonic band gap optimizations. *Optics Express*, 26(23):30052–30060, 2018.
- [27] F. Romano and F. Sciortino. Patterning symmetry in the rational design of colloidal crystals. *Nature communications*, 3:975, 2012.
- [28] J. Russo, F. Romano, L. Kroc, F. Sciortino, L. Rovigatti, and P. Šulc. SAT-assembly: A new approach for designing self-assembling systems. *Journal of Physics: Condensed Matter*, 34(35):354002, 2022.
- [29] N. Een. MiniSat: A SAT solver with conflict-clause minimization. In *Proc. SAT-05: 8th Int. Conf. on Theory and Applications of Satisfiability Testing*, pages 502–518, 2005.
- [30] E. Poppleton, M. Matthies, D. Mandal, F. Romano, P. Šulc, and L. Rovigatti. oxDNA: coarse-grained simulations of nucleic acids made simple. *Journal of Open Source Software*, 8(81):4693, 2023.
- [31] B. E. Snodin, F. Randisi, M. Mosayebi, P. Šulc, J. S. Schreck, F. Romano, T. E. Ouldridge, R. Tsukanov,



- E. Nir, A. A. Louis, et al. Introducing improved structural properties and salt dependence into a coarse-grained model of DNA. *The Journal of chemical physics*, 142(23):06B613-1, 2015.
- [32] P. Šulc, F. Romano, T. E. Ouldridge, L. Rovigatti, J. P. K. Doye, and A. A. Louis. Sequence-dependent thermodynamics of a coarse-grained DNA model. *Journal of Chemical Physics*, 137(13):5101, 2012.
- [33] T. E. Ouldridge, A. A. Louis, and J. P. Doye. Structural, mechanical, and thermodynamic properties of a coarse-grained DNA model. *The Journal of chemical physics*, 134(8):02B627, 2011.
- [34] J. Bohlin, M. Matthies, E. Poppleton, J. Procyk, A. Mallya, H. Yan, and P. Šulc. Design and simulation of DNA, RNA and hybrid protein–nucleic acid nanostructures with oxView. *Nature protocols*, 17(8):1762–1788, 2022.
- [35] J. Zhang, Y. Xu, Y. Huang, M. Sun, S. Liu, S. Wan, H. Chen, C. Yang, Y. Yang, and Y. Song. Spatially patterned neutralizing icosahedral DNA nanocage for efficient SARS-CoV-2 blocking. *Journal of the American Chemical Society*, 144(29):13146–13153, 2022.
- [36] Y. Tian, T. Wang, W. Liu, H. L. Xin, H. Li, Y. Ke, W. M. Shih, and O. Gang. Prescribed nanoparticle cluster architectures and low-dimensional arrays built using octahedral DNA origami frames. *Nature nanotechnology*, 10(7):637–644, 2015.
- [37] C. Lin, S. D. Perrault, M. Kwak, F. Graf, and W. M. Shih. Purification of DNA-origami nanostructures by rate-zonal centrifugation. *Nucleic acids research*, 41(2):e40–e40, 2013.
- [38] Y. Wang, L. Dai, Z. Ding, M. Ji, J. Liu, H. Xing, X. Liu, Y. Ke, C. Fan, P. Wang, et al. DNA origami single crystals with Wulff shapes. *Nature Communications*, 12(1):3011, 2021.
- [39] S. Lee, T. Vo, and S. C. Glotzer. Entropy compartmentalization stabilizes open host–guest colloidal clathrates. *Nature Chemistry*, pages 1–8, 2023.

# Supplementary Material

## Contents

<b>S1 Computational design framework</b>	<b>2</b>
S1.1 SAT-assembly design of pyrochlore lattice . . . . .	2
S1.2 Patchy particle simulations . . . . .	3
S1.3 OxDNA simulations . . . . .	6
<b>S2 Experimental methods and materials</b>	<b>11</b>
S2.1 DNA origami and sequence design . . . . .	11
S2.2 DNA origami annealing and purification . . . . .	11
S2.3 Fabrication of pyrochlore superlattices . . . . .	11
S2.4 Measurement of the melting profile . . . . .	12
S2.5 Silicification and SEM imaging . . . . .	12
S2.6 AuNP functionalization and incorporation . . . . .	13
S2.7 Grid preparation and imaging with TEM and STEM . . . . .	13
S2.8 SAXS measurements and modeling . . . . .	13
S2.8.1 Representation of DNA origami for SAXS analysis . . . . .	13
S2.8.2 SAXS Data Analysis . . . . .	14
S2.8.3 Small-Angle X-Ray Scattering (SAXS) Data Acquisition of DNA Origami Lattices . . . . .	15
S2.8.4 SAXS modeling . . . . .	17
<b>S3 Additional experimental graphs and figures</b>	<b>20</b>
<b>S4 DNA Sequences</b>	<b>32</b>
S4.1 Sequence design . . . . .	32
S4.2 Icosahedral DNA origami . . . . .	32
S4.2.1 Staple sequences . . . . .	32
S4.2.2 Handle sequences . . . . .	38
S4.3 Octahedral DNA origami . . . . .	41
S4.3.1 Staple sequences . . . . .	41
S4.3.2 Functionalization sequence . . . . .	45
S4.3.3 Handle sequence . . . . .	46
<b>References</b>	<b>52</b>

arXiv:2310.10995v1 [cond-mat.soft] 17 Oct 2023

# S1 Computational design framework

## S1.1 SAT-assembly design of pyrochlore lattice

We use the SAT-assembly framework to design nanostructures that self-assemble into the target lattice. We use the design framework introduced in Ref. [1, 2] that formulates the inverse design problem as a Boolean Satisfiability problem (SAT) in terms of binary variables and logic clauses. SAT problems can be efficiently solved using available tools such as MiniSAT [3].

For completeness, we list here all the variables and clauses that were used to find the solution that forms pyrochlore lattice. The color interaction is given by binary variables  $x_{c_i, c_j}^{\text{int}}$  which are 1 if color  $c_i$  is compatible with color  $c_j$  and 0 otherwise. The patch coloring for each PP species is described by binary variables  $x_{s, p, c}^{\text{pcol}}$  which are 1 if patch  $p$  of species  $s$  has color  $c$  and 0 otherwise. The arrangement of the particle species in the lattice is described by  $x_{l, s, o}^L$  which is 1 if the position  $l$  is occupied by a PP of species  $s$  in the specific orientation  $o$ . The variable  $x_{l, k, c}^A$  is 1 if slot  $k$  of lattice position  $l$  is occupied by a patch with color  $c$  and 0 otherwise. The clauses and variables are defined for all possible combinations of colors  $c \in [1, N_c]$ , patches  $p \in [1, N_p]$ , slots  $k \in [1, N_p]$ , PP species  $s \in [1, N_s]$ , orientations  $o \in [1, N_o]$ , and lattice positions  $l \in [1, L]$ . For each particle orientation  $o$ , we assign a mapping  $\phi_o$ . The mapping  $\phi_o(k) = p$  for a given orientation  $o$  means that PP's patch  $p$  overlaps with slot  $k$  in a given lattice position, for example  $\phi_1 = (1, 2, 3, 4, 5, 6) \rightarrow (2, 3, 1, 5, 6, 4)$ . For a particle with 6 patches, there are  $N_o = 12$  such orientations.

As an input for the SAT solver, the problem has to be formulated in terms of clauses  $C_j$ , each of them containing variables  $x_i$  connected by OR clauses. The final SAT problem corresponds to all respective clauses  $C_j$  connected by AND clauses. To conform with this input format, the Boolean clauses introduced in Table 1 in the main text can be all reformulated as detailed below (we use symbols " $\wedge$ ", " $\vee$ ", and " $\neg$ " to denote AND, OR, and NOT operations respectively):

1. Each color  $c_i$  can only bind to one other color  $c_j$  (we exclude self-complementary colors):

$$\forall c_i < c_j < c_k \in [1, N_c] : C_{c_i, c_j, c_k}^{\text{int}} = \neg x_{c_i, c_j}^{\text{int}} \vee \neg x_{c_i, c_k}^{\text{int}}. \quad (\text{S1})$$

2. Each patch  $p$  of each PP species  $s$  is assigned exactly one color:

$$\forall s \in [1, N_s], p \in [1, N_p], c_l < c_k \in [1, N_c] : C_{s, p, c_k, c_l}^{\text{pcol}} = \neg x_{s, p, c_k}^{\text{pcol}} \vee \neg x_{s, p, c_l}^{\text{pcol}}. \quad (\text{S2})$$

3. Each lattice position  $l$  is only assigned exactly one PP species with exactly one assigned orientation:

$$\forall l \in [1, L], s_i < s_j \in [1, N_s], o_i < o_j \in [1, N_o] : C_{l, s_i, o_i, s_j, o_j}^L = \neg x_{l, s_i, o_i}^L \vee \neg x_{l, s_j, o_j}^L. \quad (\text{S3})$$

4. For all pairs of slots  $k_i$  and  $k_j$  that are in contact in neighboring lattice positions  $l_i, l_j$  (as given by the unit cell topology listed in Table S1.1), the patches that occupy them need to have complementary colors.

$$\forall c_i \leq c_j \in [1, N_c] : C_{l_i, k_i, l_j, k_j, c_i, c_j}^{\text{lint}} = \left( x_{l_i, k_i, c_i}^A \wedge x_{l_j, k_j, c_j}^A \right) \implies x_{c_i, c_j}^C,$$

which can be equivalently rewritten as

$$C_{l_i, k_i, l_j, k_j, c_i, c_j}^{\text{lint}} = \neg x_{l_i, k_i, c_i}^A \vee \neg x_{l_j, k_j, c_j}^A \vee x_{c_i, c_j}^C, \quad (\text{S4})$$

5. The slot of lattice position  $l$  is colored with the same color as the patch of the PP species occupying it:

$$\forall l \in [1, L], k \in [1, N_p], o \in [1, N_o], s \in [1, N_s], c \in [1, N_c] : C_{l, s, o, c, k}^{\text{LS}} = x_{l, s, o}^L \implies \left( x_{l, k, c}^A \iff x_{s, \phi_o(k), c}^{\text{pcol}} \right),$$

which can be equivalently rewritten as

$$C_{l, s, o, c, k}^{\text{LS}} = \left( \neg x_{l, s, o}^L \vee \neg x_{l, k, c}^A \vee x_{s, \phi_o(k), c}^{\text{pcol}} \right) \wedge \left( \neg x_{l, s, o}^L \vee x_{l, k, c}^A \vee \neg x_{s, \phi_o(k), c}^{\text{pcol}} \right) \quad (\text{S5})$$

PP species	Patch Coloring					
I:	(A,1)	(B,2)	(C,3)	(D,4)	(E,5)	(F,6)
II:	(A,7)	(B,8)	(C,9)	(D,10)	(E,11)	(F,12)
III:	(A,13)	(B,14)	(C,15)	(D,16)	(E,17)	(F,18)
IV:	(A,19)	(B,20)	(C,21)	(D,22)	(E,23)	(F,24)
Color interactions						
(1,15), (2,8), (12,17), (13,20), (16,23), (3,21), (4,18), (5,11), (6,24), (7,19), (9,14), (10,22)						

Table S1: Pyrochlore crystal lattice patchy particle design with 4 patchy particle species and 24 colors. The six patches on each species are labeled A-F respectively. Patch Coloring column shows colors (labeled 1-24) assigned to each patch and Color interactions show which colors are compatible. Compatible colors correspond to complementary DNA overhang strands in the DNA origami designs.

6. All  $N_s$  PP species have to be used at least once in the assembled lattice:

$$\forall s \in [1, N_s] : C_s^{\text{all spec.}} = \bigvee_{\forall l \in [1, L], o \in [1, N_o]} x_{l,s,o}^L, \quad (\text{S6})$$

where for each  $s$ , the conditions are connected by OR clause over all lattice positions and orientations.

7. Each color  $c$  of  $N_c$  total number of colors is assigned to at least one patch of one of the PP species:

$$\forall c \in [1, N_c] : C_c^{\text{all cols.}} = \bigvee_{\forall s \in [1, N_s], p \in [1, N_p]} x_{s,p,c}^{\text{pcol}} \quad (\text{S7})$$

8. Finally, we introduced an additional set of clauses that ensure that any pair of particles (of the same or different species) cannot bind by more than one bond at a time:  $\forall s_i, s_j \in [1, N_s], c_i^1, c_i^2, c_j^1, c_j^2 \in [1, N_c]$  :

$$C_{s_i, s_j, p_1^i, p_2^i, p_1^j, p_2^j, c_i^1, c_i^2, c_j^1, c_j^2}^{\text{no two}} = \neg \left( x_{s_i, p_1^i, c_i^1}^{\text{pcol}} \wedge x_{s_i, p_2^i, c_i^2}^{\text{pcol}} \wedge x_{s_j, p_1^j, c_j^1}^{\text{pcol}} \wedge x_{s_j, p_2^j, c_j^2}^{\text{pcol}} \wedge x_{c_i^1, c_j^1}^{\text{int}} \wedge x_{c_i^2, c_j^2}^{\text{int}} \right), \quad (\text{S8})$$

where  $p_1^i, p_2^i, p_1^j, p_2^j$  are all possible pairs of patches on PP of type  $s_i$  and  $s_j$  respectively for which there is a possible orientation so that they can both bind if they have compatible colors.

9. We furthermore require that in the identified solution, no particle species has a patch that would be able to bind to any other patch on the same particle. This additional constraint is introduced due to constraints with DNA origami preparation, as each DNA origami with specific staple strands corresponding to patches is prepared separately, and we aim to avoid formation of dimers or unused staple strands binding to formed origami:

$$\forall s \in [1, N_s], p_i, p_j \in [1, N_p], c_k, c_l \in [1, N_c] : C_{s, p_i, p_j, c_k, c_l}^{\text{no self binding}} : \neg x_{s, p_i, c_k}^{\text{pcol}} \vee \neg x_{s, p_j, c_l}^{\text{pcol}} \vee \neg x_{c_k, c_l}^{\text{int}} \quad (\text{S9})$$

The smallest solution in terms of number of different particle species  $N_s$  that satisfies all the clauses listed above, as identified with MiniSAT solver [3], requires use of four distinct particle species. We chose species with maximum number of colors ( $N_c = 6N_s$ ), which are specified in Table S1.

## S1.2 Patchy particle simulations

The patchy particle simulations were used to test solutions obtained from the SAT-solvers algorithm and probe their assembly into a target lattice. In patchy-particle simulations of pyrochlore lattice assembly, each particle is represented by a sphere covered by 6 patches at distance  $d_p = 0.5$  distance units (d.u.) from the center of the sphere.

Position $l_i$	Slot $s_i$	Position $l_j$	Slot $s_j$
0	0	7	0
0	1	4	3
0	2	1	5
0	3	9	1
0	4	6	4
0	5	3	2
10	1	12	1
1	0	12	4
10	3	11	1
1	1	13	3
11	5	14	2
1	2	2	5
12	5	13	5
13	0	15	0
1	3	7	1
14	4	15	4
1	4	4	4
2	0	14	0
2	1	11	3
2	2	3	5
2	3	12	3
2	4	13	4
3	0	9	0
3	1	6	3
3	3	14	1
3	4	11	4
4	0	5	4
4	1	15	3
4	2	14	5
4	5	7	2
5	0	12	0
5	1	6	1
5	2	10	2
5	3	14	3
5	5	15	5
6	0	10	0
6	2	12	2
6	5	9	2
7	3	8	1
7	4	10	4
7	5	11	2
8	0	11	0
8	2	10	5
8	3	13	1
8	4	9	4
8	5	15	2
9	3	15	1
9	5	13	2

Table S2: Topology of the unit cell of a pyrochlore

To mimic the icosahedral DNA wireframe origami design, the positions of the patches correspond to the selected six vertices of an icosahedron. These positions, defined in terms of the orthonormal base associated with the patchy particle, are

$$\mathbf{p}_1 = a(0, 1, \xi), \mathbf{p}_2 = a(0, -1, \xi), \mathbf{p}_3 = a(\xi, 0, 1), \mathbf{p}_4 = a(0, -1, -\xi), \mathbf{p}_5 = a(0, 1, -\xi), \mathbf{p}_6 = a(-\xi, 0, -1), \quad (\text{S10})$$

where  $\xi = (1 + \sqrt{5})/2$  and  $a = d_p/\sqrt{1 + \xi^2}$ .

To model the octahedral wireframe DNA origami designs, we position the patches on the surface of the particle in cubic arrangement:

$$\mathbf{p}_1 = d_p(0, 0, 1), \mathbf{p}_2 = d_p(1, 0, 0), \mathbf{p}_3 = d_p(0, 1, 0), \mathbf{p}_4 = d_p(0, 0, -1), \mathbf{p}_5 = d_p(-1, 0, 0), \mathbf{p}_6 = d_p(0, -1, 0), \quad (\text{S11})$$

The position of patch  $i$  in the simulation box coordinate system is given by

$$\mathbf{r}_{p_i} = \mathbf{r}_{\text{cm}} + p_{ix}\mathbf{e}_1 + p_{iy}\mathbf{e}_2 + p_{iz}\mathbf{e}_3 \quad (\text{S12})$$

where  $\mathbf{r}_{\text{cm}}$  is the position of the center of mass of the patchy particle, and  $\mathbf{e}_{1,2,3}$  are the x, y, and z orthonormal base vectors associated with the patchy particle's orientation.

The interaction potential between a pair of patches on two distinct particles is

$$V_{\text{patch}}(r_p) = \begin{cases} -1.001\delta_{ij} \exp\left[-\left(\frac{r_p}{\alpha}\right)^{10}\right] - C & \text{if } r_p \leq r_{p\text{max}} \\ 0 & \text{otherwise} \end{cases} \quad (\text{S13})$$

where  $\delta_{ij}$  is 1 if patch colors  $i$  and  $j$  can bind and 0 otherwise,  $r_p$  is the distances between a pair of patches. The constant  $C$  is set so that for  $V_{\text{patch}}(r_{p\text{max}}) = 0$ ,  $r_{p\text{max}} = 0.18$  d.u. (distance units). The parameter  $\alpha = 0.12$  d.u. sets the patch width, where patches do not strongly interact if they are separated by distances larger than  $\alpha = 0.12$ . We approximately set the patch width based on oxDNA model simulations [4, 5, 6] of the DNA origami monomers (Sec. S1.3 and Fig. S3), where we measure the distribution of the distance between the last and the first bases of the single-stranded overhang. In order to capture the fact that single-stranded overhang can reach longer distances than its typical end-to-end distance, we approximately take the patch width  $\alpha$  to be the mean plus standard deviation of the overhang length values measured in oxDNA molecular dynamics simulations at 25°C (ran for  $10^9$  steps with time step 10 fs). To convert this length from oxDNA to distance units of the patchy particle simulations, we divide it by the diameter of the wireframe origami, which we define as twice the mean distance from the center of mass of the DNA origami to the first base of the single-stranded overhang, as measured in the oxDNA simulations.

The patchy particles further interact through excluded volume interactions ensuring that two particles do not overlap:

$$V_{\text{exc}}(r, \epsilon, \sigma, r^*) = \begin{cases} V_{\text{LJ}}(r, \epsilon, \sigma) & \text{if } r < r^*, \\ \epsilon V_{\text{smooth}}(r, b, r^c) & \text{if } r^* < r < r^c, \\ 0 & \text{otherwise.} \end{cases} \quad (\text{S14})$$

where  $r$  is the distance between the centers of the patchy particles, and  $\sigma$  is set to  $2R = 0.8$ , twice the desired radius of the patchy particle. The choice of a radius ( $R = 0.4$  distance units) smaller than  $d_p$  has been done to mimic wireframe DNA origami, which are flexible and not spherical. In particular, we wanted the patchy model to be able to capture the fact that two faces of the icosahedral DNA origami, each with three patches, can be aligned in a way that can form up to three bonds with a second origami if patch coloring allows for it. Such states have been identified to lead to misassembly, and we use the SAT framework to avoid them. The repulsive potential is a piecewise function, consisting of Lennard-Jones potential function

$$V_{\text{LJ}}(r, \sigma) = 8 \left[ \left(\frac{\sigma}{r}\right)^{12} - \left(\frac{\sigma}{r}\right)^6 \right]. \quad (\text{S15})$$

that is truncated using a quadratic smoothening function

$$V_{\text{smooth}}(x, b, x^c) = b(x^c - x)^2, \quad (\text{S16})$$

with  $b$  and  $x_c$  are set so that the potential is a differentiable function that is equal to 0 after a specified cutoff distance  $r^c = 0.8$ .

The patchy particle systems are simulated using rigid-body Molecular Dynamics with an Andersen-like thermostat [7]. During the simulation, each patch was only able to be bound to one other patch at the time, and if the binding energy between a pair of patches, as given by Eq. (S13), is smaller than 0, none of the patches can bind to any other patch until their pair interaction potential is again 0.

To verify designs obtained from SAT-assembly, we ran for each designed systems the patchy particle simulations (consisting of 2048 particles, 512 of each species) at a range of temperatures (from 0.1 to 0.125 in simulation units) at number density 0.1 to identify an optimal temperature where the system nucleates and grows into a pyrochlore lattice (Fig. S1). We found that at given density, the icosahedral patchy particle design nucleates into a pyrochlore lattice in a range of tested temperatures (0.116 to 0.123). At lower temperatures, it forms quenched glassy state, and at higher temperatures remains in gas phase. For the octahedral patchy particle design, we found that the system successfully nucleated at temperatures 0.118 and 0.119. For larger temperatures that we considered (Fig. S1b), the systems did not successfully nucleate a crystal, and it misassembled at lower temperatures.

Besides the model outlines above, we have further implemented an additional model to represent icosahedral origami designs: a rigid-body icosahedron model. The interactions between patches remain the same, given by Eq. (S13). We however replace the excluded volume interaction by a new potential

$$V_{\text{rigid b.}}(\mathbf{r}_i, \mathbf{r}_j, \boldsymbol{\Omega}_i, \boldsymbol{\Omega}_j) = \begin{cases} \infty & \text{if icosahedrons } i \text{ and } j \text{ overlap,} \\ 0 & \text{otherwise,} \end{cases} \quad (\text{S17})$$

which we calculate for icosahedral particles  $i$  and  $j$  positioned at  $\mathbf{r}_i, \mathbf{r}_j$  respectively, with their orientation given by  $\boldsymbol{\Omega}_i$  and  $\boldsymbol{\Omega}_j$ . Each particle is represented in this rigid body model as an icosahedron with distance from center of mass to its vertex equal to  $R = 0.5$  distance units. Given the non-continuous nature of this potential, we use Monte Carlo simulations (with translations and rotations) to simulate these systems. Any move that would result in two icosahedral-shaped particles to overlap is always rejected, as it would result in infinite energy. We confirmed that the kinetically trapped state present for 1-species solution in the spherical system is also present in the rigid body icosahedron simulation. Similarly, we verified with the rigid body simulation that the solutions that are designed to avoid the state where one particle can bind to another one by two bonds at the same time eventually assemble into a pyrochlore lattice. The typical configurations identified in single-species systems that we studied are shown in Fig. S2.

Finally, we have also explored the role of number of colors when the number of particle species is fixed. The SAT clauses listed above have a two-species solution (which was also shown to form pyrochlore [1]) if we leave out the conditions listed in Eqs. S9. For the two-species case, we have also tried solutions with number of colors equal to 6, 8, 10, and 12 respectively. We observed that solutions with  $N_c = 10$  and  $N_c = 8$  also assembled well into a pyrochlore, but took longer to nucleate than the  $N_c = 12$  case. We also carried out simulations for a solution with  $N_c = 6$  at a range of temperatures ranging from 0.12 to 0.138  $k_B/\epsilon$ , but we only observed either gas state or glassy state formations and we did not observe successful pyrochlore nucleation in the simulation running time (up to  $3 \times 10^9$  MD steps, corresponding to about 3 weeks of CPU running time). Hence, we focused only on the solution with maximum possible number of colors ( $6 \times$  the number of species).

### S1.3 OxDNA simulations

The nucleotide-level simulations of DNA nanostructures have been carried out using the oxDNA2 parametrization of the coarse-grained model of DNA [6, 5, 8]. All simulations were performed at 1 M salt concentration, with time-step of 15 fs and temperature 25°C unless stated otherwise. We used Andersen-like thermostat [7] for molecular dynamics simulations. The simulations were performed using GPU implementation [9, 10] of the simulation code. The simulations of monomers and fourmers (Figs. S3 and S4) were setup using oxView design tool [11, 12], which was also used to interactively set the lengths of the single-stranded overhangs connecting the respective origamis. The simulations of the 2x2x2 unit cell cluster was setup by using the assembled part of the crystal from patchy particle simulation, where each DNA origami monomer were docked onto the position of the patchy particle and

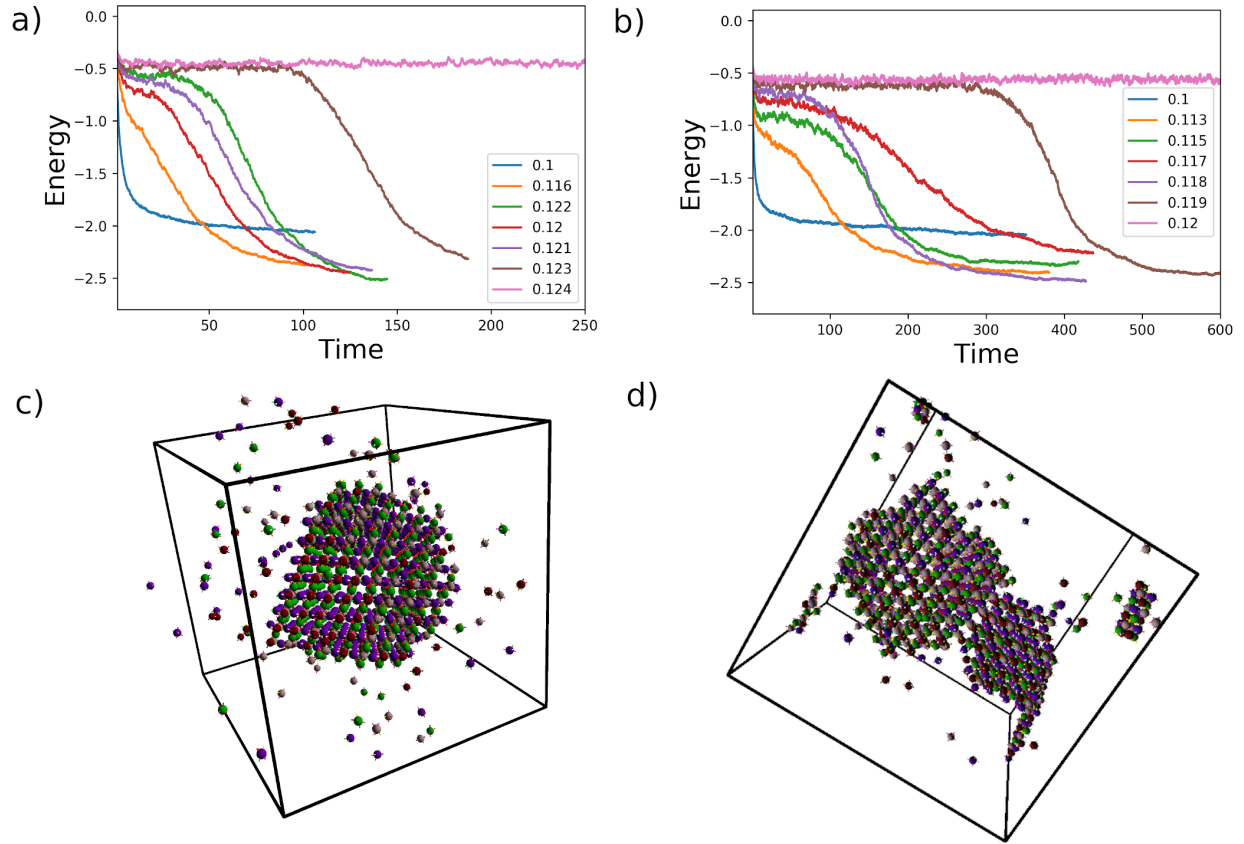


Figure S1: Energy per particle (in simulation energy units  $\varepsilon$ ) as a function of simulation time units for different simulation temperatures (in units of  $k_B/\varepsilon$ ) for icosahedral patchy particle (a) and octahedral patchy particle (b). We show a snapshot of the last state of the simulation at temperature  $T = 0.122 k_B/\varepsilon$  for icosahedral patchy particles (c) and at  $T = 0.118 k_B/\varepsilon$  octahedral patchy particles (d).



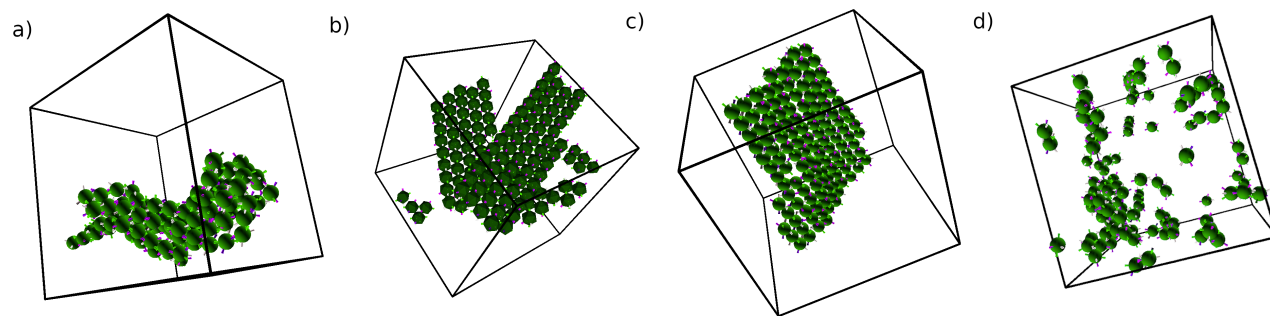


Figure S2: Snapshots from equilibrated final states of patchy particle simulations with a single particle species. At low temperature (a), the particles assemble into disordered quenched state. At intermediate temperature range, the particles assemble into alternative free-energy minima of a sheets where pairs of interacting particles interact through two patches (shown in (c) for spherical patchy simulation and in (b) for rigid body with icosahedral shape simulation). At high temperature, the system remains in gas state (d).

spring potential forces were applied to connect complementary DNA overhangs that represent the patches. The system was relaxed using Monte Carlo simulations and oxDNA relaxation potential, following the protocol from [12], before the production run of the crystal cluster was run.

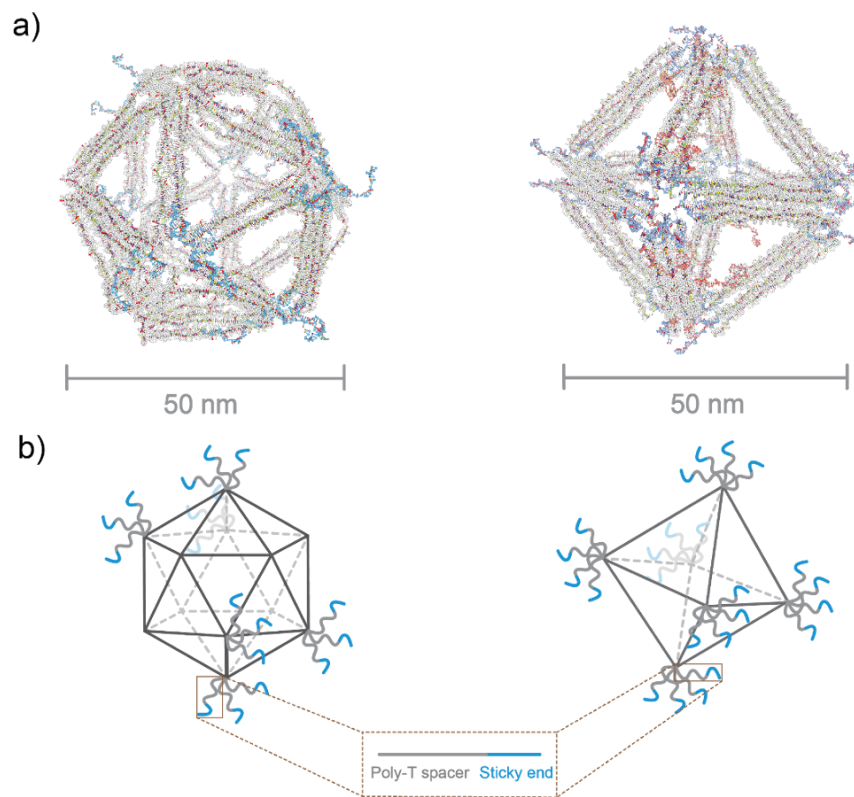


Figure S3: DNA origami design for the self-assembly of lattices. a) Origami design visualized in oxView [12] with blue strands representing the handle strands. b) Schematics showing the origami design. For each handle strand, poly-T spacers are placed before the sticky end sequence for binding, allowing flexibility for the recognition and binding of the sticky end pairs in lattice annealing.

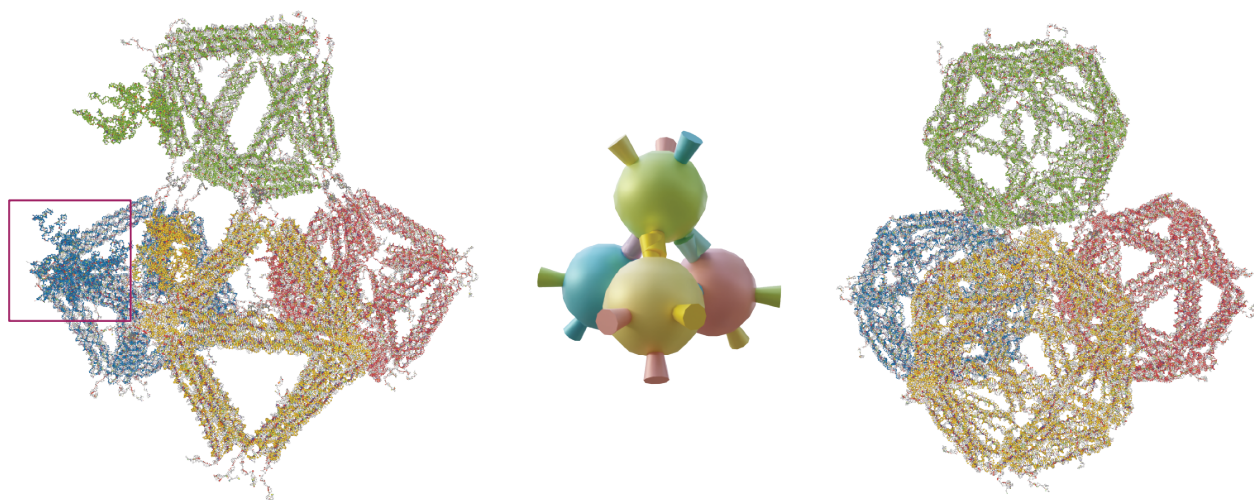


Figure S4: Tetramer in the topology of tetrahedron assembled with octahedron and icosahedron DNA origami, visualized in oxView. Tetrahedral assemblies stack on each other with the designed pathway forms further the pyrochlore lattice. The existence of scaffold loop in the octahedral DNA origami (one of them is highlighted in red square) could affect inter-particle connection due to the spatial proximity while icosahedral origami-based lattice design does not have such concern.

## S2 Experimental methods and materials

### S2.1 DNA origami and sequence design

Octahedral DNA origami (ODO), originally designed and reported by Tian et al [13] is adapted and used here. Icosahedral DNA origami (IDO) was first introduced by Zhang et al [14] and further adapted and used here. For both structures, each edge is composed of at least 4 helices to ensure the structural rigidity. The handles for directional bonding are placed on the vertices of the polyhedral shape and are properly distributed for even connection.

The sequence of handles are carefully designed so that the melting temperature difference between each pair of sticky ends are minimized and also the binding between each sequence pair is orthogonal to each other to prevent cross-talk. NUPACK[15] is used for the sequence design, with customized scripts.

### S2.2 DNA origami annealing and purification

Octahedral DNA origami are folded by mixing 20 nM M13mp18 scaffold, 200 nM of each designed staples, including the one designed to bind gold nanoparticles, and specifically 400 nM of each of the handle (sticky end strands) making the connection in 1 X TAE  $Mg^{2+}$  buffer (40 mM Tris, 20 mM acetic acid, 1 mM EDTA, 12.5 mM  $Mg^{2+}$  pH 8.0). The mixed solution is then annealed by cooling from 75°C to 20 °C slowly to obtain the target DNA structure with the following program: from 75 °C to 65 °C at a rate of 0.1 °C per 0.5 min, from 65 °C to 40 °C at a rate of 0.1 °C per 4 min, from 40 °C to 20 °C at 0.1 °C per 2 min, then held at 20 °C at the end of the cycle. Excess of the staple strands of the origami are purified through amicon ultrafiltration. Briefly, 100 kD amicon columns are passivated with fresh buffer and then annealed sample is loaded along with buffer to fill the column. The centrifugation is done with a rate between 2k rcf to 2.5k rcf followed by refilling the column with more buffer. Such procedure is done for overall 5 to 8 times, with higher loading amount taking more iterations to be purified.

Icosahedral DNA origami is annealed with the same program with the octahedral origami but usually in a higher concentration (40 - 50 nM) for further purification. It is noted that the yield of correctly formed monomer icosahedral origami is lower than the octahedral one and requires more attention and care in purification to afford clean monomers for lattice assembly. Rate zonal centrifugation, originally reported by Lin et al [16], is used to purify the monomers which guarantees higher yield compared to gel band excision and extraction. Briefly, in a 3.5 ml thick-wall ultracentrifuge tube, a glycerol gradient is created by adding 400  $\mu$ L of different percentage of glycerol solution in 1 x TAE  $Mg^{2+}$  buffer layer by layer. For overall 7 layers, the 45% glycerol solution is added the first and therefore at the bottom layer and the 5% glycerol solution is at the bottom with 5% concentration decrement per layer in between. 200  $\mu$ L of annealed icosahedral DNA origamis are then applied on the top. Without waiting overnight for a quasi-continuous gradient, the tube is loaded onto the swinging-bucket rotor (Beckman SW 55 Ti) and spun at 50000 rpm for 1 hour at 4 °C. The centrifugation program is set to be "Slow" for acceleration and "No brake" for deceleration, allowing for slow and smooth rate transition for a better separation of the sample. Afterwards, fractions (200  $\mu$ L per fraction) are taken out and placed in individual tubes which are further evaluated with agarose gel electrophoresis (AGE). The fractions corresponding to monomers, ideally with no or limited contamination of multimers/malformed structure which appear above the monomer band in AGE, are collected and concentrated as well as buffer exchanged through amicon ultrafiltration. The buffer washing step in amicon ultrafiltration is done for 6 times with 2400 rcf to remove the leftover glycerol which could affect the diffusion of DNA origamis in solution if not completely filtered.

For both DNA origami species, the concentration after purification is determined through Nanodrop based on the absorbance on 260 nm. Unused samples are stored at 4 °C refrigerator until further processing.

### S2.3 Fabrication of pyrochlore superlattices

For each origami species there are 4 particle types with 6 corresponding sticky end sets to map the interaction matrix for the assembly of pyrochlore lattices. Purified origami monomers, namely 4 individual particle species, are mixed together with equal ratio (1:1:1:1) and the final monomer concentration is set to be 10 nM. The mixed samples are annealed with a customized protocol based on the melting temperature of the superlattices.

For the pyrochlore lattice assembled with octahedral DNA origami, the annealing protocol is as follows: 55 °C for 2 hours, 54 to 52 °C with 0.1 °C per 8 hours, 52 °C for 24 hours, and then incubated at RT for forever.

For the pyrochlore lattice assembled with icosahedral DNA origami, the annealing protocol is as follows: 45 °C for 2 hours, 43 to 41 °C with 0.1 °C per 8 hours and then incubated at RT for forever.

For the screening of the nucleation temperature for the pyrochlore lattice with icosahedral building blocks, the mixed solution is incubated at 45 °C for 2 hours followed by incubation at the designated temperatures (41.1 °C, 41.3 °C, 41.4 °C, 41.5 °C, 41.7 °C, 41.9 °C) and finally incubated at RT for forever.

The thermal annealing of mixed solutions are done in thermocyclers above. The mix-and-anneal strategy is done through a customized set-up in which PCR tubes containing the sample are fixed to shaker and the devices are placed in a thermal incubator. Particularly, unless noted, all the SEM images shown are annealed with thermocyclers. The annealing protocol set in thermal incubators is as follows: 45 °C for 2 hours, 43 to 41 °C with 0.2 °C per 24 hours and the system is then allowed to cool down to RT before being harvested for characterization.

The fabricated lattices are stored in 4 °C after annealing. From our experience the assembled lattices are stable in fridge for more than 6 months - no visual differences are spotted with SEM examination after silica embedding for freshly annealed samples and fridge stored samples. Batch to batch difference exists and it is largely caused by pipeting and therefore stoichiometry accuracy, which leads to the change of average size of the lattices as visualized by SEM.

## S2.4 Measurement of the melting profile

Melting profile is used to customize the annealing protocol for the superlattices. It is measured by monitoring the aggregate size for a range of temperature through Dynamic Light Scattering (DLS, Malvern Zetasizer Nano). Specifically, the temperature ramps down from 55 °C to 30 °C with a ramping rate of 0.2°C per 240 seconds. Disposable 40  $\mu$ L Cuvette is used after cleaning and kept capped during the measurement to reduce the evaporation of water. 100  $\mu$ L of sample, pre-mixed with purified all 4 particle species, is loaded so that the melting profile would be similar to the one associated to lattice annealing.

## S2.5 Silicification and SEM imaging

To preserve the structure of under EM conditions, a thin layer of silica was coated on the DNA origami superlattices with the method originally described by Wang et al[17] and further adapted by us. Briefly, the annealed sample is buffer exchanged through gently removing the supernatant and replace with fresh buffer of 1xTAE 12.5mM  $Mg^{2+}$ . [ $Mg^{2+}$ ] reaches to the expected level after several times of pipetting, along with the amount of monomer and oligomer which would potentially affect the imaging quality of SEM. Samples are lightly centrifuged (1k rpm, 1min) to ensure the fabricated lattices are deposited at the bottom of the tube. TMAPS (50% in Methanol, TCI), diluted with methanol, is then added to the sample with microsyringe and the solution mix is subjected to shaking (800rpm, 30min, 4°C) to facilitate the diffusion and therefore even binding of TMAPS to the DNA phosphate backbone. Subsequently, TEOS (Sigma-Aldrich) is added to the solution after dilution with methanol and the same shaking protocol is executed for the sample. Notably, to embed silica onto large lattices elongated mixing (up to 2h) is needed to ensure the diffusion of silanes into the internal part of the lattice, as also indicated by Lewis et al [18]. A direct result of insufficient mixing is the collapse of lattice upon drying as shown in Fig. S13. The molar ratio of nucleotide: TMAPS : TEOS is 1:9:18 for the production of a thin layer of silica. The sample mixed with silanes is then incubated at RT for 12 hours undisturbed, wrapped within an aluminum foil. White cloudy precipitants are visible afterwards, indicating the successful formation of silica coated substances. Fresh ultrapure water is finally added to fill the tube to 2ml for the purpose of quenching the reaction, followed by light pipeting, centrifuging and supernatant removal to get rid of the excess silanes and silica particles. The washing process is done for at least 3 times with water, followed by one last washing step with isopropanol.

10  $\mu$ L embedded sample is taken from the bottom of the tube and further dropped cast on a silicon wafer cleaned with ethanol. The droplet is then dried in room temperature to expose the silicated superlattices to the air. SEM images are obtained through Auiga (Zeiss) and Helios 5 UX (ThermoScientific). Accelerating voltages, currents and other imaging parameters are adjusted to minimize the charging effect.

Frame Geometry	Bundle Length (nm)	Truncated Diagonal (nm)	Extrapolated Edge Length (nm)	Extrapolated Diagonal (nm)	Lattice Parameter (nm)	Nearest Neighbor (nm)	Inter-vertex Distance (nm)
Octahedron	27.79	39.30	38.34	54.22	156.4	55.30	16.00
Icosahedron	21.42	40.74	27.86	53.0	159.1	56.26	15.52

Table S3: Parameters of the DNA origami wireframe structures and their extrapolated ideal polyhedral shapes.

Cross-section of the silicated sample is created with Focused Ion Beam (FIB) installed on Helios 5 UX. A sacrificial layer of Platinum is deposited to the top of the sample to avoid unintended milling. For ion beam imaging, 30 kv and 7 pA is used to reduce the charging with charge neutralizer switched on while the current is increased to 41 pA for the creation of cross-section to accelerate the process.

## S2.6 AuNP functionalization and incorporation

10nm AuNP (Nanopartz) is functionalized with DNA through the salt aging method, adapted from Tian et al[19]. Briefly, thiolated DNA is synthesized by IDT and reduced with TCEP (tris[2-carboxyethyl] phosphine) to be prepared for the conjugation onto AuNP. With a ratio of 1:100, excess TCEP is added to the solution of thiolated DNA and the mixture is shaken at room temperature for an hour with 800rpm. Desalting column (G-25, GE Healthcare) is used to remove the remaining TCEP along with the reduced side-product. The purified product is further added into the AuNP solution in a ratio of 1:300 and another hour is given to the mixture for initial DNA attachment. Phosphate buffer is then added until 10 mM concentration is reached. After 1 hour, 2 M NaCl solution is mixed with the solution from the previous step gradually to reach a final concentration of 300 mM over the course of 5 hours, sonication up to 30 seconds is allowed after the addition of NaCl. The solution is finally aged at room temperature for at least 18 hours. Excess DNA is removed from the functionalized AuNP through repeating the process of centrifugation at 15000 rcf and buffer exchange (1 x PBS, remove the supernatant and add fresh buffer). The concentration of AuNP is determined by measuring the absorbance at 520 nm.

To incorporate the AuNP into the pyrochlore lattice, annealed sample is mixed with functionalized AuNP for 2 times excess. After gentle pipetting, the solution is annealed from 45 to 30 °C with a rate of 0.2 °C/hour.

## S2.7 Grid preparation and imaging with TEM and STEM

Carbon coated copper grids are glow discharged for 30 seconds and incubated at room temperature for 5 min before the following operation. To image the individual DNA origami building blocks for the assembly of the superlattice, 5  $\mu$ L solution of purified origami is dropcasted on the grid, followed by incubation for 5 min. Excess liquid is then blotted with a piece of filter paper and the grid is then negatively stained with 5  $\mu$ L solution of 2% uranyl acetate for 90 s, after which the grid is blotted thoroughly with filter paper and allowed to air dry for at least 20 min. To image the lattices, 5  $\mu$ L of silicated lattices, after thorough washing with water, is taken from the bottom of the tube and added to the glow discharged grid. Silicated lattice is used here to ensure the structural integrity. 20 min of incubation in the humid chamber is allowed for the lattice sample to sediment and the grid is blotted with filter paper afterwards. The grid is then allowed to air dry without further staining for EM imaging.

TEM imaging is done on Talos L120C (TFS), operated at an accelerating voltage of 120 kV.

STEM images are taken using a Titan 300/80 (FEI) in high-angle annular dark field (HAADF) mode, operated at an accelerating voltage of 300 kV.

## S2.8 SAXS measurements and modeling

### S2.8.1 Representation of DNA origami for SAXS analysis

For the SAXS analysis, we approximate the DNA origami wireframe structures as ideal polyhedrons. We extrapolate edges as lines from the center of cylindrical dsDNA bundles that will meet at the vertices of the ideal polyhedron, as shown in Fig. S5. This ideal polyhedron is used to model the spatial arrangements of the bundles for SAXS data analysis, in particular the form factor, of a given DNA wireframe. The analysis of the SAXS data in this work uses the parameters listed in Table S3.

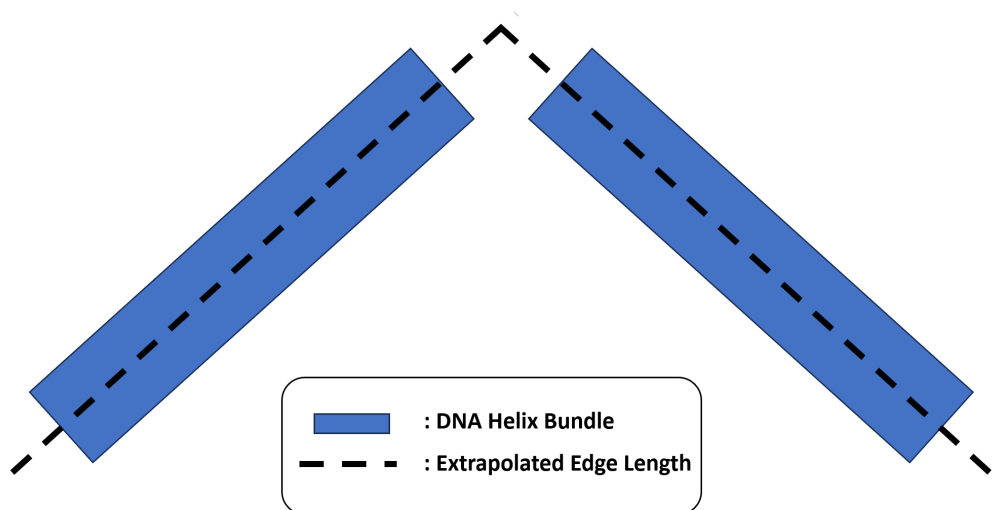


Figure S5: A 2D cartoon depicting how the junction between DNA bundles (blue rectangles) results in a truncated polyhedron, but that their spatial arrangement can be described mathematically via the extrapolated edge lengths (dashed lines)

The bundle length can be estimated by multiplying the number of base pair steps in the bundle by 0.34 nm, the length of a base pair in the ideal B-form helix. From this bundle length, a truncated diagonal can be determined through geometric relations for a given frame geometry. The extrapolated edge length and diagonal are empirically determined from SAXS data through fitting the form factor of the DNA origami. After the unit cell is determined from SAXS data, the lattice parameter and nearest neighbor distances are used to estimate the inter-vertex distance between two bound vertices. The inter-vertex is the distance from the outer edge of one frame to another, which is the nearest neighbor distance subtracted by the truncated diagonal and is physically determined by the spacer and sticky end sequences of the binding patches on the frames.

The parameters used to model the octahedron origami are in line with those used for prior SAXS analysis. The bundle length, 21.42 nm, used for the icosahedron origami comes from the design reported in the by Zhang et al [14]. There is a slight discrepancy between our estimate of the truncated diagonal, 40.74 nm, and their reported truncated diagonal, 43 nm, possibly due to the fact that their estimate might be based on negative TEM staining, which could have deformed the structures.

### S2.8.2 SAXS Data Analysis

The SAXS data analysis consists of three steps: 1) modelling the building block (DNA origami) used in the self-assembly, 2) arranging the building blocks into the expected unit cell, and 3) simulating the SAXS pattern from the model unit cell and fitting the pattern to the data. This process is described in greater detail in Section S2.8.4. For DNA origami frames, the helix bundles that serve as the edges of the frames are represented as single cylinders. The bundle length and thickness are used as the cylinder height and diameter respectively. The cylinders are then rotated and translated such that the edge corresponding to the extrapolated polyhedron runs through the center of the cylinder, continuing until the frame is fully constructed. The icosahedron has 30 edges and therefore consists of 30 cylinders, whereas the octahedron has 12 edges and consists of 12 cylinders. For gold nanoparticles which are attached inside octahedral DNA origami, the known form factor of a sphere is used. Therefore, a form factor is fit to the data corresponding to systems with gold nanoparticles, such as the pyrochlore lattice made out of octahedral DNA origami with gold nanoparticles inside. When modelling the gold nanoparticle (AuNP), it is important to

account for size polydispersity to better match the data as this can have a profound effect on the form factor of a sphere.

Once the building blocks are modelled, they need to be placed into the sites corresponding to the unit cell of the expected lattice. In this analysis, the sites corresponding to the pyrochlore lattice are determined through the CrystalMaker software (from CrystalMaker Software Ltd, Oxford, England ([www.crystallmaker.com](http://www.crystallmaker.com))), and exported as fractional coordinates that need to be scaled by the physical lattice parameters. Theoretical Bragg peaks corresponding to the pyrochlore are generated with the software CrystalDiffract.

The lattice parameters are extracted from the experimental data by converting the first peak position from q-space to real space and accounting for the peak indices, using the following formula:

$$q_{hkl} = \frac{2\pi}{a} \sqrt{h^2 + k^2 + l^2} \quad (\text{S18})$$

Where  $q_{hkl}$  is the  $q$  position of any given peak,  $a$  is the lattice parameter of a cubic lattice, and  $h$ ,  $k$ , and  $l$ , are the crystallographic indices for the peak. The first peak in the SAXS data used to determine the lattice parameter in the pyrochlore lattices corresponds to the [1 1 1] peak. From this formula, the octahedron origami pyrochlore lattice has a lattice parameter of 156.4 nm and the icosahedron origami pyrochlore lattice has a lattice parameter of 159.1 nm. The unit cell and building blocks are then appropriately scaled to fit the SAXS data. Fine tuning of other parameters, such as peak shape and Debye-Waller factor, a thermal disorder parameter, further improves the fitting of the model.

The icosahedron origami pyrochlore lattice data shows good agreement with the  $I(q)$  model, as shown in Figure S6, and agrees with most of the model in terms of peak height ratios. The model departs in terms of relative peak intensity at the peaks around  $0.28 \text{ nm}^{-1}$  and diverges when approaching the high  $q$  space data, due to instrument limitations. The scattering data from the pyrochlore constructed with icosahedra origami is left as  $I(q)$  because of the difficulty in deconvoluting the form factor of an empty icosahedral frame from the structure factor of the pyrochlore. The analytical form factors of the different objects are shown in Figure S8. From the SAXS data, the icosahedron origami frames have an extrapolated diagonal of 53.0 nm. The icosahedron pyrochlore lattice parameter is 159.1 nm, and the nearest neighbor distance is 56.26 nm.

The structure factor data is in good agreement with the modelled structure factor for the pyrochlore of octahedron loaded with gold nanoparticles (AuNP), as shown in Figure S7. The data is presented as structure factor data because the AuNPs provide a simple measurable form factor to remove from the data. The  $S(q)$  data show a small peak around  $0.15 \text{ nm}^{-1}$  that does not appear in either the model structure factor or the Bragg peaks from the pyrochlore, which can be due possible defects in the crystal. The data eventually diverges in the high  $q$  space, due to instrument limitations. The octahedron origami pyrochlore has a lattice parameter of 156.4 nm, which results in a nearest neighbor distance of 55.30 nm.

The complexity of the form factor contribution to scattering intensity is dependent upon the complexity of the object. A polydisperse AuNP has low complexity and is therefore easier to deconvolute from the scattering intensity data of the octahedron pyrochlore. However, it is more difficult to deconvolute the icosahedron form factor's contribution to the scattering intensity because of its more complex features. It is challenging to determine the capability of the instrument to measure the complex features of the icosahedral form factor. Therefore, the data from the icosahedral pyrochlore is displayed as  $I(q)$  rather than  $S(q)$ .

### S2.8.3 Small-Angle X-Ray Scattering (SAXS) Data Acquisition of DNA Origami Lattices

Origami assemblies were measured in solution at the Complex Materials Scattering (CMS, 11-BM) beamline at the National Synchrotron Light Source II (NSLS-II), Brookhaven National Laboratory (BNL). The photon energy of the beam at CMS is 13.5 keV with a beam size of  $200 \mu\text{m} \times 200 \mu\text{m}$  with an approximate flux of 1011 photons/sec. The sample-to-detector distance was set at 5.05 m. The detector used for the measurements was a Pilatus 1M with a pixel size of  $172 \mu\text{m} \times 172 \mu\text{m}$ . Samples were loaded into borosilicate glass capillaries that were then sealed with glue or wax. The bottom of the capillaries were then probed at the bottom of the capillary where origami lattices had settled. Two-dimensional scattering patterns were captured on are detectors downstream of the sample. The two-dimensional scattering patterns were then converted into one-dimensional scattering intensity profiles ( $I(q)$ ) via



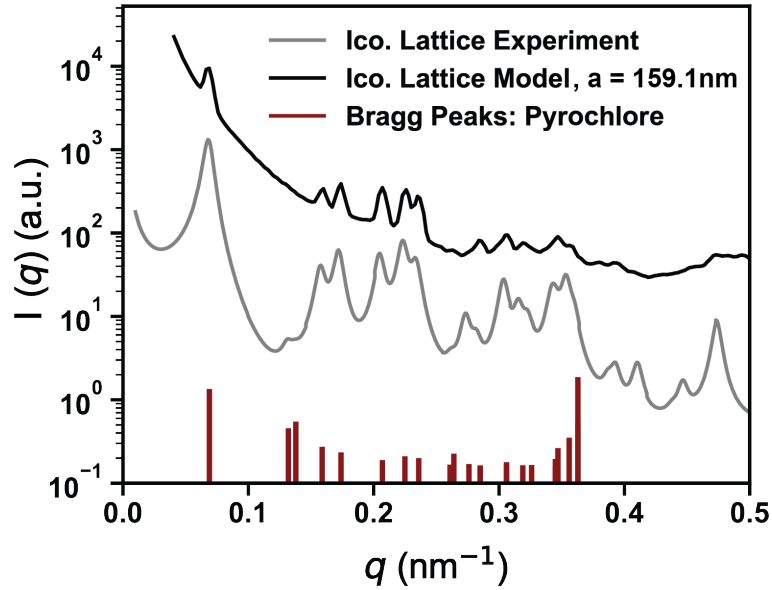


Figure S6: Scattered intensity,  $I(q)$ , of the pyrochlore lattice constructed with icosahedral DNA origami, where the blue and black curves correspond to the experimental data and modelling respectively. The red lines correspond to the Bragg peak positions of a pyrochlore lattice.

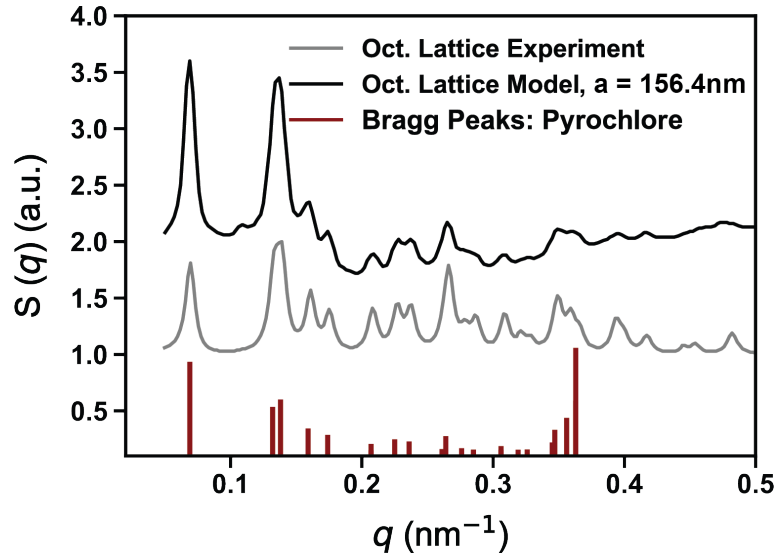


Figure S7: Structure factor,  $S(q)$ , data from the pyrochlore of octahedral origami loaded with gold nanoparticles, where the blue and black curves correspond to the experimental data and modelling respectively. The red lines correspond to the Bragg peaks of the pyrochlore lattice.

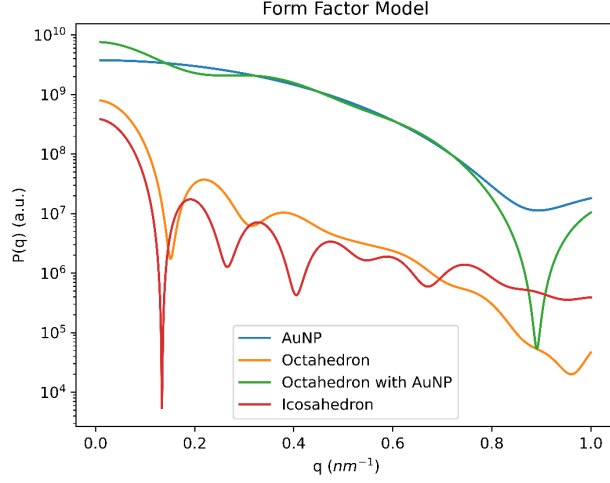


Figure S8: Modelled form factor,  $P(q)$ , profiles for the different origami frames and gold nanoparticles.

azimuthal integration, as a function of the scattering vector  $q$ , where  $q = \frac{4\pi}{\lambda} \sin\left(\frac{\theta}{2}\right)$ .  $\lambda$  and  $\theta$  are the wavelength of the incident x-rays and the full scattering angle, respectively. The resulting  $I(q)$  curves spanned from around  $0.04 \text{ nm}^{-1}$  to  $1 \text{ nm}^{-1}$  with a resolution of  $0.002 \text{ nm}^{-1}$ , in reciprocal space.

#### S2.8.4 SAXS modeling

SAXS modeling was primarily performed using ScatterSim software, a python software package for simulating the 1D curves associated with crystalline superlattices built from arbitrary nano-objects [20].

**Modeling Polydisperse Gold Nanospheres:** The model for polydisperse AuNP was built using “PolydisperseNanoObject” in the ScatterSim package [20]. This generates a specified object while varying a key parameter of the object. In this case, “PolydisperseNanoObject” was given a gold sphere generated by “SphereNanoObject”. We used  $(r_{\text{AuNP}})$  must be supplied and here,  $r_{\text{AuNP}} = 4.99 \text{ nm}$ . This radius was determined by analytically fitting the underlying form factor of intensity data gathered at the beamtime with spheres of different size. “PolydisperseNanoObject” requires an additional parameter,  $\sigma_r$ , which accounts for the standard deviation of the sphere. In this work, the  $\sigma_r$  of the AuNP was found by a fit to be  $0.483 \text{ nm}$ . The scattering length density (SLD) of the aqueous environment was  $SLD_{\text{water}} = 9.43 \times 10^{-6} \text{ \AA}^{-2}$  and the SLD of gold is  $SLD_{\text{gold}} = 119.16 \times 10^{-6} \text{ \AA}^{-2}$ . With these parameters, the form factor of AuNP can be calculated using:

$$F_{\text{sphere}}(q, R, \rho') = \frac{4\pi}{3} R^3 \rho' \frac{\sin(qR) - qR \cos(qR)}{(qR)^3} \quad (\text{S19})$$

where  $\rho'$  is the scattering contrast  $SLD_{\text{gold}} - SLD_{\text{water}}$ . We then applying polydispersity dependent on radius  $r$  with average value  $\bar{r}$  with its standard deviation  $\sigma_r$ .

$$\langle F(q) \rangle_r = \int P(h, \bar{r}, \sigma_r) F_{\text{sphere}}(q, h, \rho') dh \quad (\text{S20})$$

and

$$\langle |F(q)|^2 \rangle_r = \int P(h) |F_{\text{sphere}}(q, h, \rho')|^2 dh \quad (\text{S21})$$

and where the Gaussian distribution is

$$P(r, \bar{r}, \sigma_r) = \frac{1}{\sqrt{2\pi\sigma_r^2}} e^{-\frac{(r-\bar{r})^2}{2\sigma_r^2}}. \quad (\text{S22})$$

In ScatterSim this is accomplished by randomly creating spheres with radii that are sampled from the corresponding probability distribution and averaging their resultant form factor amplitudes or intensities ( $F(q)$  and  $|F(q)|^2$  respectively).

**Modeling Octahedral DNA origami:** The octahedron model was built using “OctahedronCylindersNanoObject” in the ScatterSim package. This generates an octahedral DNA frame where each of six helix bundles (6HB) at the 12 edges of the octahedron frame is approximated as a cylinder with a specified radius ( $r_{6HB}$ ) and height ( $h_{6HB}$ ). The parameters used in this work were as follows:  $r_{6HB} = 4.156$  nm,  $h_{6HB} = 27.79$  nm. Additionally, an extrapolated edge length ( $L_{\text{Octahedron}}$ ) of the DNA octahedron must be supplied, since the true shape of the origami is a truncated octahedron. In this work, the edge length was  $L_{\text{Octahedron}} = 38.34$  nm. The SLD of 6HB is approximated as that of double stranded DNA (dsDNA),  $SLD_{\text{dsDNA}} = 11 \times 10^{-6} \text{ \AA}^{-2}$ . These parameters agree with both the design and known physical features of the octahedron design as well as previous work [19, 21]. The octahedral DNA origami loaded with a polydisperse gold nanoparticle (Octa-AuNP) was treated as a non-overlapping “composite” object of the two different components. This is possible to model in ScatterSim as a “CompositeNanoObject”, where the interference between sub-components is accounted for. The SAXS modeling with these objects did not include distortions of the octahedron shapes and polydispersity of their constituent cylinder components. Adding these distortions introduces many additional parameters, increases model complexity, and increases calculation times. Additionally, the resulting model has negligible improvement in fit over the results shown in this work.

**Modeling Icosahedral DNA origami:** The icosahedral model was built using “CylinderNanoObject” in ScatterSim to generate each individual four helix bundle (4HB) at each edge of the icosahedron. Each cylinder was then rotated and translated to the positions corresponding to the edge positions of the icosahedron. All 30 cylinders were then combined through “CompositeNanoObject”. Each cylinder was set with a specified radius and height of  $r_{4HB} = 2.5$  nm,  $h_{4HB} = 21.42$  nm. The extrapolated edge length of the icosahedron was set to  $L_{\text{icosahedron}} = 27.86$  nm. These parameters are aligned with the dimensions simulated via oxDNA and the previously reported design [14]. The SLD of the 4HB is approximated as  $SLD_{\text{dsDNA}}$ .

**Modeling Crystal Lattices of DNA origami:** To model the pyrochlore lattices of DNA origami, the Octa-AuNP or icosahedron composites were used as simple objects for the construction of the pyrochlore unit cell using ScatterSim. Once the unit cell is properly organized, the scattering intensity profile can be calculated via:

$$I(q) = cZ_0(q)G(q) + P(q)(1 - \beta(q)G(q)) \quad (\text{S23})$$

where  $c$  is an overarching scaling factor,  $P(q)$  is the form factor contribution of the composite object which contains all objects in the lattice to the signal intensity, and the lattice factor is:

$$Z_0(q) = \frac{1}{q^2} \sum_{hkl}^{m_{hkl}} \left| \sum_{j=1}^N \langle F_j(q_{hkl}) \rangle_{\epsilon} e^{2\pi i(x_j h + y_j k + z_j l)} \right|^2 L(q - q_{hkl}) \quad (\text{S24})$$

where  $L(q - q_{hkl})$  is a peak shape function. Lattice structure and symmetry were taken into account through sampling over the correspondent Miller indices  $q_{hkl}$ .  $G(q)$  is the Debye-Waller factor which accounts for thermal vibrations within the lattice and is defined as:

$$G(q) = e^{-q^2 \sigma_{\text{Drms}}^2}, \quad (\text{S25})$$

where  $\sigma_{\text{Drms}}^2$  is the rms displacement of lattice elements. Finally

$$\beta(q) = \frac{|\langle F(q) \rangle_{\epsilon}|^2}{\langle |F(q)|^2 \rangle_{\epsilon}} \quad (\text{S26})$$

which comes from any polydispersity in parameter  $\epsilon$ . When thermal vibrations increase, the Debye-Waller factor,  $G(q)$ , results in reduced ordered scattering from  $Z_0(q)$  and increased diffuse scattering from unordered elements. In this work, the effect of  $\beta(q)$  was only considered for the radius of the AuNP. SAXS modeling of lattice scattering is then carried out as follows: First, given certain lattice components, we used morphological and scattering parameters as described by designs and informed by those obtained from single-particle form factor analysis. This includes parameters like size, shape, and SLD. Next, we built lattice components and calculated  $P(q)$  and  $\beta(q)$ . The lattice

components were then arranged into the unit cell of a pyrochlore lattice, and lattice constants were extracted by fitting the primary peak of the experimental data with the constructed lattice model. Finally,  $G(q)$ , peak shape, scaling factors, and background were adjusted to best match modeled scattering with experimental measurements. In this work, no direct non-linear least squares fitting of intensity profiles was conducted because convergence of such fitting is limited due to the contribution to scattering of diffuse scattering elements and the time required by the complex architecture of a collection of composite objects.

### S3 Additional experimental graphs and figures

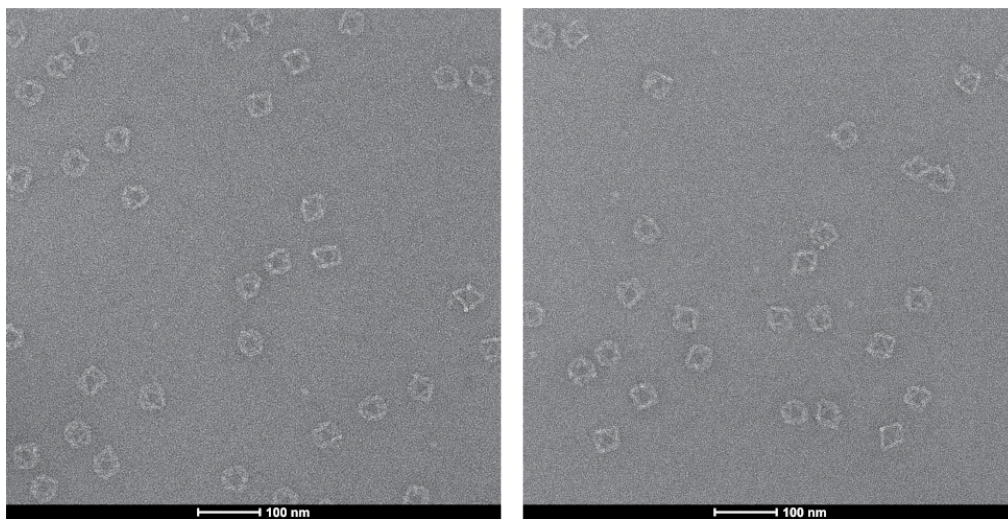


Figure S9: Negative stain TEM images of the octahedral DNA origami, purified with ultrafiltration.

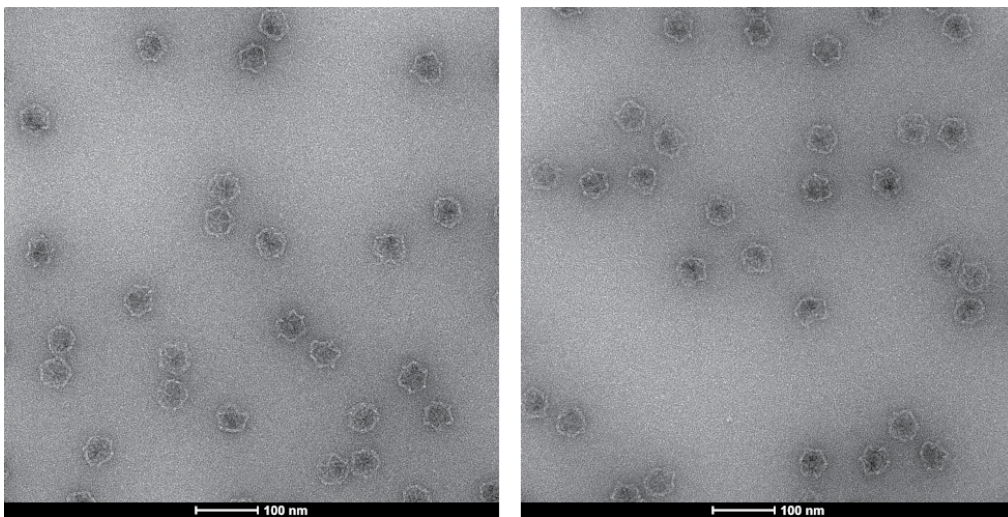


Figure S10: Negative stain TEM images of the icosahedral DNA origami, purified with rate zonal purification and therefore free from the malformed multimers that would potentially affect the lattice growth.

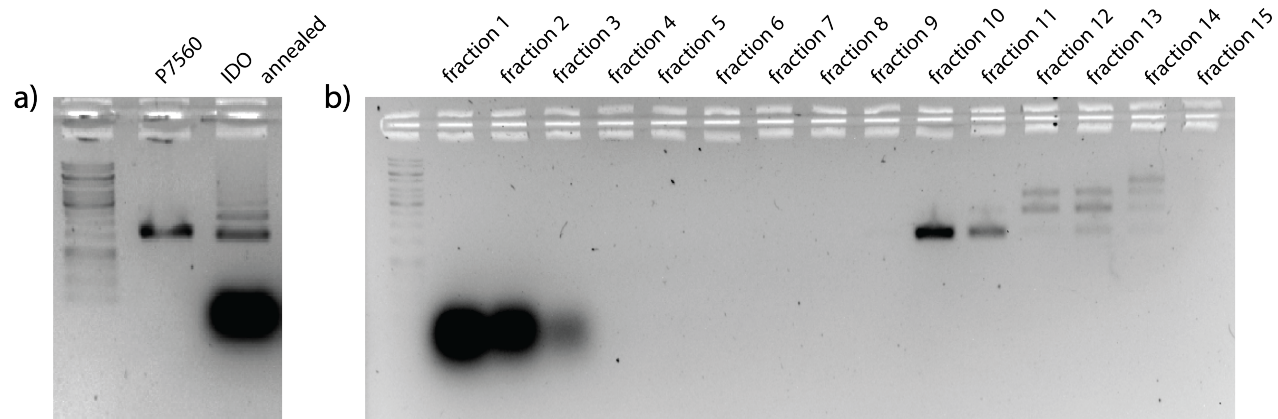


Figure S11: Agarose gel result on the synthesis and purification of IDO. a) Raw IDO from annealing shows a mixture of targeted structure with unwanted multi-mer/malformed structures above the targeted gel band. b) Purification of the annealed IDO with rate zonal centrifugation: gel result on all the fractions collected after the ultra-centrifugation. Batch to batch differences exist for the purification and in this case, only fraction 10 and 11 are collected for further assembly process.

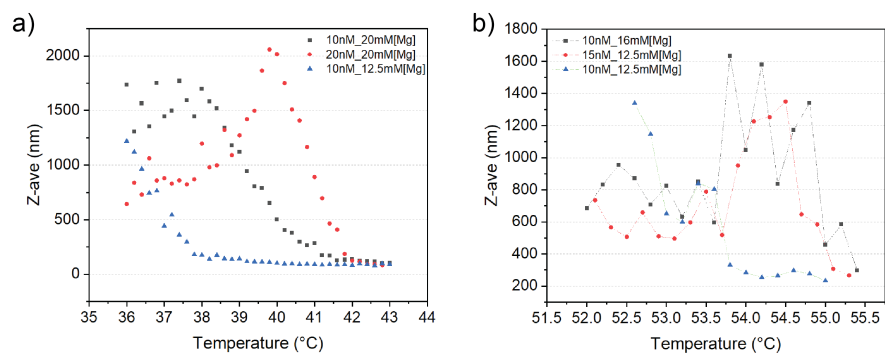


Figure S12: DLS spectrum of the self-assembly systems involved at different conditions. DLS measures the change of Z-average (intensity weighted mean hydrodynamic size of the ensemble) against temperature. In a typical experiment, the cuvette is equilibrated at the starting temperature for at least 5 min before the execution of program, which when initiated decreases the temperature at a rate of  $0.2^{\circ}\text{C}$  per 4 min. In the figure the spectra corresponding to a) icosahedron and b) octahedron building blocks are shown, with varied concentration of  $\text{Mg}^{2+}$  and the assembling unit themselves. Note in b) the data points are connected with dashed lines for better differentiation. A qualitative comparison shows that the concentration increase of either the units or  $\text{Mg}^{2+}$  increase the melting temperature and shrink the "annealing window" (the temperature starting from origamis just bind to each other to the point no further increasing of the assembly size is observed). It is noted that for the spectra of the lattice assembly with octahedron origami, the initial size is much higher than the one shown in panel a and also the expected monomer size. We reason that it is because of the strong binding strength of the handle to connect octahedron units, as the melting temperature of the lattice is close to  $54^{\circ}\text{C}$  and incubation of the system at  $55^{\circ}\text{C}$  for limited time does not dissociate all the connected units into dispersed monomers. In the meantime, the starting temperature can only be set at  $55^{\circ}\text{C}$  or lower as higher temperature will dissolve the origami itself. While we elongated the incubation time of the system at  $55^{\circ}\text{C}$  for up to 2 hours, we suspect still not all the building blocks will stay mono-dispersed for the assembly and may contribute to the final inferior quality of the pyrochlore lattice assembled with the octahedron origami.



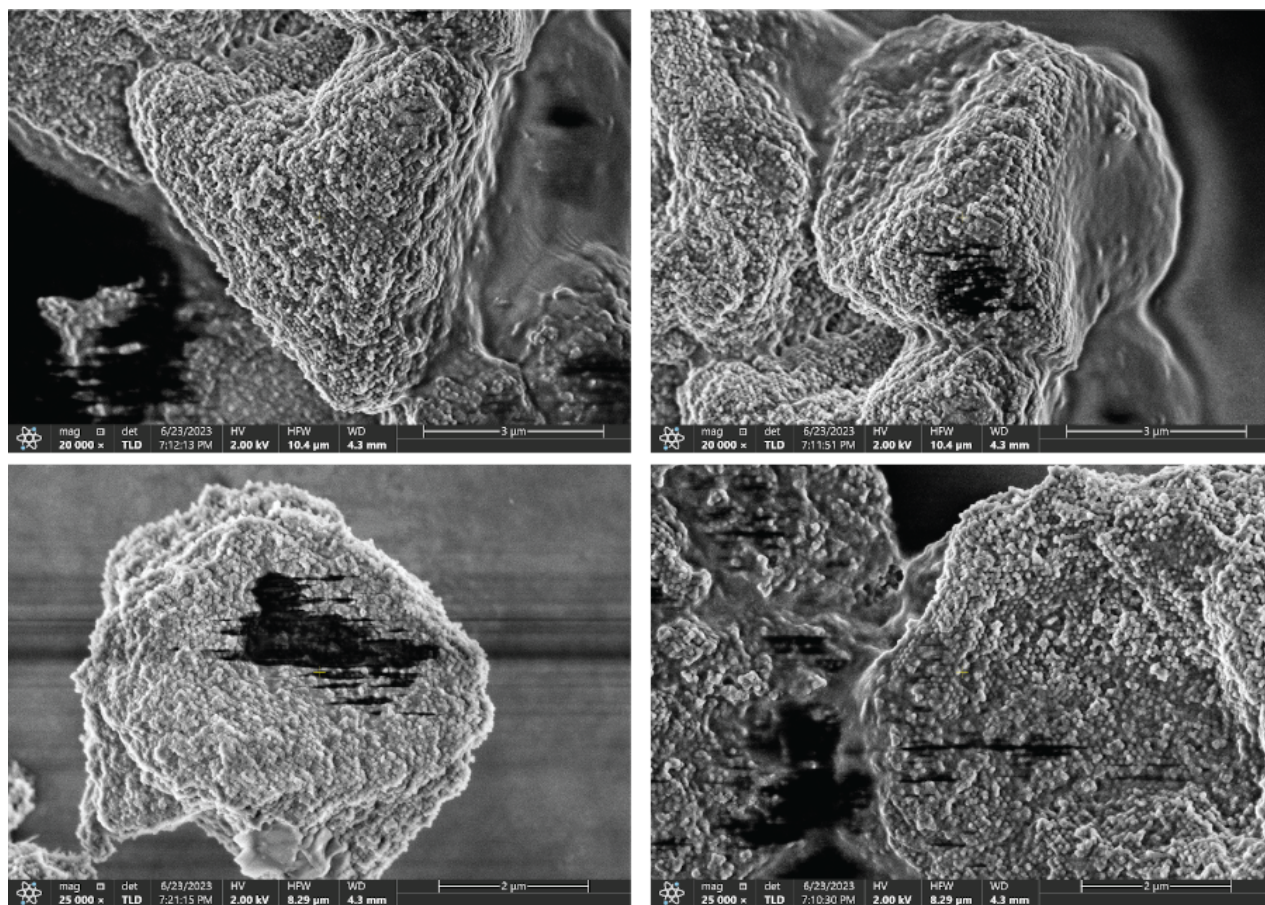


Figure S13: Typical examples showing the distorted/collapsed lattice imaged with SEM, with suboptimal silica coating being the major reason.

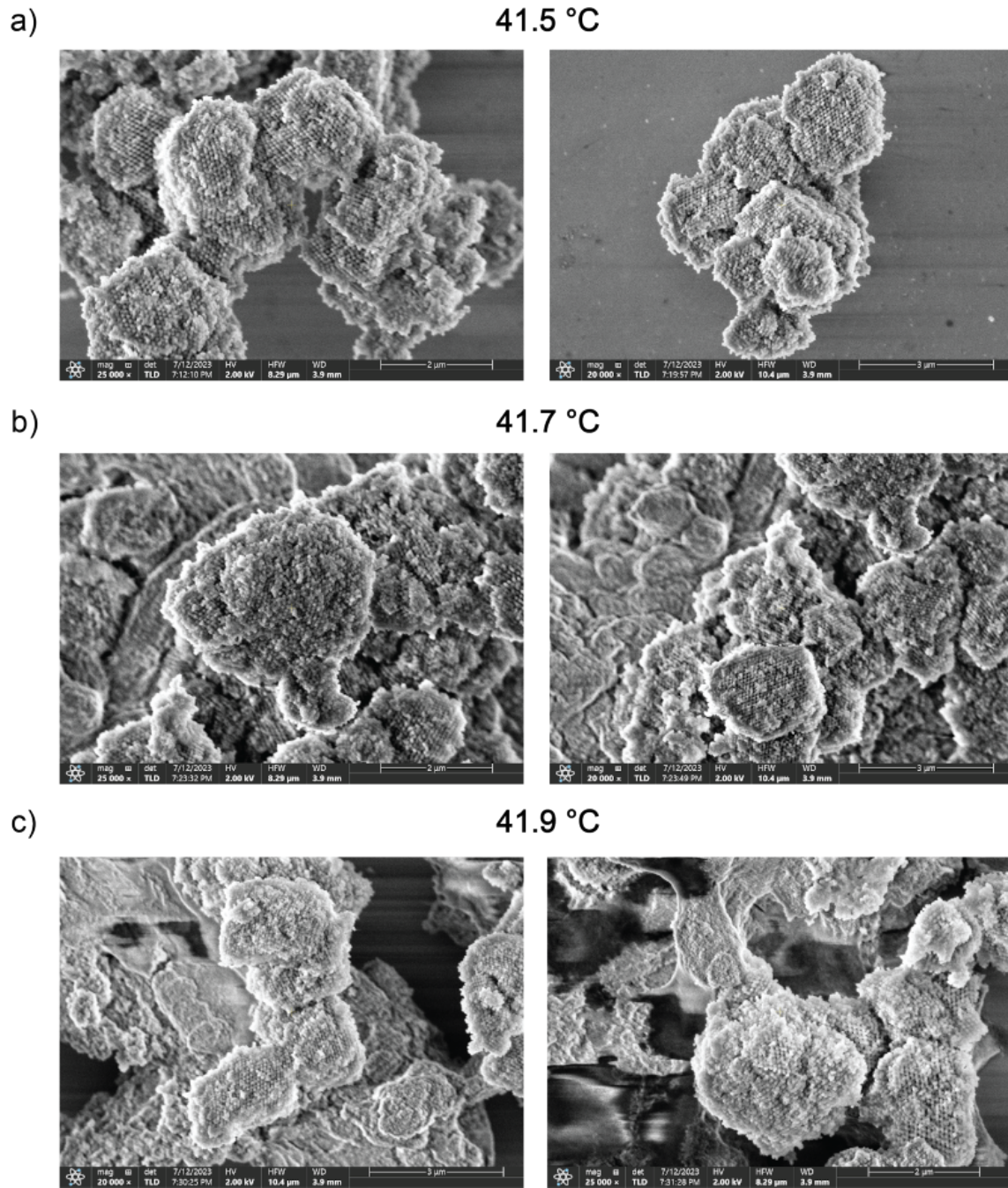


Figure S14: Isothermal annealing of the pyrochlore lattice with the icosahedral building blocks. The mixed samples are incubated at a higher temperature for the dissociation of the interactions and then allowed to be incubated at the specified temperature for a week. The temperature series in this figure is 41.5 °C, 41.7 °C and 41.9 °C.

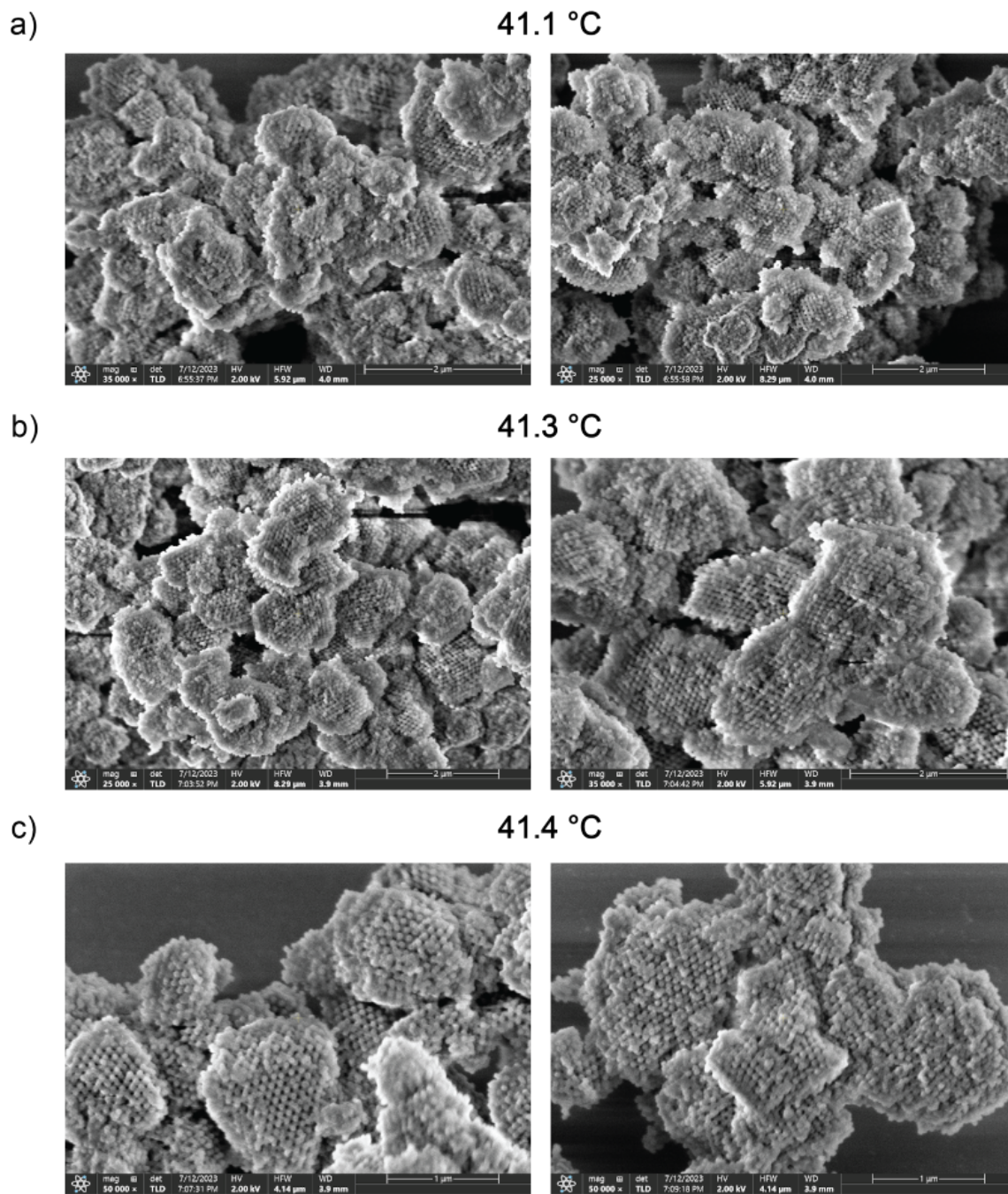


Figure S15: Isothermal annealing of the pyrochlore lattice with the icosahedral building blocks. The temperature series in this figure is 41.1 °C, 41.3 °C and 41.4 °C.

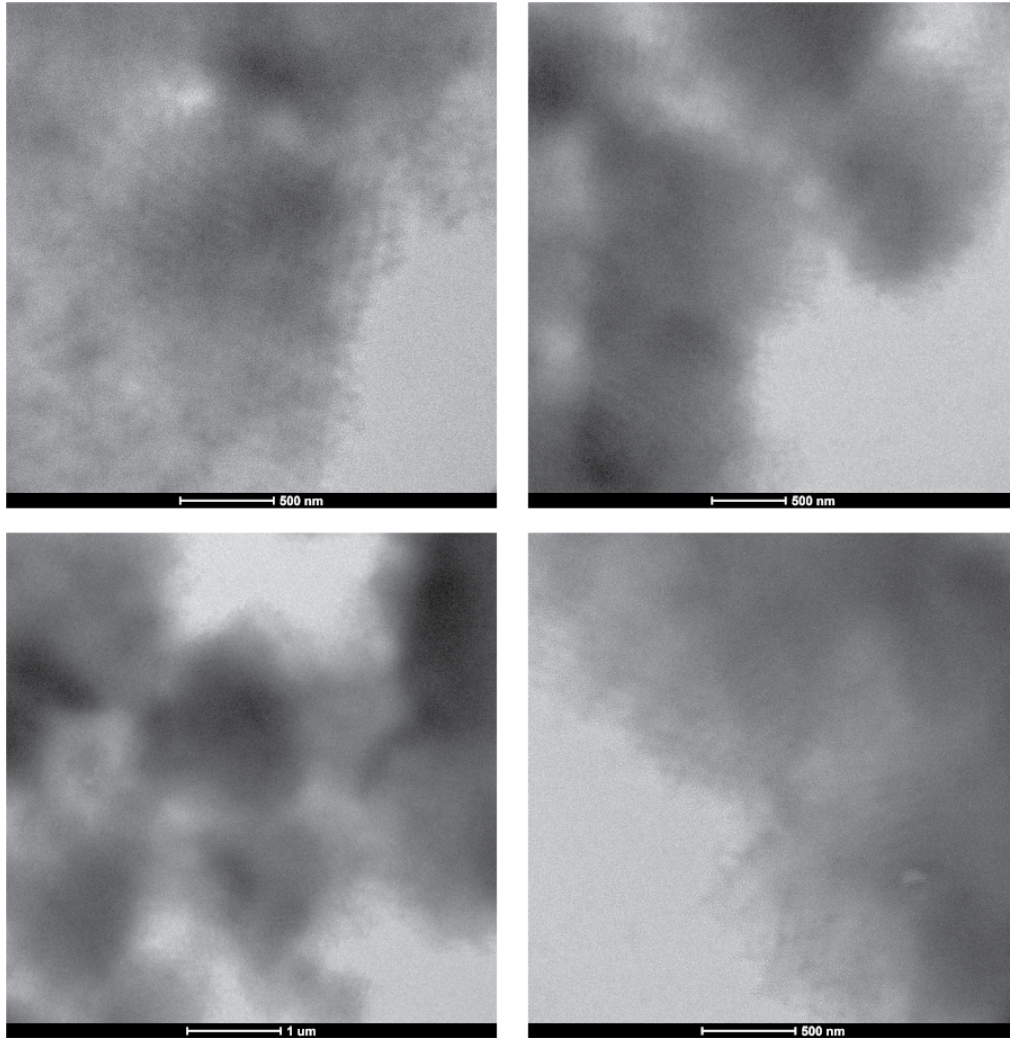


Figure S16: TEM imaging the silicated pyrochlore lattice assembled with icosahedron DNA origami. Despite the lack of negative staining, due to the elevated sample height and silica embedding, it is straightforward to identify and therefore examine the assembled lattices in low magnification mode. On the other hand, it becomes nearly impossible for the electron beam to penetrate through the superlattice, except for the small grains or the peripheral regions with reduced sample height. The images shown are taken based on such principle for the purpose of examining the result of the programmed assembly.

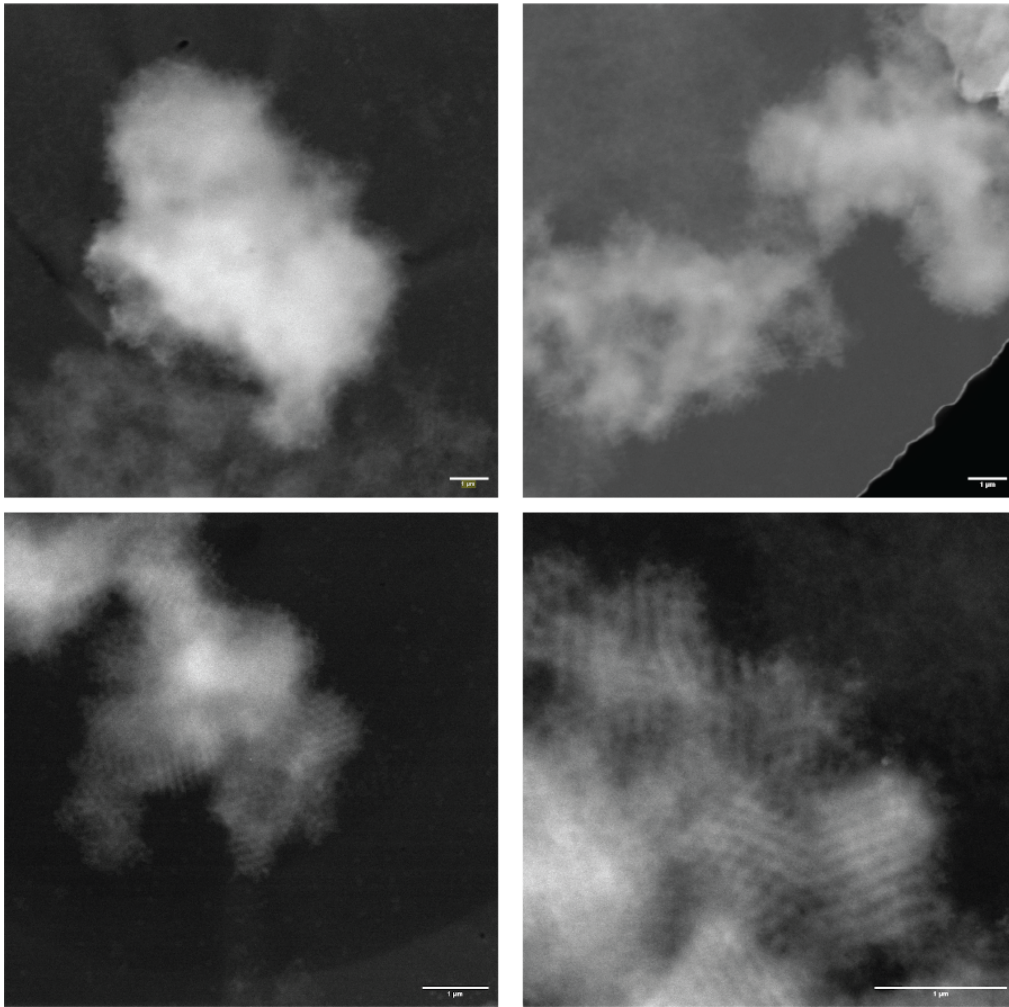


Figure S17: STEM imaging the silicated pyrochlore lattice assembled with icosahedron DNA origami in HAADF mode. While at a higher acceleration voltage and better contrast with STEM-HAADF, similar issues as mentioned with TEM imaging exist. Images are taken on a sample assembled in a less optimal condition in this case, in which small grains are more abundant to be imaged and examined.

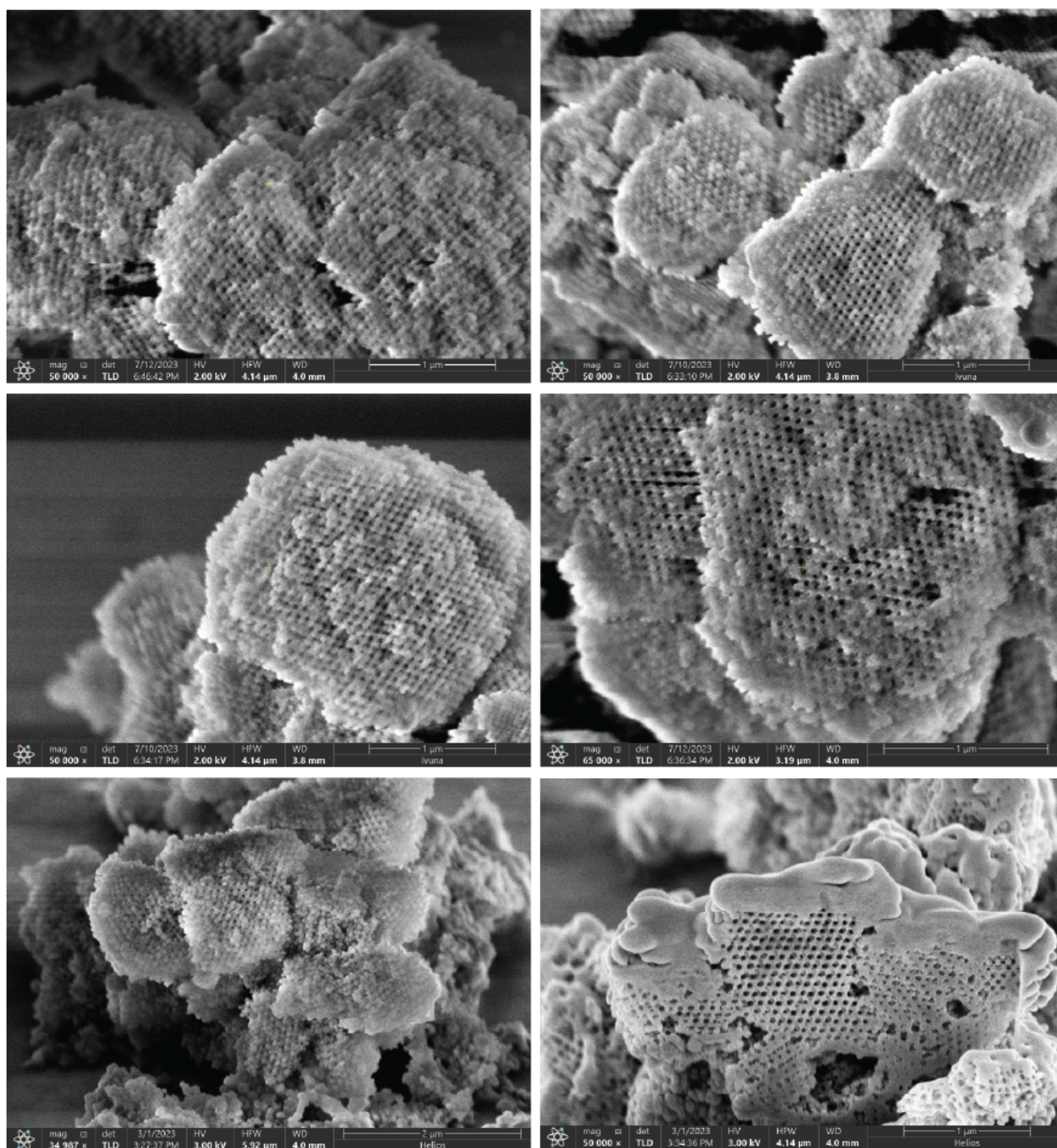


Figure S18: Additional figures for the ODO pyrochlore lattices with zoomed-in and out views and cross-sections of the lattices generated by FIB. The blur of the edges and boundary are likely caused by the charging effect and possibly slightly overcoating of the silica.

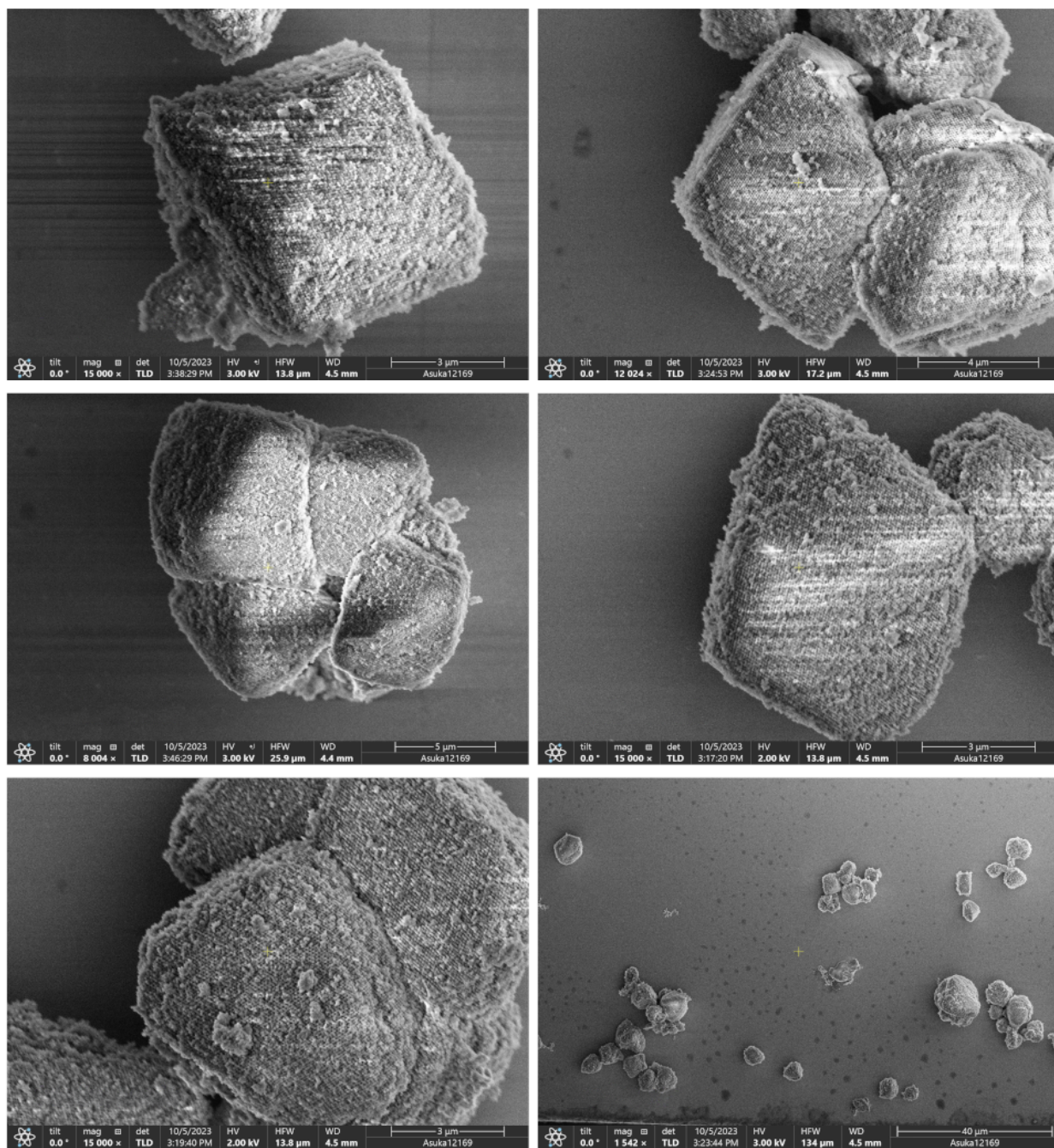


Figure S19: Additional figures for the IDO pyrochlore lattices annealed with thermocycler and embedded in silica with zoomed-in views and zoomed-out view (bottom right). Charging effect is observed as no metal was sputtered onto the surface.

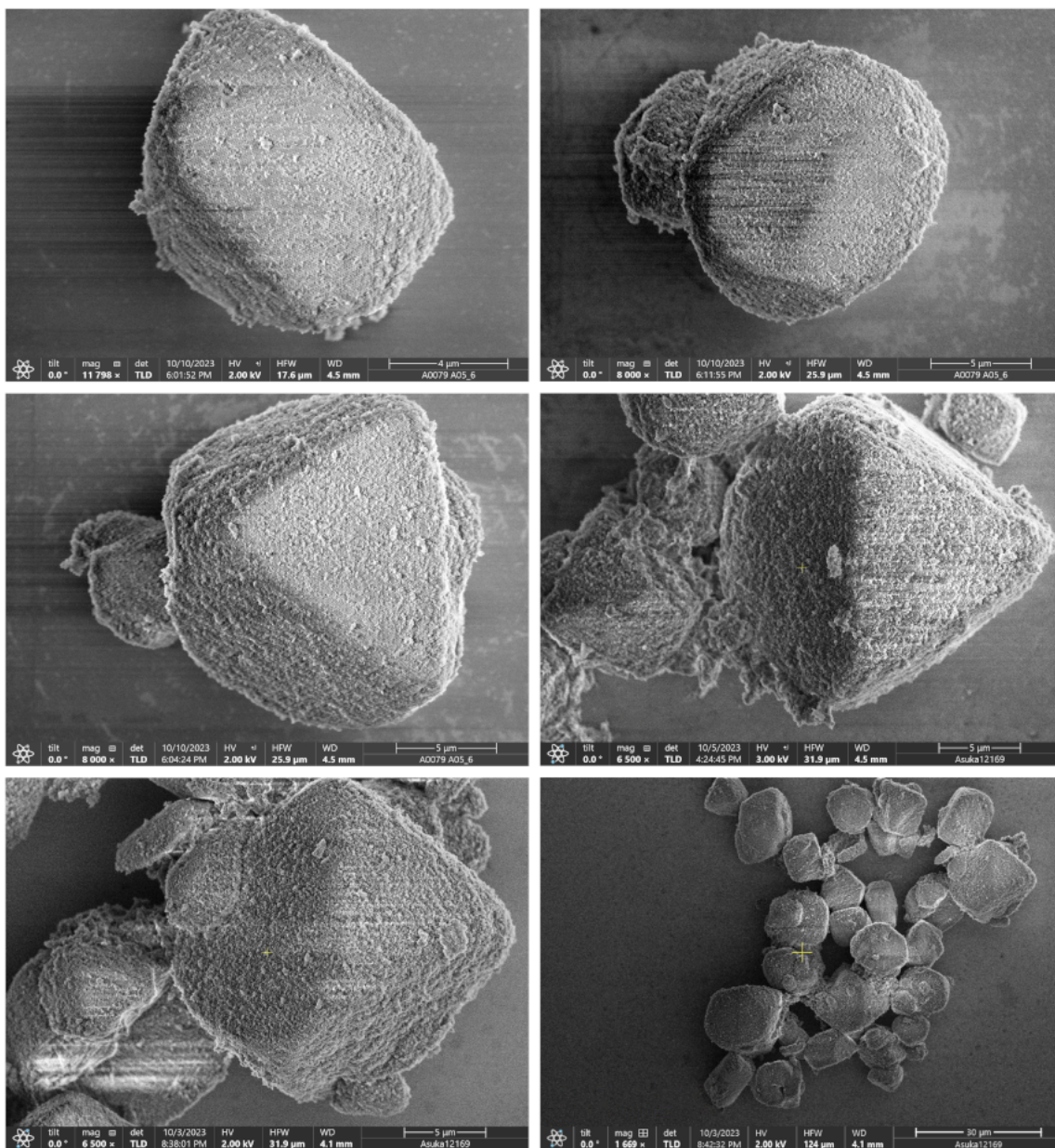


Figure S20: Additional figures for the IDO pyrochlore lattices annealed within a thermal incubator while actively mixed and further embedded in silica with zoomed-in views and zoomed-out view (bottom right). Charging effect is observed as no metal was sputtered onto the surface.



## S4 DNA Sequences

### S4.1 Sequence design

In order to find a set of 24 sequences (12 complementary pairs) for the design consisting of 4 particle species, each with 6 unique patches, we have first enumerated all possible duplex sequences of length 7. We have then selected a subset which had nearly the same binding-free energy according to the SantaLucia nearest-neighbor model [22]. We removed any sequences that would be predicted to form a stable secondary structure. We then considered all possible pairs of the overhang sequences (which were not complementary to each other) and used NUPACK [15] to find the lowest free energy of binding that these non-complementary sequences can form. We have then selected a subset of 12 pairs of sequences so that the lowest free-energy of a duplex formed between two non-complementary sequences was as high as possible across the pairs considered. The resulting handle sequences have been incorporated into a staple strand with poly-T overhangs. All these sequences have been placed at the 3' end of the staple strands. The sequences are listed as Handles" in the following tables, that list all the sequences that compose each DNA origami particle. The staple strands used in all the DNA origami species are the same except for the staples sequences that include the handles.

### S4.2 Icosahedral DNA origami

#### S4.2.1 Staple sequences

core_strand_5	ATTAAACCTTTTTATTAGCCCAATAGGAACCC
core_strand_10	GAAGTGTTCCTGTCCAGATAAGTCCTGAACAA
core_strand_17	ATCTAAAGTTTTCTGTGCGAGCACGTATAACGT
core_strand_24	GAAAGCCGGAAAGGAGAAGTACGGTGTCTGGA
core_strand_31	AGCCCCAATTGTAAACACTACGTGAACCATCA
core_strand_39	AGGCGGATCCCGGAATGTAGCGACAGAATCAA
core_strand_50	TGACAACAGGATTAGGCTCAGCAGCGAAAGAC
core_strand_56	AAGCGAACTAGAGAGTAAAAAAAAGGCTCCAA
core_strand_63	ATACGTAAGAGGCCAAACTTTACCCTGACTATT
core_strand_70	GCATTAAGTAGACTGGTACCAAAAACATTATG
core_strand_76	ATAACCTGAAAAGGTGTCAGGTCATTGCCTGA
core_strand_83	ATCAAAAATCCCTCAGATGGTAATAAGTTTTAA
core_strand_93	CAGACCAGTGATATTCTGCTCATTTCAGTGAAT
core_strand_98	GCAACACTAACCAAAACCGCGACCTGCTCCAT
core_strand_105	CCTTATGCGAGCGGAACATTATTACAGGTAGA
core_strand_112	GTTGTAAACGTTATTATAAGTGTCCCTTAGTGC
core_strand_118	ACTCCAGCGGTGAGAAGCGATCGGTGCGGGCC
core_strand_126	AGAGATAAGAACCACCAAGAAAAGTAAGCAGA
core_strand_136	ACAATAACAAAGTCAGAAGATGATGAAACAAA
core_strand_142	ACAACATAAAGGATTTACAAAATTATTTGCACG
core_strand_149	GAGTGAATAATTTTCCGAACCTCAAATATCAA

core_strand_156	CGCATTTCAACCACCACTCGATAAAGACGGAG
core_strand_162	CCGACAGTGGGCACGAGACCGTAATGGGATAG
core_strand_169	ATTACGCAAAGGTGGCTTATTTATCCCAATCC
core_strand_179	TTTCATCTTCAAGATTTTACTAGAAAAAGCCT
core_strand_184	GAAAGCGTGGCTATTATCCGGCTTAGGTTGGG
core_strand_191	AACAACGCCAGTAATCAATCGTCTGAAATGG
core_strand_198	TTTCTTTTCTGAGTAGCCCCAGCAGGCGAAA
core_strand_204	TTAAATTTAACGCCATACTGCCCGCTTTCCAG
core_strand_212	CCCAATAGATTCTAAGTCAACCGATTGAGGGA
core_strand_3	TGTAGCATCGCCACCCTAACACTGCCGCCACCGAGAACAA
core_strand_11	AATAATCGGACGACAAATATCCAGTAATTCTCCACCGAG
core_strand_18	AAAGGGATACCACACCCGTTAGAACACGCTGCGACGTTAG
core_strand_25	GATTTAGTAGAGCTTATCCATATATTTTTGCGAGGAAGGG
core_strand_34	GGAACCCTAAGAACGTAAGTTTTTCAAGAGTCTAAGCAAA
core_strand_43	GGTCATAGCATTAGCATTAGCGTCCAGTAGCGTTGATAT
core_strand_48	AAGACTTTTATTCGGTAACGAGGGAGAGGCTGAGACTCCT
core_strand_57	ATTTCTTAAGAAAGGATTTAATTGTCAGCGGATCCAACAG
core_strand_64	CCGAAAGACTCAAATGAAGCAAAGTATTCATTCCAACCTA
core_strand_71	TAAAAATTCAAAGAATATACTTTTCAGAGGGGGTAATAGT
core_strand_78	AGCATGTCAGCTGATAAGCAAACAGATATTCATTGGGGC
core_strand_86	CCCCTGCCTGAATTTAGTGCCTTGTGGAAAGCACCACCGG
core_strand_91	TTGAGATGCAAGAGTACCCTGACGTGAGGCAGGTCAGACG
core_strand_99	GAACTGACCGCGAAACGCCGGAACCAGCGATTACCAGACG
core_strand_106	GATACATAACCAGTCAGTCAGTTGAGCGGAACAAAGAAACC
core_strand_113	CTAATCTACAGGAGAACAACCTTACTCGTATTAATCCTT
core_strand_121	GATTAAGTGCCGAAAATTACGCCAATGTGTAGGTAAAGA
core_strand_129	ACGGAATAATAATAAGCAAAGTTACCACCACCCTCAGAGC
core_strand_134	ACCTTTTTCCAAGTTAAAACAAAAGAGAATTAAGTGAACA
core_strand_143	GATGAATAATCCTGATAAATAAAGGCAATTCAATAGATAA
core_strand_150	AATTGAGGAACAGTGCTCAATATCTATTAACAATCGTCCG
core_strand_157	TTCTGTGGACCTCCTGGTACCGACATCGCCATTAAAAAT
core_strand_164	TTGAGGGGTAAATGTGGTGTAGACCAGCTTTTAAGCAAC
core_strand_172	CCTTTACACGCTAACGAACGATTTTCTGAATAGAAAATA
core_strand_177	ACGCTCAAAATACCGATCATATGCTGCGGGAGGTTTTGAA
core_strand_185	AAGAACGCAAGAGTCACTATATGTAGATTAAGGACAATAT
core_strand_192	GGGACATTACCGCCAGCATTGGCATATCCAGACAGAGGCA

core_strand_199	CAAAAGAAATTGCCCTTGATGGTGTTFGATTAGTAATAAC
core_strand_207	CGGGGAGATGTAAAGCCCTGTCGTAGCCGGAATTTTTTAA
core_strand_215	ACCGTCACCACAATCAAAATATTGAATAAGTTAGAAGGCT
core_strand_6	ATGTACCGTCAGAACCCACTCATCCTCAGAACTCCACAGAGTTTAGTAAGTTTCGT
core_strand_12	GAAAAATATAAAACAACCAGTGAGGGTCCAGACGCTGTCTTAAGGTAATCCTAATT
core_strand_19	GCTTTCCTCGCCGCGCTCTTTCACGCGTAACCTTTAGACAGTAGCGGTTCCAGAGCG
core_strand_26	AGTTTCATATTGCTGAGGCGAGAAGATGGCTTTTGACCATAGAGGTCAACAGTTGA
core_strand_35	CCCAAATCGGACTCCAAGATTGTACACTATTAAGGGGAGTTTGGAAATGGGGTCCG
core_strand_42	GTTTGCCTAGGCCGGATCGAGAGGACCATTACCCCCCTTACAAAATCAAGACTGTA
core_strand_51	AGCATCGGCGCTGAGGCCACGCATAACCGATATTCATGAGAAGTATTATAGCAACG
core_strand_58	AAGGAGCCACAACATAAAAGCAAACGTGAGAATAACAGCTTCAACAGTTTATCGGTT
core_strand_65	ATAGTCAGCTTTAAACCGAAGGCAGAATCCCCCTTCAAATGTCATAAACGGATTGC
core_strand_72	ACCCTGTATAGCAAAAATCATAACAGGCAAGGTTTAGAACAGTTTTCGCGGGGAGA
core_strand_79	GAGTCTGGAATTAATGTATTTTCAACCGTCTAATCATATATCAATATAGAGAATC
core_strand_85	CGGGGTCACCGTTCCACCAGAGCCGCGAGTCTCTATTTTCGGAGCCAGAAAGTAACAG
core_strand_94	AAGGCTTGATCTTGACGCTGGCTGACCTTCATGTTAATTCAGGAGGTAGAAACAC
core_strand_100	GTTACTTAAAAGTACACCTCGTTTATACCAAGCAACTTTGTTGACCCCGAGGCGCA
core_strand_107	AAGATTCAGACGTTGGGAACGGCTCATTATAACGCCAAAATCATTTTGATTTAGG
core_strand_114	TGAATTGTGCCAGGGTCAGTGCCAAGCTTCTTTTACGCTTTCGACAATGACAATG
core_strand_122	TCTTCGCTCCAGGCAACGGCACCGCTTCTGGTTGGGTAACGCCTGAGTAGCTGGCG
core_strand_128	TAGCCGAAAGCAAGAAAATTGAGTTAAGCCACCCAAAAGCCTCAGAGCCAGAAGG
core_strand_137	CATCAAGACAAAATCGCTGATTGCTTTGAATATAATGGAATTAGACGGTTAATTAC
core_strand_144	TAAACAGTGTTTGGAAAGCCGTCATCAATATATACAGTAAAGATGATGAAAATTGCG
core_strand_151	ACCCTCAACACGCTGATTCTGTAACCGCTGCAAGGTTATGCGGTCAGTGGTCAGT
core_strand_158	GATCCCCGGGTTGGTGCATTTCTCCGAACTCTTGAAATTGCCCTAAAAGCTCGAAT
core_strand_165	GTCACGTTGAGCGAGTGCCATCTGCATCAACAACGACGACTCCTGTAGTGGGCGCA
core_strand_171	AAATAAGAAGCGTCTTGCAAACGTCTTACCAAGAGAGAATCAATTTTATTTGTTA
core_strand_180	GTTTAGTACCGTGTGAAAATTTAATGGTTTGACAGTAGGGTCCCGACTGTTATACA
core_strand_186	TTATATAAATAGTGAAGTGGCACAACGCTGAGGAGAAAACGATAGCTTAAATGCTG
core_strand_193	ATTATTTACCATTGCAAATTTAGGACAATATTCTGGCCAAGCTGGTAAGATTCACC
core_strand_200	ATCCTGTTTCACCGCCAGACGGGCAACAGCTGTAGCCCGAAATACTTCGTTCCGAA
core_strand_208	TCGGGAAACTGGGGTGTGAGCTCAGCATAAAGGGCGTTTAAACATACGGCCAGCTG
core_strand_214	GGGAAGGTATAGAAAATCAGATATTTATTTTGTGCGACTTGACACCACGGACGGAAT
core_strand_4	GCAAGCCGAAGTACCGGCCACCCTCAGAGCCA
core_strand_13	TAAAAGAGTTTATAAATATGTTTCAGCTAATGCA
core_strand_20	TAAATGAATTTTGTGCTTAATGCGCCGCTACA

core_strand_27	AAGAAAGCGCGAACGTATATAATGCTGTAGCT
core_strand_36	TATTTAAAAAACAGGAACGTCAAAGGGCGAAA
core_strand_45	AAGTATAGAAGTGCCGAACGTCAACCAATGAAA
core_strand_49	CAAGAGAAACCATCGCCTTGCAGGGAGTTAAA
core_strand_59	GTCAGGATCAGACCGGAGGAATTGCGAATAAT
core_strand_66	AAACGAAATGCCACTAAGTTCAGAAAACGAGA
core_strand_73	AAAATGTTATCCAATATTAAGCAATAAAGCCT
core_strand_80	GCGAGCTGTTTAGCTACCGGAGAGGGTAGCTA
core_strand_88	AACCGCCTCACCGGAAGTAAGCGTCATACATG
core_strand_92	ATTGGCCTGCGCATAGAAGAACCGGATATTCA
core_strand_101	ACGATAAAATCATAACACGGAGATTTGTATCA
core_strand_108	ACCAGAAGGATTTTAAGAAGAAAAATCTACGT
core_strand_115	TGCCCCGAAACGACGGCGGATGTTCTTCTAAGT
core_strand_123	TTCAAAGCAGCTTTCAGCGCCATTCGCCATT
core_strand_131	CGCCACCACCACAAGACAATGAAATAGCAAT
core_strand_135	CCCTGAACGGATTCGCCGCAGAGGCGAATTAT
core_strand_145	TACATTTGTAGATTAGTTATACTTCTGAATAA
core_strand_152	TATTAATTAACCTTGCGAGCCAGCAGCAAATG
core_strand_159	ACCGAACGACATAAATTAATGAGTAAACAGGG
core_strand_166	TCGTCCGGTGC GGCCCTAACAAACCCGTCGGATT
core_strand_174	CATACATAGTATGTTATCCAGAGCCTAATTTG
core_strand_178	GCCTTAAATCTGACCTTAAATAAGGCGTAAA
core_strand_187	TTTTGAATAAGAATACTTTATCAAAATCATAG
core_strand_194	TTTTCGAGCAACATGTACAGGAAAAACGCTCA
core_strand_201	ATCACTTGCACCAGTGTGGCCCTGAGAGAGTT
core_strand_209	CCAATAGGTTGTTAAACCTAATGAGTGAGCTA
core_strand_217	TATCCGGTCAAGCAAATTCATATGGTTTACCA
corner_strand_1	TATAATTTTTAGTACCGACAATCCTTATCATTTTTTTCCAAGAACGGGT
corner_strand_2	GCGCCAAAGACATTCAGGGATAGCATTTCATCG
corner_strand_7	GGGCGCGTACTATACTACAACGCC
corner_strand_8	CCACCCTCATTTTAGAAACCAATC
corner_strand_14	ATCGGCAAAATTTTATCAACAATATCACGCA
corner_strand_15	GAACGCGCCTGTTGGAGGCCGATT
corner_strand_16	TCACTTTTTTGTACTCAGGAGCAGCCCTCATATTTTTGTTAGCGTAACG
corner_strand_22	TTTTTGAGAGATTGCGAACGAGTA
corner_strand_23	TTCCACCCCGATTTATTTTTGAGCTTGACGGG

corner_strand_30	AGACATTTTTGTCAAATCACCGTACCCCGTTTTTTTTGATAATCAGAAA
corner_strand_33	CAACATGTTTTATAGCACTAAATC
corner_strand_37	ACTCACATTAATTGGGCGATGGCCCGTTAATA
corner_strand_38	GGGTTTTTTTTTGCTCAGTACC
corner_strand_41	AAAAGTTTTTAAACGCAAAGAGCCATTTGGGATTTTTATTAGA
corner_strand_44	GCTTTTGATGATTTTCGGCATT TTC
corner_strand_47	CCATCGATAGCATGGGATCGTCACCATTAGCG
corner_strand_52	AATAATTTTTATCCTCATTA AACCTATTATTTTTTTCTGAAA
corner_strand_53	ATGACCATAAATTTTTGAGGACTA
corner_strand_54	GGCCGCTTTTGCTTTTCGAGGTGA
corner_strand_55	CCAATTTTTTACTGCGGAATCATCGGTTTTATTTTTATTTCGAGCTTCA
corner_strand_61	AATTTTTTCACGTTAAGAGGAAGC
corner_strand_62	CATGAGAAGTTTCCATTTTTTAAACGGGTAAA
corner_strand_67	GACGGTCAATCTCAAAAATCAGGTAGAATAC
corner_strand_68	AAAGGGGATGTCAACGCAAGGA
corner_strand_69	TTCTATTTTTCTAATAGTAGTA
corner_strand_77	AACCGTCTATCATATCGTAAACT
corner_strand_81	CAGAGCATAAAGTCTACAAAGGCTAGCATCAA
corner_strand_82	GCCAGTTAGCGTTTGCTTTTTCATCTTTTCATA
corner_strand_84	AAACCGAGGAATACAGGAGTGTACGCCGCCA
corner_strand_87	GCTACAGAGGCTACAGTTAATGC
corner_strand_89	ACTAATTTTTAACACTCATCTAAAGAGGACAGTTTTTATGAACGGTGTA
corner_strand_90	TGCCCCGTATAATACGTAACAAAGCACAAACA
corner_strand_95	TAATAAAACGAATGTAAATTGGGC
corner_strand_96	TTACCCAAATCATATAAGGGAACC
corner_strand_97	AAGTTTTTTTTGAGTAACATTAGGAATTACGATTTTTGGCATAGTAAGA
corner_strand_102	AGCCTTTATTTTTGTGTCGAAATTAGCGAG
corner_strand_103	TCGCCTGATAAATCAACTAATGCA
corner_strand_104	CCGCCTTTTTGCCAGCATTGATCAACTTTAATTTTTTCATTGTGAATTA
corner_strand_110	CTCCGTGGGAACCTAACCCCGCTT
corner_strand_111	GCAATGCCAGGGTTTTTTTTTCCCAGTCACGAC
corner_strand_116	AATACCACATTTATGCGCACGACTATTTTAA
corner_strand_117	AATCTTTTTGCGTCTGGCCTAGTATCGGCCTTTTTTCAGGAAGATCGC
corner_strand_119	AGGCTTTTTTTTTGCAAAGACCTCATATATTTTTTTTTAAAT
corner_strand_120	GGTTGTGAATTCTTGCTGCAAGGC
corner_strand_124	GATGAACGGTATCTGTTGGGAAGGAGGCCGG

corner_strand_125	TTGAGTTTTTCGCTAATATCAG
corner_strand_130	CCAGTTACAAAATACGCAATAATA
corner_strand_133	AGCTATCTTACCTCCTGAGCAAAAAGAGGGTAA
corner_strand_139	AAAAATCTAAAGTTCATTTGAATT
corner_strand_140	TCATTTCAATTATGTTTAAACGTCA
corner_strand_141	ATAAATTTTTACAGAGGTGAGCTAAAATATCTTTTTTTTTAGGAGCACTA
corner_strand_147	TGGAAGGGTTAGTCAGTTGAAAGG
corner_strand_148	GCGCAACAGTACATAATTTTTATCAATATATGT
corner_strand_154	CATTAATGAATTGTCATAGCTGT
corner_strand_155	GGCCTTTTTTTGAATCGGCTGA
corner_strand_163	CAGGCTGCGCAATCATCTGCCAGT
corner_strand_167	CTTAAGCTACGTAAACGGCGGATTATATAGG
corner_strand_168	CCCTCTTTTTAGAACCGCCACAACCTGGCATGATTTTTTTAAGACTCCTT
corner_strand_170	TATTCATTAAATTAACAGCCATAAACATAT
corner_strand_173	ATTTAACAATTTGAAAATAGCAG
corner_strand_176	ACGTCAAAAATCCGGAATCATAAAGTTGCT
corner_strand_181	TGAAATACCTATGTATAAAGCCA
corner_strand_182	TAAGAATAAACATATCGCAAGACA
corner_strand_183	TCAAATTTTTCTATCGGCCTTCAGAGATAGAATTTTTCCCTTCTGACCT
corner_strand_188	TCGTAATCATGTACCTTTTTAACCGTCTTTA
corner_strand_189	GTCTGAGAGACTTCAGTAATAAAA
corner_strand_190	GGCGTTTTTTTTAGCGAACCTTAATTGAGATTTTATCGCCATATTT
corner_strand_195	TACGAGCATGTTTATTTGACGCTAAGAGAA
corner_strand_196	AGGTGCCGTAATCCCTTATAAAT
corner_strand_197	CACACGCGTATTGGGCTTTTTGCCAGGGTGGTT
corner_strand_202	AGTCACACGACTCCACGCTGGTTTGAAGAAC
corner_strand_203	TTTTGTTTTTTTAAAATTCGCA
corner_strand_205	ATGCGTTTTTCGAACTGATAGTTATCCGCTCATTTTTCAATTC
corner_strand_206	GCAGCAAGCGGTTTCGGCCAACGCG
corner_strand_210	TCGTAACCGTGTTGCGTTGCGCTCCAAAAAT
corner_strand_211	TAGGATTTTTATCATTACCGCG
corner_strand_213	AATTCCTACCATAAAGGGCGACATAACGCGA
corner_strand_216	GCGCGTTTTTCATGGTGAATTATC

Table S4: Staple sequence for the icosahedral DNA origami

### S4.2.2 Handle sequences

Handle_A0.1	TTCCCAATTCTTTTGAAAATCTCCACCTTTATTTTTTTTTTTTTTTTGTGTGTC
Handle_A0.2	ATTGCTTTTTTCCTTTTGATATAGATACATTTTTTTTCGCAAATGGTCATTTTTTT TTTTTTTTTGTGTGTC
Handle_A0.3	ATCAAAAAGATTCTAAATCGGTTGATAGCGTTTTTTTTTTTTTTTTTGTGTGTC
Handle_A1.1	TTTGCTTTTTTAAACAACCTTTGATACCGATAGTTTTTTTGCGCCGACAATTTTTTT TTTTTTTTTACATCGC
Handle_A1.2	TATCAGCTTGCTTGGTTGCTTTGAATGGGATTTTTTTTTTTTTTTTTTACATCGC
Handle_A1.3	CACCAGTACAATGCACCGTAATCAAGGTGATTTTTTTTTTTTTTTTTTACATCGC
Handle_A2.1	TAGGGTTTTTCGCTGGCAAGTGGAACGGTACGTTTTTCCAGAATCCTGATTTTTTT TTTTTTTTTTATGTGCGC
Handle_A2.2	GGAGCTAAACATAATATGCAACTACGGGCGCTTTTTTTTTTTTTTTTTATGTGCGC
Handle_A2.3	AATTATTTTTACCGTTGTAGCGATAGGGTTGATTTTTTGTGTTGTTTTTTTTTTTTTT TTTATGTGCGC
Handle_A3.1	ATTTTTTTTTGCACCCAGCTAAACATAAAAACTTTTTAGGGAATTTTTTTTTTTTTTT TTCTTTCGGT
Handle_A3.2	ATGCAAATCCATCATCACCTTGCTCTTAGAATTTTTTTTTTTTTTTCTTTCGGT
Handle_A3.3	TCCTTTTTTTGAAAACATAGCTTTTTCAAATATTTTTATTTTAGTTAATTTTTTTT TTTTTTTTCTTTCGGT
Handle_A4.1	TCCCGCCAAAATAACCTACCATATGAAGTATTTTTTTTTTTTTTTTTTGGAGCTA
Handle_A4.2	TGGCAAATCAATGGTGCTTGTTACGCAGAAGTTTTTTTTTTTTTTTTTGGAGCTA
Handle_A4.3	TAGACTTTTTTTTACAAACAACGCCCTGGAGTTTTTTGACTCTATGATATTTTTTTT TTTTTTTTTGGAGCTA
Handle_A5.1	TAGATTTTCAGTCTAACGGAACAATTATCATTTTTTTTTTTTTTTTTTAGAGGCA
Handle_A5.2	CAGAACGAGTATGAAGCCCTTTTTACCAGAGTTTTTTTTTTTTTTTTTAGAGGCA
Handle_A5.3	CATATTTTTTTCCTGATTATCCAGTACCTTTTTTTTTTACATCGGGAGAATTTTTTT TTTTTTTTTAGAGGCA
Handle_B0.1	TTCCCAATTCTTTTGAAAATCTCCACCTTTATTTTTTTTTTTTTTTTTTAGCTTGC
Handle_B0.2	ATTGCTTTTTTCCTTTTGATATAGATACATTTTTTTTCGCAAATGGTCATTTTTTT TTTTTTTTTAGCTTGC
Handle_B0.3	ATCAAAAAGATTCTAAATCGGTTGATAGCGTTTTTTTTTTTTTTTTTAGCTTGC
Handle_B1.1	TTTGCTTTTTTAAACAACCTTTGATACCGATAGTTTTTTTGCGCCGACAATTTTTTT TTTTTTTTTGCATGTA
Handle_B1.2	TATCAGCTTGCTTGGTTGCTTTGAATGGGATTTTTTTTTTTTTTTTTTGCATGTA
Handle_B1.3	CACCAGTACAATGCACCGTAATCAAGGTGATTTTTTTTTTTTTTTTTTGCATGTA

Handle_B2.1	TAGGGTTTTTCGCTGGCAAGTGGAACGGTACGTTTTTCCAGAATCCTGATTTTTT TTTTTTTTTCGGATTGT
Handle_B2.2	GGAGCTAAACATAATATGCAACTACGGGCGCTTTTTTTTTTTTTTTTCGGATTGT
Handle_B2.3	AATTATTTTTACCGTTGTAGCGATAGGGTTGATTTTTGTGTTGTTTTTTTTTTTTT TTCGGATTGT
Handle_B3.1	ATTTTTTTTTGCACCCAGCTAAACATAAAAACTTTTTAGGGAATTTTTTTTTTTTTT TTCGGAACAT
Handle_B3.2	ATGCAAATCCATCATCACCTTGCTCTTAGAATTTTTTTTTTTTTTTTCGGAACAT
Handle_B3.3	TCCTTTTTTTGAAAACATAGCTTTTTCAAATATTTTTATTTTAGTTAATTTTTTT TTTTTTTTTCGGAACAT
Handle_B4.1	TCCCGCCAAAATAACCTACCATATGAAGTATTTTTTTTTTTTTTTTAGCTCCA
Handle_B4.2	TGGCAAATCAATGGTGCTTGTTACGCAGAAGTTTTTTTTTTTTTTTAGCTCCA
Handle_B4.3	TAGACTTTTTTTTACAAACAACGCCCTGGAGTTTTTGGACTCTATGATATTTTTTT TTTTTTTTTAGCTCCA
Handle_B5.1	TAGATTTTCAGTCTAACGGAACAATTATCATTTTTTTTTTTTTTTTACTTGACG
Handle_B5.2	CAGAACGAGTATGAAGCCCTTTTACCAGAGTTTTTTTTTTTTTTTACTTGACG
Handle_B5.3	CATATTTTTTTCCTGATTATCCAGTACCTTTTTTTTTTACATCGGGAGAATTTTTTT TTTTTTTTACTTGACG
Handle_C0.1	TTCCCAATTCTTTTGAAAATCTCCACCTTTATTTTTTTTTTTTTTTCTCGTTGT
Handle_C0.2	ATTGCTTTTTTTCCTTTTGATATAGATACATTTTTTTTCGCAAATGGTCATTTTTTT TTTTTTTTCTCGTTGT
Handle_C0.3	ATCAAAAAGATTCTAAATCGGTTGATAGCGTTTTTTTTTTTTTTTTTCTCGTTGT
Handle_C1.1	TTTGCTTTTTTAAACAACCTTTGATACCGATAGTTTTTTTGCGCCGACAATTTTTTT TTTTTTTTTACAATCCG
Handle_C1.2	TATCAGCTTGCTTGGTTGCTTTGAATGGGATTTTTTTTTTTTTTTTACAATCCG
Handle_C1.3	CACCAGTACAATGCACCGTAATCAAGGTGTATTTTTTTTTTTTTTTTACAATCCG
Handle_C2.1	TAGGGTTTTTCGCTGGCAAGTGGAACGGTACGTTTTTCCAGAATCCTGATTTTTTT TTTTTTTTTGACACACA
Handle_C2.2	GGAGCTAAACATAATATGCAACTACGGGCGCTTTTTTTTTTTTTTTTGACACACA
Handle_C2.3	AATTATTTTTACCGTTGTAGCGATAGGGTTGATTTTTGTGTTGTTTTTTTTTTTTT TTGACACACA
Handle_C3.1	ATTTTTTTTTGCACCCAGCTAAACATAAAAACTTTTTAGGGAATTTTTTTTTTTTTT TTCGCTTTA
Handle_C3.2	ATGCAAATCCATCATCACCTTGCTCTTAGAATTTTTTTTTTTTTTTCCGCTTTA
Handle_C3.3	TCCTTTTTTTGAAAACATAGCTTTTTCAAATATTTTTATTTTAGTTAATTTTTTT TTTTTTTTCCGCTTTA



Handle_C4.1	TCCCGCCAAAATAACCTACCATATGAAGTATTTTTTTTTTTTTTTTTTCGTCAAGT
Handle_C4.2	TGGCAAATCAATGGTGCTTGTTACGCAGAAGTTTTTTTTTTTTTTTTTCGTCAAGT
Handle_C4.3	TAGACTTTTTTTTACAAACAACGCCCTGGAGTTTTTTGACTCTATGATATTTTTTT TTTTTTTTTCGTCAAGT
Handle_C5.1	TAGATTTTCAGTCTAACGGAACAATTATCATTTTTTTTTTTTTTTTTACCGAAAG
Handle_C5.2	CAGAACGAGTATGAAGCCCTTTTACCAGAGTTTTTTTTTTTTTTTTTACCGAAAG
Handle_C5.3	CATATTTTTTTCCTGATTATCCAGTACCTTTTTTTTTTACATCGGGAGAATTTTTTT TTTTTTTTTACCGAAAG
Handle_D0.1	TTCCCAATTCTTTTGAAAATCTCCACCTTATTTTTTTTTTTTTTTTGCAAGCTA
Handle_D0.2	ATTGCTTTTTTTCCTTTTGATATAGATACATTTTTTTTCGCAAAATGGTCATTTTTTT TTTTTTTTTGCAAGCTA
Handle_D0.3	ATCAAAAAGATTCTAAATCGGTTGATAGCGTTTTTTTTTTTTTTTTTTGCAAGCTA
Handle_D1.1	TTTGCTTTTTTAAACAACCTTGATACCGATAGTTTTTTTGCGCCGACAATTTTTTT TTTTTTTTTACAACGAG
Handle_D1.2	TATCAGCTTGCTTGGTTGCTTTGAATGGGATTTTTTTTTTTTTTTTACAACGAG
Handle_D1.3	CACCAGTACAATGCACCGTAATCAAGGTGTATTTTTTTTTTTTTTTTACAACGAG
Handle_D2.1	TAGGGTTTTTCGCTGGCAAGTGGAACGGTACGTTTTTCCAGAATCCTGATTTTTT TTTTTTTTTGCGACATA
Handle_D2.2	GGAGCTAAACATAATATGCAACTACGGGCGCTTTTTTTTTTTTTTTTGCACATA
Handle_D2.3	AATTATTTTTTACCGTTGTAGCGATAGGGTTGATTTTTGTGTGTTTTTTTTTTTTTT TTGCACATA
Handle_D3.1	ATTTTTTTTTGCACCCAGCTAAACATAAAAACTTTTTAGGGAATTTTTTTTTTTTTT TTATGTTCCG
Handle_D3.2	ATGCAAATCCATCATCACCTTGCTCTTAGAATTTTTTTTTTTTTTTTATGTTCCG
Handle_D3.3	TCCTTTTTTTGAAAACATAGCTTTTCAAATATTTTTTATTTTAGTTAATTTTTTT TTTTTTTTTATGTTCCG
Handle_D4.1	TCCCGCCAAAATAACCTACCATATGAAGTATTTTTTTTTTTTTTTTTTAAAGCGG
Handle_D4.2	TGGCAAATCAATGGTGCTTGTTACGCAGAAGTTTTTTTTTTTTTTTTTAAAGCGG
Handle_D4.3	TAGACTTTTTTTTACAAACAACGCCCTGGAGTTTTTTGACTCTATGATATTTTTTT TTTTTTTTTAAAGCGG
Handle_D5.1	TAGATTTTCAGTCTAACGGAACAATTATCATTTTTTTTTTTTTTTTTGCCTCTA
Handle_D5.2	CAGAACGAGTATGAAGCCCTTTTACCAGAGTTTTTTTTTTTTTTTTTGCCTCTA
Handle_D5.3	CATATTTTTTTCCTGATTATCCAGTACCTTTTTTTTTTACATCGGGAGAATTTTTTT TTTTTTTTTGCCTCTA

Table S5: Handle sequence for the icosahedral DNA origami

### S4.3 Octahedral DNA origami

#### S4.3.1 Staple sequences

core_octa-1	TCAAAGCGAACCAGACCGTTTTATATAGTC
core_octa-2	GCTTTGAGGACTAAAGAGCAACGGGGAGTT
core_octa-3	GTAAATCGTCGCTATTGAATAACTCAAGAA
core_octa-4	AAGCCTTAAATCAAGACTTGCGGAGCAAAT
core_octa-5	ATTTTAAGAAGCTGGCTTGAATTATCAGTGA
core_octa-6	GTAAAAATTTCGCATTATAAACGTAAACTAG
core_octa-7	AGCACCATTACCATTACAGCAAATGACGGA
core_octa-8	ATTGCGTAGATTTTCAAACAGATTGTTTG
core_octa-9	TAACCTGTTTAGCTATTTTCGCATTCATTC
core_octa-10	GTCAGAGGGTAATTGAGAACACCAAATAG
core_octa-11	CTCCAGCCAGCTTTCCCCTCAGGACGTTGG
core_octa-12	GTCCACTATTAAGAACCAGTTTTGGTTCC
core_octa-13	TAAAGGTGGCAACATAGTAGAAAATAATAA
core_octa-14	GATAAGTCCTGAACAACTGTTTAAAGAGAA
core_octa-15	GGTAATAGTAAAATGTAAGTTTTACACTAT
core_octa-16	TCAGAACCGCCACCCTCTCAGAGTATTAGC
core_octa-17	AAGGGAACCGAACTGAGCAGACGGTATCAT
core_octa-18	GTAAAGATTCAAAGGCCTGAGTTGACCCCT
core_octa-19	AGGCGTTAAATAAGAAGACCGTGTGCAAG
core_octa-20	CAGGTCGACTCTAGAGCAAGCTTCAAGGCG
core_octa-21	CAGAGCCACCACCCTCTCAGAACTCGAGAG
core_octa-22	TTCACGTTGAAAATCTTGCGAATGGGATTT
core_octa-23	AAGTTTTAACGGGGTCGGAGTGTAAGTGG
core_octa-24	TTGCGTATTGGGCGCCCGGGGTGCGCTC
core_octa-25	GTCACCAGAGCCATGGTGAATTATCACCAATCAGAAAAGCCT
core_octa-26	GGACAGAGTTACTTTGTGCGAAATCCGCGTGTATCACCGTACG
core_octa-27	CAACATGATTTACGAGCATGGAATAAGTAAGACGACAATAAA
core_octa-28	AACCAGACGCTACGTTAATAAAAACGAACATACCACATTCAGG
core_octa-29	TGACCTACTAGAAAAAGCCCCAGGCAAAGCAATTTTCATCTTC
core_octa-30	TGCCGGAAGGGGACTCGTAACCGTGCATTATATTTTAGTTCT
core_octa-31	AGAACCCCAAATCACCATCTGCGGAATCGAATAAAAATTTTT
core_octa-32	GCTCCATTGTGTACCGTAACACTGAGTTAGTTAGCGTAACCT
core_octa-33	AGTACCGAATAGGAACCCAAACGGTGTAACCTCAGGAGGTTT
core_octa-34	CAGTTTGAATGTTTAGTATCATATGCGTAGAATCGCCATAGC

core_octa-35	AAGATTGTTTTTTTAAACCAAGAAACCATCGACCCAAAAACAGG
core_octa-36	TCAGAGCGCCACCACATAATCAAAATCAGAACGAGTAGTATG
core_octa-37	GATGGTTGGGAAGAAAAATCCACCAGAAATAATTGGGGCTTGA
core_octa-38	CTCCTTAACGTAGAAAACCAATCAATAATTCATCGAGAACAGA
core_octa-39	AGACACCTTACGCAGAACTGGCATGATTTTCTGTCCAGACAA
core_octa-40	GCCAGCTAGGCGATAGCTTAGATTAAGACCTTTTTAACCTGT
core_octa-41	CCGACTTATTAGGAACGCCATCAAAAATGAGTAACAACCCCA
core_octa-42	GTCCAATAGCGAGAACCAGACGACGATATTC AACGCAAGGGA
core_octa-43	CCAAAATACAATATGATATTC AACCGTTAGGCTATCAGGTAA
core_octa-44	AACAGTACTTGAAAACATATGAGACGGGTCTTTTTTAATGGA
core_octa-45	TTTCACCGCATTAAAGTCGGGAAACCTGATTTGAATTACCCA
core_octa-46	GAGAATAGAGCCTTACCGTCTATCAAATGGAGCGGAATTAGA
core_octa-47	ATAATTAATTTTAAAAA CTTTTTCAA CTTTTTAAACAACGCC
core_octa-48	GCACCCAGCGTTTTTTATCCGGTATTCTAGGCGAATTATTCA
core_octa-49	GGAAGCGCCACAAACAGTTAATGCCCGACTCCTCAAGATA
core_octa-50	GTTTGCCTATTCACAGGCAGGTCAGACGCCACCACACCACCC
core_octa-51	CGCGAGCTTAGTTTTTCCCAATTCTGCGCAAGTGTAAGCCT
core_octa-52	AGAAGCAACCAAGCCAAAAGAATACACTAATGCCAAA CTTCC
core_octa-53	ATTAAGTATAAAGCGGCAAGGCCAAAGAACTAATAGGGTACC
core_octa-54	CAGTGCCTACATGGGAATTTACCGTTCCACAAGTAAGCAGAT
core_octa-55	ATAAGGCGCCAAAAGTTGAGATTTAGGATAACGGACCAGTCA
core_octa-56	TGCTAAACAGATGAAGAAACCACCAGAATTTAAAAAAAGGCT
core_octa-57	CAGCCTTGTTTTTGTATTAAGAGGCTGACTGCCTATATCAGA
core_octa-58	CGGAATAATTCAACCCAGCGCCAAAGACTTATTTTAAACGCAA
core_octa-59	CGCCTGAATTACCCTAATCTTGACAAGACAGACCATGAAAGA
core_octa-60	ACGCGAGGCTACAACAGTACCTTTTACAAATCGCGCAGAGAA
core_octa-61	CAGCGAACATTTAAAAGAGAGTACCTTTACTGAATATAATGAA
core_octa-62	GGACGTTTAAATTCGACGAGAAAACACCACCTAATGCAGAT
core_octa-63	AAAGCGCCAAAGTTTATCTTACCGAAGCCCAATAATGAGTAA
core_octa-64	GAGCTCGTTGTAAACGCCAGGGTTTTCCAAAGCAATAAAGCC
core_octa-65	AATTATTGTTTTTCATGCCTTTAGCGTCAGATAGCACGGAAAC
core_octa-66	AAGTTTCAGACAGCCGGGATCGTCACCCTTCTGTAGCTCAAC
core_octa-67	ACAAAGAAATTTAGGTAGGGCTTAATTGTATACAACGGAATC
core_octa-68	AACAAAATAACTAGGTCTGAGAGACTACGCTGAGTTTCCCT
core_octa-69	CATAACCTAAATCAACAGTTCAGAAAACGTCATAAGGATAGC
core_octa-70	CACGACGAATTCGTGTGGCATCAATTCTTTAGCAAAAATTACG

core_octa-71	CCTACCAACAGTAATTTTATCCTGAATCAAACAGCCATATGA
core_octa-72	GATTATAAAGAAACGCCAGTTACAAAATTTACCAACGTCAGA
core_octa-73	AGTAGATTGAAAAGAATCATGGTCATAGCCGGAAGCATAAGT
core_octa-74	TAGAATCCATAAATCATTTAACAATTTCTCCCGGCTTAGGTT
core_octa-75	AAAGGCCAAATATGTTAGAGCTTAATTGATTGCTCCATGAGG
core_octa-76	CCAAAAGGAAAGGACAACAGTTTCAGCGAATCATCATATTCC
core_octa-77	GAAATCGATAACCGGATACCGATAGTTGTATCAGCTCCAACG
core_octa-78	TGAATATTATCAAATAATGGAAAGGGTTAATATTTATCCCAA
core_octa-79	GAGGAAGCAGGATTCGGGTAAAATACGTAAAACACCCCCCAG
core_octa-80	GGTTGATTTTCCAGCAGACAGCCCTCATTCGTCACGGGATAG
core_octa-81	CAAGCCCCACCCTTAGCCCGGAATAGGACGATCTAAAGTTT
core_octa-82	TGTAGATATTACGCGGCGATCGGTGCGGGCGCCATCTTCTGG
core_octa-83	CATCCTATTCAGCTAAAAGGTAAAGTAAAAAGCAAGCCGTTT
core_octa-84	CAGCTCATATAAGCGTACCCCGGTTGATGTGTCGGATTCTCC
core_octa-85	CATGTCACAAACGGCATTAAATGTGAGCAATTCGCGTTAAAT
core_octa-86	AGCGTCACGTATAAGAATTGAGTTAAGCCCTTTTTAAGAAAG
core_octa-87	TATAAAGCATCGTAACCAAGTACCGCACCGGCTGTAATATCC
core_octa-88	ATAGCCCGCGAAAATAATTGTATCGGTTTCGCCACAATGAGT
core_octa-89	AGACAGTTCATATAGGAGAAGCCTTTATAACATTGCCTGAGA
core_octa-90	AACAGGTCCCGAAATTGCATCAAAAAGATCTTTGATCATCAG
core_octa-91	ACTGCCCTTGCCCCGTTGCAGCAAGCGGCAACAGCTTTTTCT
core_octa-92	TCAAAGGGAGATAGCCCTTATAAATCAAGACAACAACCATCG
core_octa-93	GTAATACGCAAACATGAGAGATCTACAACCTAGCTGAGGCCGG
core_octa-94	GAGATAACATTAGAAGAATAACATAAAAAGGAAGGATTAGGA
core_octa-95	CAGATATTACCTGAATACCAAGTTACAATCGGGAGCTATTTT
core_octa-96	CATATAACTAATGAACACAACATACGAGCTGTTTCTTTGGGG
core_octa-97	ATGTTTTGCTTTTGATCGGAACGAGGGTACTTTTTCTTTTGATAAGAGGTCATT
core_octa-98	CTTCGCTGGGCGCAGACGACAGTATCGGGGCACCGTCGCCATTCAGGCTGCGCA
core_octa-99	GATATTCTAAATTGAGCCGGAACGAGGCCCAACTTGGCGCATAGGCTGGCTGAC
core_octa-100	TGTCGTCATAAGTACAGAACCGCCACCCATTTTCACAGTACAACTACAACGCC
core_octa-101	CGATTATAAGCGGAGACTTCAAATATCGCGGAAGCCTACGAAGGCACCAACCTA
core_octa-102	AACATGTACGCGAGTGGTTTGAATAACCTAAACACATTCTTACCAGTATAAAGC
core_octa-103	GTCTGGATTTTGCCTTTTAAATGCAATGGTGAGAAATAAATTAATGCCGGAGAG
core_octa-104	GCCTTGAATCTTTTCCGGAACCGCCTCCCAGAGCCCAGAGCCGCCCGCCAGCATT
core_octa-105	CGCTGGTGCTTTCTGAATCGGCCAACGAGGGTGGTGATTGCCCTTCACCGCCT
core_octa-106	ACATAACTTGCCCTAACTTTAATCATTGCATTATAACAACATTATTACAGGTAG

core_octa-107	TTATTTTTACCGACAATGCAGAACGCGCGAAAAATCTTTCCTTATCATTCCAAG
core_octa-108	TTTCAATAGAAGGCAGCGAACCTCCCGATTAGTTGAAACAATAACGGATTGCGC
core_octa-109	GGGCGACCCCAAAAGTATGTTAGCAAACATAAAAGAGTCACAATCAATAGAAAAAT
core_octa-110	ATGACCACTCGTTTGGCTTTTGCAAAAGTTAGACTATATTCATTGAATCCCCCT
core_octa-111	TCCAAATCTTCTGAATTATTTGCACGTAGGTTAACGCTAACGAGCGTCTTTCC
core_octa-112	GGGTTATTTAATTACAATATATGTGAGTAATTAATAAGAGTCAATAGTGAATTT

Table S6: Staple sequence for the octahedral DNA origami

### S4.3.2 Functionalization sequence

Oct_AuNPhandles_1	ATCCATCACTTCATACTCTACGTTGTTGTTGTTGTTGTTGGGGTGCCAGTTGAGACCATTAGATACAATTTTCACTGTGTGAAATTGTTATCC
Oct_AuNPhandles_2	ATCCATCACTTCATACTCTACGTTGTTGTTGTTGTTGTTTCAGAGCTGGGTAAACGACGGCCAGTGCGATCCCCGTAGTAGCATTAAACATCCA
Oct_AuNPhandles_3	ATCCATCACTTCATACTCTACGTTGTTGTTGTTGTTGTTTTCAGCGGTACAGAGCGGGAGAATTAAGTGCCTAATTTTCGGAACCTATTATTCT
Oct_AuNPhandles_4	ATCCATCACTTCATACTCTACGTTGTTGTTGTTGTTGTTTTCAGCGGTACAGAGCGGGAGAATTAAGTGCCTAATTTTCGGAACCTATTATTCT
Oct_AuNPhandles_5	ATCCATCACTTCATACTCTACGTTGTTGTTGTTGTTGTTGTAGCGCCATTAAATTGGGAATTAGAGCGCAAGGCGCACCGTAATCAGTAGCGA
Oct_AuNPhandles_6	ATCCATCACTTCATACTCTACGTTGTTGTTGTTGTTGTTAGCCGAAAGTCTCTCTTTGATGATACAAGTGCCTTAAGAGCAAGAAACAATGA
Oct_AuNPhandles_7	ATCCATCACTTCATACTCTACGTTGTTGTTGTTGTTGTTGTGGGAAATCATATAAATATTTAAATTGAATTTTGTCTGGCCTTCCTGTAGCC
Oct_AuNPhandles_8	ATCCATCACTTCATACTCTACGTTGTTGTTGTTGTTGTTCCACGCGCAAAATGGTTGAGTGTGTTTCGTGGACTTGCTTTCGAGGTGAATTT
Oct_AuNPstaples_1	GGGGTGCCAGTTGAGACCATTAGATACAATTTTCACTGTGTGAAATTGTTATCC
Oct_AuNPstaples_2	TCAGAGCTGGGTAAACGACGGCCAGTGCGATCCCCGTAGTAGCATTAAACATCCA
Oct_AuNPstaples_3	TTAGCGGTACAGAGCGGGAGAATTAAGTGCCTAATTTTCGGAACCTATTATTCT
Oct_AuNPstaples_4	TGATTATCAACTTTACAATAAGGAATCCAAAAAGTTTGTAGTAACATTATCAT
Oct_AuNPstaples_5	GTAGCGCCATTAAATTGGGAATTAGAGCGCAAGGCGCACCGTAATCAGTAGCGA
Oct_AuNPstaples_6	AGCCGAAAGTCTCTCTTTTGTGATGATACAAGTGCCTTAAGAGCAAGAAACAATGA
Oct_AuNPstaples_7	GTGGGAAATCATATAAATATTTAAATTGAATTTTGTCTGGCCTTCCTGTAGCC
Oct_AuNPstaples_8	CCCACGCGCAAAATGGTTGAGTGTGTTTCGTGGACTTGCTTTCGAGGTGAATTT
AuNP_conjugation	TATGAAGTGATGGATGAT-SH

Table S7: Functionalization sequence for the octahedral DNA origami. The one named with "AuNPhandle" is used to capture DNA functionalized AuNP while the one named with "AuNPstaple" is just the staple without the handle for doing so. The one named as AuNP\_conjugation is used to be conjugated to AuNPs.

### S4.3.3 Handle sequence

Handle_A0.0	GCTCACAATTCCGTGAGCTAACTCACTGGAAGTAATGGTCAATTTTTTTTTTTTTTT TTTTTTTTTCCCTGCTCC
Handle_A0.1	GGCCCTGAGAGAAGCAGGCGAAAATCATTGCGTAGAGGCGGTTTTTTTTTTTTTTT TTTTTTTTTCCCTGCTCC
Handle_A0.2	CTTAAACAGCTTATATATTCGGTCGCTTGATGGGGAACAAGATTTTTTTTTTTTTTTT TTTTTTTTTCCCTGCTCC
Handle_A0.3	TTTGCGGATGGCCAACTAAAGTACGGGCTTGCAGCTACAGAGTTTTTTTTTTTTTTT TTTTTTTTTCCCTGCTCC
Handle_A1.0	ATCAAAATCATATATGTAAATGCTGAACAAACACTTGCTTCTTTTTTTTTTTTTTTT TTTTTTTTTGACATGCGC
Handle_A1.1	CAACGCTCAACAGCAGAGGCATTTTCAATCCAATGATAAATATTTTTTTTTTTTTTTT TTTTTTTTTGACATGCGC
Handle_A1.2	AACGGGTATTAAGGAATCATTACCGCCAGTAATTCAACAATATTTTTTTTTTTTTTTT TTTTTTTTTGACATGCGC
Handle_A1.3	TGATTGCTTTGAGCAAAAAGAAGATGAAATAGCAGAGGTTTTGTTTTTTTTTTTTTTT TTTTTTTTTGACATGCGC
Handle_A2.0	ACTGTTGGGAAGCAGCTGGCGAAAGGATAGGTCAAGATCGCATTTTTTTTTTTTTTT TTTTTTTTTCGCCAAGTC
Handle_A2.1	ATAAATCATAATAAATCGGTTGTACTGTGCTGGCATGCCTGTTTTTTTTTTTTTTT TTTTTTTTTCGCCAAGTC
Handle_A2.2	GGTAGCTATTTTAGAGAATCGATGAAAACATTAAATGTGTAGTTTTTTTTTTTTTTT TTTTTTTTTCGCCAAGTC
Handle_A2.3	AGCTTTCATCAACGGATTGACCGTAAAATCGTATAATTTTTTTTTTTTTTTTTTTT TTTTTTTTTCGCCAAGTC
Handle_A3.0	AATAGCAATAGCACCAGAAGGAAACCTAAAGCCACTGGTAATTTTTTTTTTTTTTTT TTTTTTTTTGCGTGTCAC
Handle_A3.1	GACAGGAGGTTGAAACAAATAAATCCGCCCCCTCGCCACCCTTTTTTTTTTTTTTTT TTTTTTTTTGCGTGTCAC
Handle_A3.2	CAGAAATCAAGTTTCGGCATTTTCGGTTAAATATATCACCAGTTTTTTTTTTTTTTT TTTTTTTTTGCGTGTCAC
Handle_A3.3	TCATATGGTTTACGATTGAGGGAGGGAAACGCAATACATACATTTTTTTTTTTTTTTT TTTTTTTTTGCGTGTCAC
Handle_A4.0	CAAATGCTTTAAAAAATCAGGTCTTTAAGAGCAGCCAGAGGGTTTTTTTTTTTTTTT TTTTTTTTTGCGGCATAC

Handle_A4.1	AAACGAAAGAGGGCGAAACAAAGTACTGACTATATTCGAGCTTTTTTTTTTTTTTT TTTTTTTTTGCGGCATAC
Handle_A4.2	CTTCATCAAGAGAAAATCAACGTAACAGAGATTTGTCAATCATTTTTTTTTTTTTTT TTTTTTTTTGCGGCATAC
Handle_A4.3	AAAGATTCATCAGGAATTACGAGGCATGCTCATCCTTATGCGTTTTTTTTTTTTTT TTTTTTTTTGCGGCATAC
Handle_A5.0	AGAGCCTAATTTGATTTTTTGTTTAAATCCTGAAATAAAGAATTTTTTTTTTTTTTT TTTTTTTTTGCGCTGCAAC
Handle_A5.1	TTTGCGGAACAATGGCAATTCATCAATCTGTATAATAATTTTTTTTTTTTTTTTT TTTTTTTTTGCGCTGCAAC
Handle_A5.2	GAAACATGAAAGCTCAGTACCAGGCGAAAAATGCTGAACAAATTTTTTTTTTTTTTT TTTTTTTTTGCGCTGCAAC
Handle_A5.3	TGTAGCATTCCAACGTTAGTAAATGAAGTGCCGCGCCACCCTTTTTTTTTTTTTTT TTTTTTTTTGCGCTGCAAC
Handle_B0.0	GCTCACAAATTCGTGAGCTAACTCACTGGAAGTAATGGTCAATTTTTTTTTTTTTTT TTTTTTTTTCGCTGTACC
Handle_B0.1	GGCCCTGAGAGAAGCAGGCGAAAATCATTGCGTAGAGGCGGTTTTTTTTTTTTTT TTTTTTTTTCGCTGTACC
Handle_B0.2	CTTAAACAGCTTATATATTCGGTTCGCTTGATGGGGAACAAGATTTTTTTTTTTTTTT TTTTTTTTTCGCTGTACC
Handle_B0.3	TTTGCGGATGGCCAACTAAAGTACGGGCTTGCAGCTACAGAGTTTTTTTTTTTTTT TTTTTTTTTCGCTGTACC
Handle_B1.0	ATCAAAATCATATATGTAAATGCTGAACAAACACTTGCTTCTTTTTTTTTTTTTTT TTTTTTTTTGCGCATGTC
Handle_B1.1	CAACGCTCAACAGCAGAGGCATTTCAATCCAATGATAAATATTTTTTTTTTTTTTT TTTTTTTTTGCGCATGTC
Handle_B1.2	AACGGGTATTAAGGAATCATTACCGCCAGTAATTCAACAATATTTTTTTTTTTTTTT TTTTTTTTTGCGCATGTC
Handle_B1.3	TGATTGCTTTGAGCAAAAAGAAGATGAAATAGCAGAGTTTTGTTTTTTTTTTTTTT TTTTTTTTTGCGCATGTC
Handle_B2.0	ACTGTTGGGAAGCAGCTGGCGAAAGGATAGGTCAAGATCGCATTTTTTTTTTTTTTT TTTTTTTTTCGCTCGAAC
Handle_B2.1	ATAAATCATAATAAATCGGTTGTACTGTGCTGGCATGCCTGTTTTTTTTTTTTTT TTTTTTTTTCGCTCGAAC
Handle_B2.2	GGTAGCTATTTAGAGAATCGATGAAAACATTAATGTGTAGTTTTTTTTTTTTTT TTTTTTTTTCGCTCGAAC



Handle_B2.3	AGCTTTCATCAACGGATTGACCGTAAAATCGTATAATATTTTTTTTTTTTTTTTTTTT TTTTTTTTTCGCTCGAAC
Handle_B3.0	AATAGCAATAGCACCAGAAGGAAACCTAAAGCCACTGGTAATTTTTTTTTTTTTTTTTT TTTTTTTTTGCTGACGAC
Handle_B3.1	GACAGGAGGTTGAAACAAATAAATCCGCCCCCTCCGCCACCCTTTTTTTTTTTTTTTTT TTTTTTTTTGCTGACGAC
Handle_B3.2	CAGAATCAAGTTTCGGCATTTCGGTTAAATATATCACCAGTTTTTTTTTTTTTTTTTT TTTTTTTTTGCTGACGAC
Handle_B3.3	TCATATGGTTTACGATTGAGGGAGGGAAACGCAATACATACATTTTTTTTTTTTTTTTT TTTTTTTTTGCTGACGAC
Handle_B4.0	CAAATGCTTTAAAAAATCAGGTCTTTAAGAGCAGCCAGAGGGTTTTTTTTTTTTTTTT TTTTTTTTTGATGCCGC
Handle_B4.1	AAACGAAAGAGGGCGAAACAAAGTACTGACTATATTCGAGCTTTTTTTTTTTTTTTTT TTTTTTTTTGATGCCGC
Handle_B4.2	CTTCATCAAGAGAAATCAACGTAACAGAGATTTGTCAATCATTTTTTTTTTTTTTTTT TTTTTTTTTGATGCCGC
Handle_B4.3	AAAGATTCATCAGGAATTACGAGGCATGCTCATCCTTATGCGTTTTTTTTTTTTTTTT TTTTTTTTTGATGCCGC
Handle_B5.0	AGAGCCTAATTTGATTTTTTTGTTTAAATCCTGAAATAAAGAATTTTTTTTTTTTTTTTT TTTTTTTTTCCAGAGCCC
Handle_B5.1	TTTGCGGAACAATGGCAATTCATCAATCTGTATAATAATTTTTTTTTTTTTTTTTTTTT TTTTTTTTTCCAGAGCCC
Handle_B5.2	GAAACATGAAAGCTCAGTACCAGGCGAAAAATGCTGAACAAATTTTTTTTTTTTTTTTT TTTTTTTTTCCAGAGCCC
Handle_B5.3	TGTAGCATTCCAACGTTAGTAAATGAAGTGCCGCGCCACCCTTTTTTTTTTTTTTTTT TTTTTTTTTCCAGAGCCC
Handle_C0.0	GCTCACAATTCCGTGAGCTAACTCACTGGAAGTAATGGTCAATTTTTTTTTTTTTTTTT TTTTTTTTTAGCGAACCC
Handle_C0.1	GGCCCTGAGAGAAGCAGGCGAAAATCATTGCGTAGAGGCGGTTTTTTTTTTTTTTTTTT TTTTTTTTTAGCGAACCC
Handle_C0.2	CTTAAACAGCTTATATATTCGGTCGCTTGATGGGGAACAAGATTTTTTTTTTTTTTTTT TTTTTTTTTAGCGAACCC
Handle_C0.3	TTTGCGGATGGCCAACTAAAGTACGGGCTTGCAGCTACAGAGTTTTTTTTTTTTTTTT TTTTTTTTTAGCGAACCC
Handle_C1.0	ATCAAAATCATATATGTAAATGCTGAACAAACACTTGCTTCTTTTTTTTTTTTTTTTT TTTTTTTTGTTCGAGCG

Handle_C1.1	CAACGCTCAACAGCAGAGGCATTTTCAATCCAATGATAAATATTTTTTTTTTTTTTT TTTTTTTTTGTTTCGAGCG
Handle_C1.2	AACGGGTATTAAGGAATCATTACCGCCAGTAATTCAACAATATTTTTTTTTTTTTTT TTTTTTTTTGTTTCGAGCG
Handle_C1.3	TGATTGCTTTGAGCAAAAGAAGATGAAATAGCAGAGGTTTTGTTTTTTTTTTTTTT TTTTTTTTTGTTTCGAGCG
Handle_C2.0	ACTGTTGGGAAGCAGCTGGCGAAAGGATAGTCAAGATCGCATTTTTTTTTTTTTTT TTTTTTTTTGAGCAGGG
Handle_C2.1	ATAAATCATAATAAATCGGTTGTAAGTGTGCTGGCATGCCTGTTTTTTTTTTTTTT TTTTTTTTTGAGCAGGG
Handle_C2.2	GGTAGCTATTTAGAGAATCGATGAAAACATTAATGTGTAGTTTTTTTTTTTTTT TTTTTTTTTGAGCAGGG
Handle_C2.3	AGCTTTCATCAACGGATTGACCGTAAAATCGTATAATTTTTTTTTTTTTTTTTTT TTTTTTTTTGAGCAGGG
Handle_C3.0	AATAGCAATAGCACCAGAAGGAAACCTAAAGCCACTGGTAATTTTTTTTTTTTTTT TTTTTTTTGCCTCTCCC
Handle_C3.1	GACAGGAGGTTGAAACAAATAAATCCGCCCCCTCCGCCACCCTTTTTTTTTTTTTTT TTTTTTTTGCCTCTCCC
Handle_C3.2	CAGAAATCAAGTTTCGGCATTTTCGGTTAAATATATCACCAGTTTTTTTTTTTTTT TTTTTTTTGCCTCTCCC
Handle_C3.3	TCATATGGTTTACGATTGAGGGAGGGAAACGCAATACATACATTTTTTTTTTTTTTT TTTTTTTTGCCTCTCCC
Handle_C4.0	CAAATGCTTTAAAAAATCAGGTCTTTAAGAGCAGCCAGAGGGTTTTTTTTTTTTTT TTTTTTTTGGGCTCTGG
Handle_C4.1	AAACGAAAGAGGGCGAAACAAAGTACTGACTATATTCGAGCTTTTTTTTTTTTTTT TTTTTTTTGGGCTCTGG
Handle_C4.2	CTTCATCAAGAGAAATCAACGTAACAGAGATTTGTCAATCATTTTTTTTTTTTTTT TTTTTTTTGGGCTCTGG
Handle_C4.3	AAAGATTCATCAGGAATTACGAGGCATGCTCATCCTTATGCGTTTTTTTTTTTTTT TTTTTTTTGGGCTCTGG
Handle_C5.0	AGAGCCTAATTTGATTTTTGTTTTAAATCCTGAAATAAAGAATTTTTTTTTTTTTTT TTTTTTTTGTGACACGC
Handle_C5.1	TTTGCGGAACAATGGCAATTCATCAATCTGTATAATAATTTTTTTTTTTTTTTTTTT TTTTTTTTGTGACACGC
Handle_C5.2	GAAACATGAAAGCTCAGTACCAGGCGAAAAATGCTGAACAAATTTTTTTTTTTTTTT TTTTTTTTGTGACACGC

Handle_C5.3	TGTAGCATTCCAACGTTAGTAAATGAAGTGCCGCGCCACCCTTTTTTTTTTTTTTTT TTTTTTTTTGTGACACGC
Handle_D0.0	GCTCACAATTCCGTGAGCTAACTCACTGGAAGTAATGGTCAATTTTTTTTTTTTTTTT TTTTTTTTTGGTACAGCG
Handle_D0.1	GGCCCTGAGAGAAGCAGGCGAAAATCATTGCGTAGAGGCGGTTTTTTTTTTTTTTT TTTTTTTTTGGTACAGCG
Handle_D0.2	CTTAAACAGCTTATATATTCGGTCGCTTGATGGGGAACAAGATTTTTTTTTTTTTTTT TTTTTTTTTGGTACAGCG
Handle_D0.3	TTTGCGGATGGCCAACTAAAGTACGGGCTTGCAGCTACAGAGTTTTTTTTTTTTTTT TTTTTTTTTGGTACAGCG
Handle_D1.0	ATCAAAATCATATATGTAAATGCTGAACAAACACTTGCTTCTTTTTTTTTTTTTTTT TTTTTTTTTGGGTTTCGCT
Handle_D1.1	CAACGCTCAACAGCAGAGGCATTTTCAATCCAATGATAAATATTTTTTTTTTTTTTTT TTTTTTTTTGGGTTTCGCT
Handle_D1.2	AACGGGTATTAAGGAATCATTACCGCCAGTAATTCAACAATATTTTTTTTTTTTTTTT TTTTTTTTTGGGTTTCGCT
Handle_D1.3	TGATTGCTTTGAGCAAAAAGAAGATGAAATAGCAGAGGTTTTGTTTTTTTTTTTTTTT TTTTTTTTTGGGTTTCGCT
Handle_D2.0	ACTGTTGGGAAGCAGCTGGCGAAAGGATAGGTCAAGATCGCATTTTTTTTTTTTTTTTT TTTTTTTTTGACTIONGGCG
Handle_D2.1	ATAAATCATACATAAATCGGTTGTACTIONGTGCTGGCATGCCTGTTTTTTTTTTTTTTT TTTTTTTTTGACTIONGGCG
Handle_D2.2	GGTAGCTATTTTAGAGAATCGATGAAAACATTAAATGTGTAGTTTTTTTTTTTTTTT TTTTTTTTTGACTIONGGCG
Handle_D2.3	AGCTTTCATCAACGGATTGACCGTAAAATCGTATAATTTTTTTTTTTTTTTTTTTT TTTTTTTTTGACTIONGGCG
Handle_D3.0	AATAGCAATAGCACCAGAAGGAAACCTAAAGCCACTGGTAATTTTTTTTTTTTTTTTTT TTTTTTTTTGTCGTCAGC
Handle_D3.1	GACAGGAGGTTGAAACAAATAAATCCGCCCCCTCCGCCACCCTTTTTTTTTTTTTTTT TTTTTTTTTGTCGTCAGC
Handle_D3.2	CAGAAATCAAGTTTCGGCATTTCGGTTAAATATATCACCAGTTTTTTTTTTTTTTTTT TTTTTTTTTGTCGTCAGC
Handle_D3.3	TCATATGGTTTACGATTGAGGGAGGGAAACGCAATACATACATTTTTTTTTTTTTTTT TTTTTTTTTGTCGTCAGC
Handle_D4.0	CAAATGCTTTAAAAAATCAGGTCTTTAAGAGCAGCCAGAGGGTTTTTTTTTTTTTTTTT TTTTTTTTTGGGAGAGGC

Handle_D4.1	AAACGAAAGAGGGCGAAACAAAGTACTGACTATATTCGAGCTTTTTTTTTTTTTTT TTTTTTTTTGGGAGAGGC
Handle_D4.2	CTTCATCAAGAGAAATCAACGTAACAGAGATTTGTCAATCATTTTTTTTTTTTTTT TTTTTTTTTGGGAGAGGC
Handle_D4.3	AAAGATTCATCAGGAATTACGAGGCATGCTCATCCTTATGCGTTTTTTTTTTTTTT TTTTTTTTTGGGAGAGGC
Handle_D5.0	AGAGCCTAATTTGATTTTTTGTTTAAATCCTGAAATAAAGAATTTTTTTTTTTTTTT TTTTTTTTTGTTGCAGCC
Handle_D5.1	TTTGCGGAACAATGGCAATTCATCAATCTGTATAATAATTTTTTTTTTTTTTTTT TTTTTTTTTGTTGCAGCC
Handle_D5.2	GAAACATGAAAGCTCAGTACCAGGCGAAAAATGCTGAACAAATTTTTTTTTTTTTTT TTTTTTTTTGTTGCAGCC
Handle_D5.3	TGTAGCATTCCAACGTTAGTAAATGAAGTGCCGCGCCACCCTTTTTTTTTTTTTTT TTTTTTTTTGTTGCAGCC

Table S8: Handle sequence for the octahedral DNA origami

## References

- [1] F. Romano, J. Russo, L. Kroc, and P. Šulc. Designing patchy interactions to self-assemble arbitrary structures. *Physical Review Letters*, 125(11):118003, 2020.
- [2] J. Russo, F. Romano, L. Kroc, F. Sciortino, L. Rovigatti, and P. Šulc. SAT-assembly: A new approach for designing self-assembling systems. *Journal of Physics: Condensed Matter*, 34(35):354002, 2022.
- [3] N. Een. MiniSat: A SAT solver with conflict-clause minimization. In *Proc. SAT-05: 8th Int. Conf. on Theory and Applications of Satisfiability Testing*, pages 502–518, 2005.
- [4] P. Šulc, F. Romano, T. E. Ouldridge, L. Rovigatti, J. P. Doye, and A. A. Louis. Sequence-dependent thermodynamics of a coarse-grained DNA model. *The Journal of chemical physics*, 137(13):135101, 2012.
- [5] T. E. Ouldridge, A. A. Louis, and J. P. Doye. Structural, mechanical, and thermodynamic properties of a coarse-grained DNA model. *The Journal of chemical physics*, 134(8):02B627, 2011.
- [6] B. E. Snodin, F. Randisi, M. Mosayebi, P. Šulc, J. S. Schreck, F. Romano, T. E. Ouldridge, R. Tsukanov, E. Nir, A. A. Louis, et al. Introducing improved structural properties and salt dependence into a coarse-grained model of DNA. *The Journal of chemical physics*, 142(23):06B613.1, 2015.
- [7] J. Russo, P. Tartaglia, and F. Sciortino. Reversible gels of patchy particles: role of the valence. *The Journal of chemical physics*, 131(1):014504, 2009.
- [8] P. Šulc, F. Romano, T. E. Ouldridge, L. Rovigatti, J. P. K. Doye, and A. A. Louis. Sequence-dependent thermodynamics of a coarse-grained DNA model. *Journal of Chemical Physics*, 137(13):5101, 2012.
- [9] L. Rovigatti, P. Šulc, I. Z. Reguly, and F. Romano. A comparison between parallelization approaches in molecular dynamics simulations on GPUs. *Journal of computational chemistry*, 36(1):1–8, 2015.
- [10] E. Poppleton, M. Matthies, D. Mandal, F. Romano, P. Šulc, and L. Rovigatti. oxDNA: coarse-grained simulations of nucleic acids made simple. *Journal of Open Source Software*, 8(81):4693, 2023.
- [11] E. Poppleton, J. Bohlin, M. Matthies, S. Sharma, F. Zhang, and P. Šulc. Design, optimization and analysis of large DNA and RNA nanostructures through interactive visualization, editing and molecular simulation. *Nucleic acids research*, 48(12):e72–e72, 2020.
- [12] J. Bohlin, M. Matthies, E. Poppleton, J. Procyk, A. Mallya, H. Yan, and P. Šulc. Design and simulation of DNA, RNA and hybrid protein–nucleic acid nanostructures with oxView. *Nature protocols*, 17(8):1762–1788, 2022.
- [13] Y. Tian, T. Wang, W. Liu, H. L. Xin, H. Li, Y. Ke, W. M. Shih, and O. Gang. Prescribed nanoparticle cluster architectures and low-dimensional arrays built using octahedral DNA origami frames. *Nature nanotechnology*, 10(7):637–644, 2015.
- [14] J. Zhang, Y. Xu, Y. Huang, M. Sun, S. Liu, S. Wan, H. Chen, C. Yang, Y. Yang, and Y. Song. Spatially patterned neutralizing icosahedral DNA nanocage for efficient SARS-CoV-2 blocking. *Journal of the American Chemical Society*, 144(29):13146–13153, 2022.
- [15] J. N. Zadeh, C. D. Steenberg, J. S. Bois, B. R. Wolfe, M. B. Pierce, A. R. Khan, R. M. Dirks, and N. A. Pierce. NUPACK: Analysis and design of nucleic acid systems. *Journal of computational chemistry*, 32(1):170–173, 2011.
- [16] C. Lin, S. D. Perrault, M. Kwak, F. Graf, and W. M. Shih. Purification of DNA-origami nanostructures by rate-zonal centrifugation. *Nucleic acids research*, 41(2):e40–e40, 2013.

- [17] Y. Wang, L. Dai, Z. Ding, M. Ji, J. Liu, H. Xing, X. Liu, Y. Ke, C. Fan, P. Wang, et al. DNA origami single crystals with Wulff shapes. *Nature Communications*, 12(1):3011, 2021.
- [18] D. J. Lewis, L. Z. Zornberg, D. J. Carter, and R. J. Macfarlane. Single-crystal Winterbottom constructions of nanoparticle superlattices. *Nature materials*, 19(7):719–724, 2020.
- [19] Y. Tian, J. R. Lhermitte, L. Bai, T. Vo, H. L. Xin, H. Li, R. Li, M. Fukuto, K. G. Yager, J. S. Kahn, et al. Ordered three-dimensional nanomaterials using DNA-prescribed and valence-controlled material voxels. *Nature materials*, 19(7):789–796, 2020.
- [20] K. G. Yager, Y. Zhang, F. Lu, and O. Gang. Periodic lattices of arbitrary nano-objects: modeling and applications for self-assembled systems. *Journal of Applied Crystallography*, 47(1):118–129, 2014.
- [21] S.-T. Wang, B. Minevich, J. Liu, H. Zhang, D. Nykypanchuk, J. Byrnes, W. Liu, L. Bershadsky, Q. Liu, T. Wang, et al. Designed and biologically active protein lattices. *Nature communications*, 12(1):3702, 2021.
- [22] J. SantaLucia Jr and D. Hicks. The thermodynamics of DNA structural motifs. *Annu. Rev. Biophys. Biomol. Struct.*, 33:415–440, 2004.